The role of LRP2 in forebrain development of the mouse

Dissertation

zur Erlangung des akademischen Grades des Doktors der Naturwissenschaften

doctor rerum naturalium
(Dr. rer. nat.)

eingereicht im Fachbereich Biologie, Chemie, Pharmazie
der Freien Universität Berlin

vorgelegt von

ANNABEL CHRIST

September 2010

Die Arbeit wurde von 04/2007 bis 09/2010 unter der Anleitung von Prof. Dr. Thomas E. Willnow am Max-Delbrück Centrum für Molekulare Medizin in Berlin durchgeführt.

1. Gutachter: Herr Prof. Dr. Volker Haucke,
   Freie Universität Berlin

2. Gutachter: Herr Prof. Dr. Thomas E. Willnow,
   Max-Delbrück Centrum Berlin-Buch

Tag der Disputation: 26.1.2011

Summary

LRP2 is a member of the low-density lipoprotein receptor gene family, expressed in the neuroepithelial cells of the developing central nervous system. Loss of *Lrp2* expression in LRP2-deficient mice results in forebrain abnormalities with features of holoprosencephaly, causing perinatal lethality of most affected animals.

Holoprosencephaly is a common forebrain anomaly in which the cerebral hemispheres fail to separate along the midline due to a defect in midline induction. This syndrome includes a wide spectrum of malformations of face and brain structures both in humans and in animal models.

Recent studies from our lab demonstrated that LRP2 deficiency in mice leads to an increase in *bone morphogenetic protein* (*Bmp*) *4* expression in the rostral dorsal neuroepithelium, weaker and dorsally shifted *fibroblast growth factor* (*Fgf*) *8* expression and loss of *sonic hedgehog* (*Shh*) expression in the ventral telencephalon. These findings implicated the receptor in regulation of opposing actions of dorsal and ventral morphogen pathways in forebrain patterning.

Aim of my study was to elucidate the molecular mechanisms of LRP2 action in morphogen signaling and to find out why LRP2 receptor deficiency causes holoprosencephaly. In particular, I wanted to explore whether the receptor may act as key component in the BMP4 and/or SHH pathways and whether or not this activity involves regulated intramembranous proteolysis of the receptor intracellular domain.

Initially I introduced a *Bmp4* mutant allele into the *Lrp2*$^{-/-}$ line to reduce levels of this morphogen in embryos lacking LRP2. Despite a decrease in *Bmp4* expression (*Lrp2*$^{-/-}$; *Bmp4*$^{tm1blh/+}$), receptor-deficient embryos still suffered from holoprosencephalic defects, suggesting that overactivity of BMP4 in LRP2-deficient embryos is not the primary cause but likely a secondary consequence of loss of LRP2 activity.

A further detailed analysis of the expression pattern of transcription factors and morphogen pathways in early brain development showed that already before neural tube closure, *Lrp2*$^{-/-}$ embryos suffer from an impaired initial establishment of SHH protein in the rostral diencephalon ventral midline (RDVM) overlying the prechordal plate. The RDVM acts as an organizer for the developing

prosencephalon. Insufficient SHH protein activity in the RDVM leads to a decrease in *Six3* and *Shh* expression in the neuroepithelium of *Lrp2* mutants. This defect in early SHH signaling affects the coordinate activity of the three key morphogens SHH, BMP4, and FGF8 with severe consequences for early forebrain patterning processes. Individual cells within the RDVM were still able to respond to activation of the SHH pathway by SAG, suggesting that LRP2 deficiency affects an event in the SHH signaling cascade upstream of Smo, such as binding of SHH on the neuroepithelial cell surface. A potential role for LRP2 as cell surface receptor for SHH was confirmed by demonstrating specific binding of the recombinant morphogen to the neuroepithelium of wild type embryos but not LRP2-deficient embryos in an *ex vivo* model.

Finally, the crucial function of LRP2 as receptor for SHH was supported by my findings in a new mouse model that expresses the intracellular domain (ICD) of LRP2 under the endogenous promoter. Robust expression of the ICD failed to rescue forebrain defects caused by the lack of the full-length receptor, suggesting that it is the membrane-localized form of the clearance receptor that is important for proper forebrain formation.

In conclusion, my studies identified LRP2 as a novel morphogen receptor required for proper targeting of SHH protein to the RDVM. This pathway is essential for establishing the *Shh* expression domain in the ventral telencephalon and, consequently, for proper ventral medial forebrain development. My findings not only identified a novel molecular mechanism in the SHH pathway but also uncovered the cause of the holoprosencaphylic syndrome in mouse models and likely in patients with LRP2 deficiencies.

Zusammenfassung

LRP2 ist ein Mitglied der low-density Lipoprotein Rezeptor Genfamilie, der während der Entwicklung des zentralen Nervensystems in neuroepithelialen Zellen exprimiert wird. Der genetisch bedingte Verlust der *Lrp2* Expression in LRP2-defizienten Mäusen führt zu Missbildungen des Vorderhirns, welche typische Merkmale einer Holoprosenzephalie zeigen und zum perinatalen Tod der am stärksten betroffenen Tiere führen.

Holoprosenzephalie ist die häufigste Fehlbildung des Vorderhirns beim Menschen und zeichnet sich durch ein breites Spektrum an Anomalien der Gesichts- und Hirnstrukturen aus.

Frühere Studien aus unserem Labor zeigten, dass der Verlust der LRP2 Expression zu einem Anstieg der dorsalen *Bmp4* Expression, zu einer schwächeren und nach dorsal verschobenen *Fgf8* Expression sowie zu einer fehlenden *Shh* Expression im ventralen Telenzephalon Rezeptor-defizienter Mäuse führt. Diese Resultate ließen vermuten, dass der Rezeptor eine zentrale Rolle in der Regulation sich antagonisierender dorsaler und ventraler Signalwege des Vorderhirns spielt. Welcher der betroffenen Morphogen-Signalwege allerdings der primäre Ansatzpunkt der LRP2 Aktivität und welches der genaue Wirkmechanismus des Rezeptors sein könnte, war bisher jedoch vollkommen unklar.

Ziel meiner Studie war es daher den molekularen Mechanismus von LRP2 in Morphogen-Signalwegen aufzuklären und herauszufinden, warum LRP2 Defizienz Holoprosenzephalie verursacht. Im Speziellen wollte ich herausfinden ob der Rezeptor eine Schlüsselrolle im BMP4 und/oder SHH Signalweg ist und ob diese Aktivität regulierte intramembrane Spaltung der intrazellulären Domäne des Rezeptors beinhaltet.

Initial habe ich die LRP2-defiziente Mauslinie mit einer haploinsuffizienten Mauslinie für BMP4 verpaart, um die BMP4 Konzentration im Vorderhirn betroffener Tiere bereits auf transkriptioneller Ebene zu reduzieren. Die Halbierung der Transkriptionsrate von *Bmp4* hatte jedoch keinen positiven Einfluss auf den holoprosenzephalen Phänotyp LRP2-defizienter Embryonen. Aus diesen

Ergebnissen schloss ich, dass eine erhöhte *Bmp4* Expression nicht der primäre Grund für die Ausbildung der Holoprosenzephalie ist.

Eine nachfolgende detaillierte Expressionsanalyse von Transkriptionsfaktoren und Morphogenen ergab, dass sich schon vor der Schließung des Neuralrohres in *Lrp2*$^{-/-}$ Embryonen eine Störung der SHH Protein Lokalisation in der rostralen ventralen Mittellinie des Dienzephalons zeigte. Diese spezielle Region des zentralen Nervensystems fungiert als ein Organisationszentrum für das sich entwickelnde Prosenzephalon. Ungenügende SHH Aktivität in dieser Region führt zu geringerer *Six3* und *Shh* Expression im Neuroepithel LRP2-defizienter Embryonen. Dieser frühe Defekt im SHH Signalweg beeinflusst nachfolgend die Wechselwirkungen aller drei Signalwege der Musterbildung (SHH, BMP4 und FGF8) mit dramatischen Konsequenzen für die korrekte Entwicklung des Vorderhirns. Einzelne Zellen innerhalb der rostralen ventralen Mittellinie des Dienzephalons rezeptor-defizienter Mäuse waren aber immer noch fähig auf Aktivierung des SHH Signalweges zu reagieren. Diese Daten ließen den Schluss zu, dass die Aktivität von LRP2 proximal zu Smo, z.B. in der anfänglichen Bindung von SHH auf der Zelloberfläche von Zielzellen nötig sein könnte. Eine mögliche Rolle von LRP2 als Oberflächenrezeptor für SHH konnte ich tatsächlich in Organkulturen bestätigen. So zeigte sich, dass rekombinantes SHH Protein spezifisch an das Neuroepithel von Wildtyp-Embryonen nicht aber an das von LRP2-defizienten Embryonen bindet. Schließlich konnte ich die essentielle Bedeutung des Membranrezeptors LRP2 in der Vorderhirnentwicklung auch noch in einem neuen Mausmodell validieren, in dem die intrazelluläre Domäne von LRP2 unter der Kontrolle des LRP2 Promoters exprimiert wird. In diesem Tiermodell zeigte sich, dass die lösliche intrazelluläre Domäne des Rezeptors nicht in der Lage war, den Verlust des Wildtyp Rezeptors auszugleichen.

Zusammenfassend gelang mir in meinen Studien der Nachweis von LRP2 als Morphogen-Rezeptor, der für die initiale Lokalisation von SHH in der rostralen ventralen Mittellinie des Dienzephalons und damit für eine korrekte Ausbildung des ventralen, medialen Vorderhirns verantwortlich ist. Diese Ergebnisse haben nicht nur ein völlig neues Konzept im SHH Signalweg aufgedeckt sondern auch wichtige Hinweise auf mögliche Ursachen der Holoprosenzephalie bei Mausmodellen und möglicherweise auch bei Patienten mit LRP2 Gendefekten geliefert.

Contents

List of Figures

List of Tables

Abbreviations

AER	Apical ectodermal ridge
AME	Axial mesendoderm
ANR	Anterior neural ridge
AVE	Anterior visceral endoderm
BAC	Bacterial artificial chromosome
BMP	Bone morphogenetic protein
BN16 cells	Brown Norway rat yolk sac carcinoma cells
Boc	Brother of CDO
BSA	Bovine serum albumin
Cdo	Cell adhesion molecule-related/downregulated by oncogenes
Ce-LRP1	*Caenorhabditis elegans*-LRP1
Ce-IMP-2	*Caenorhabditis elegans*-IMP-2
CK1	Casein kinase 1
CNS	Central nervous system
CSL	Cranial suspensory ligament
Cx	Cortex
Dab1/2	Disabled homolog 1/2
DBP	Vitamin D-binding protein
DBS	Donnai-Barrow syndrome
Disp1	Dispatched homolog 1
DKK-1	Dickkopf-1
DMEM	Dulbecco's Modified Eagle's Medium
DS	Dissection solution
E	Embryonic day
EGF	Epidermal growth factor-type repeat
Emx1/2	Empty spiracles homolog 1/2
ER	Endoplasmic reticulum
ES cells	Embryonic stem cells
FCS	Fetal calf serum
FGF	Fibroblast growth factor
FOAR	Facio-oculo-acoustico-renal syndrome
FoxA2	Forkhead box A2
FoxH1	Forkhead box H1

Fzd	Frizzled
Gas1	Growth arrest-specific protein
Gli	Glioma-associated oncogene
GO	Early-gastrula organizer
GSK3	Glycogen synthase kinase 3
GST	Glutathione S-transferase
Gsx2	GS homeobox 2
HEPES	2-(4-(2-Hydroxyethyl)-1-piperazinyl)-ethansulfonacid
Hhip	Hedgehog-interacting protein
HPE	Holoprosencephaly
HSPG	Heparan sulfate proteoglycan
ICD	Intracellular cytoplasmic domain
IP	Immunoprecipitation buffer
IPTG	Isopropylthiogalactosidase
ISH	*In situ* hybridization
LB	Lysogeny broth
LDL	Low-density lipoprotein
LDLR	Low-density lipoprotein receptor
Leu	Leucine
LGE	Lateral ganglionic eminence
LRP	LDLR related protein
MGE	Medial ganglionic eminence
MCTF	Membrane-bound LRP2 COOH-terminal fragment
MICD	Soluble LRP2 intracellular domain
MIH	Middle interhemispheric variant of Holoprosencephaly
MMP	Metalloprotease
MS	Mid streak
MuSK	Muscle specific kinase
Nhe3	Na^+/H^+ exchanger
NICD	Intracellular domain of Notch
Nkx2.1	NK2 homeobox 1
NMDA	N-methyl-D-aspartate
OKP	Opossum kidney proximal tubule cells
Os	Optic stalk
PBS	Phosphate buffered saline
PBT	Phosphate buffered saline with Triton
PCR	Polymerase chain reaction

PFA	Paraformaldehyde
PKA	Protein kinase A
PrCP	Prechordal plate
PrE	Primitive endoderm
PTB	Phosphotyrosine binding domain
PTC	Proximal tubule culture
Ptch1	Patched homolog 1
R	Rhombomers
RAP	Receptor associated protein
RBP	Vitamin A/retinol binding protein
RIP	Regulated intramembrane proteolysis
RDVM	Rostral diencephalon ventral midline
S	Septum
SAG	Smoothened Agonist
SDS	Sodium dodecyl sulfate
SDS-PAGE	Sodium dodecyl sulfate polyacrylamide gel electrophoresis
SEZ	Subependymal Zone
SHH	Sonic hedgehog
SHH-N	N-terminal SHH
SHH-Np	SHH protein with N-terminal palmitate and C-terminal cholesterol
Six3	Sine oculis homeobox 3
Smo	Smoothened
SOB	Super optimal broth
Sufu	Suppressor of fused
TC-B_{12}	Transcobalamin vitamin B_{12}
TDGF1	Teratocarcinoma-derived growth factor 1
TGIF	TGF-β-induced factor homeobox
WNT	Wingless-related MMTV integration site proteins
Zic2	Zinc finger protein of the cerebellum 2
Zli	Zona limitans intrathalamica

1. Introduction

1.1 Developmental patterning processes

The development and patterning of multicellular organisms is critically dependent on spatial gradients formed by morphogens. Morphogens are secreted signaling molecules that induce different cell fates in a time and concentration dependent manner. During development the excretion of a particular morphogen from its source leads to the formation of different cell types in a defined spatial relationship to the source, and it provides positional information to the receiving cells.

Forebrain development is directed by morphogens, and represents a unique model of the complex interactions between opposing morphogen gradients.

Defects in morphogen signaling often lead to holoprosencephaly (HPE), the most common malformation of the human forebrain during early embryonic development. Basic mechanisms in brain development in humans and mice are conserved and thus alterations that lead to HPE can be studied in the mouse. The identification of novel factors and the mechanisms underlying the patterning processes disturbed in this syndrome will extend our understanding of the complex morphogen network during forebrain development.

In the following chapters, early forebrain development and defects that lead to HPE will be described.

1.1.1 Early forebrain development in the mouse

During gastrulation, the three germ layers of an embryo (ectoderm, mesoderm and endoderm) are reorganized, and the body plan of the mature organism is established.

At mid-streak (MS) stage of gastrulation, which starts at embryonic day (E) 6.75, when the primitive streak elongates, node precursors, which are located at the anterior tip of the primitive streak, form the early-gastrula organizer (GO). The GO is able to induce anterior neural development (J. Klingensmith *et al*., 1999; P. Tam *et al*., 1999) (Figure 1.1). At E7.5, the node, located at the anterior end of the primitive streak, is formed at the distal tip of the embryo. Mutations in *forkhead box A*2 (*Foxa2*) lead to a disturbed development of the GO and node, resulting in forebrain truncations and lack of forebrain-specific gene expression (S. Ang *et al*., 1994), demonstrating that the GO and its derivatives are important in establishing early forebrain anlagen.

Additionally, extra-embryonic tissues also play an essential role in forebrain induction. The anterior visceral endoderm (AVE) underlies the anterior epiblast that is destined to develop into anterior neuroectoderm. Recent studies reported that the AVE promotes forebrain formation by antagonizing long-range signaling of posterior bone morphogenetic protein (BMP) and therefore acts in concert with the GO and its derivatives (Figure 1.1) (Y. Yang *et al*., 2006).

By headfold stage at E7.5, the axial mesendoderm (AME) forms from the organizer and migrates to the anterior region to underlie the midline of the neural plate. During this developmental stage, the AME specifies forebrain character by restricting BMP signaling (Y. Yang *et al*., 2006).

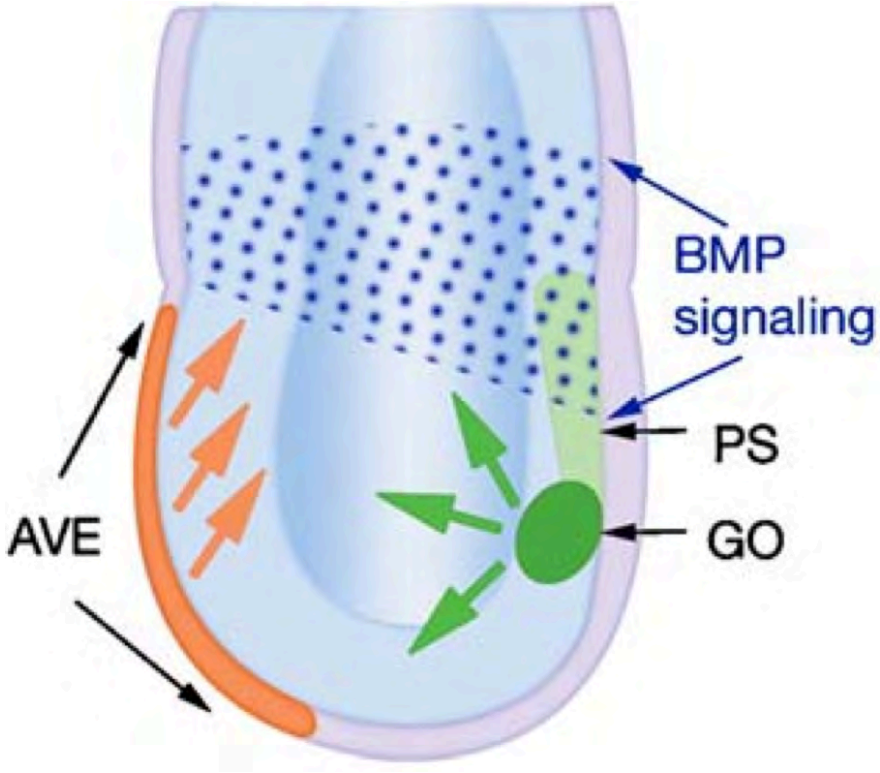

Figure 1.1: Forebrain formation at E6.75 by antagonizing BMP signaling. Anti-BMP activities emitted from the anterior visceral endoderm (AVE, orange) and the early-gastrula organizer (GO, green) restrict BMP signaling (blue dots) to the proximal epiblast, allowing forebrain establishment in anterior ectoderm. (Adapted from Y. Yang *et al*., 2006)

Starting with the onset of neurulation, sonic hedgehog (*Shh)* is expressed in the prechordal plate (PrCP), a mesodermal structure developing from the anterior end of the primitive streak, underlying the most rostral area of the neuroepithelium. The PrCP is known to be an essential organizing center for midline specification of brain, facial and oral structures (H. Li *et al*., 1997; E. Pera *et al*., 1997). It is believed that SHH signaling, originating in the PrCP, acts on the overlying anterior neuroepithelium (rostral diencephalon ventral midline, RDVM) in separating the eye field and activating genes like *Nkx2.1* and *sine oculis homeobox 3* (*Six3)* (C. Chiang *et al*., 1996; R. Chow *et al*., 2001). The activation of these genes is important for ongoing development of the forebrain and initiates *Shh* expression in the developing ventral neuroepithelium (X. Geng *et al*., 2008; Y. Jeong *et al*., 2008; L. Sussel *et al*., 1999) (Figure 1.2).

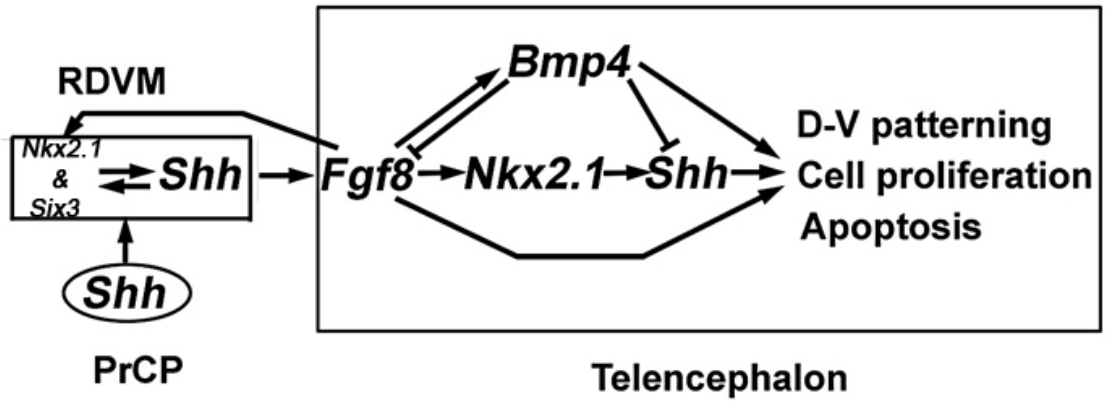

Figure 1.2: Model of SHH signaling during telencephalon development. SHH protein from the prechordal plate (PrCP) activates through long-range signaling *Nkx2.1* and *Six3* expression in the rostral diencephalon ventral midline (RDVM), which in turn activates *Shh* expression. The RDVM afterwards patterns the developing telencephalon. (Adapted from X. Geng *et al*., 2008)

Once the neural tissue has obtained anterior characteristics, its further patterning relies on the influence of signaling molecules expressed in centers both surrounding and within the forebrain (Figure 1.3)

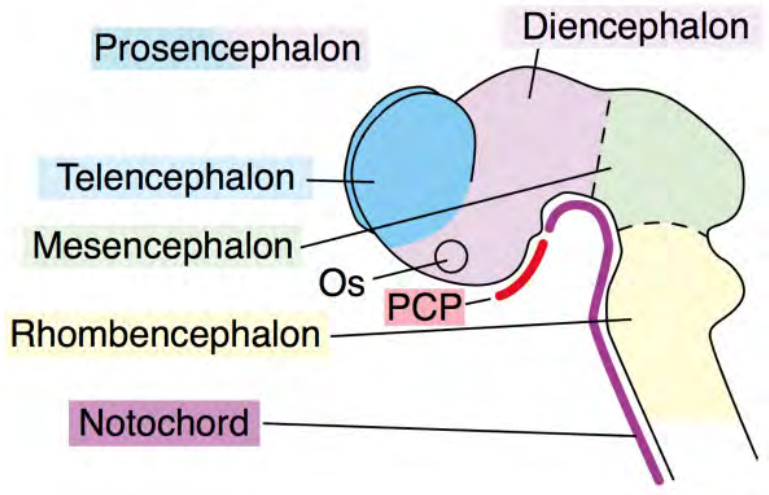

Figure 1.3: Scheme of the developing mouse brain. Lateral view of the brain around mid-gestation (E10.5) after neural tube closure. PrCP, PCP, prechordal plate; Os, optic stalk. (Adapted from P. Zaki *et al*., 2003)

The development of the forebrain is accompanied by the establishment of a secondary organizer, the anterior neural ridge (ANR). The ANR is located between the most rostral part of the neural plate and the non-neural ectoderm (G. Couly *et al*., 1988; G. Eagleson *et al*., 1995). *Fibroblast growth factor 8* (*Fgf8)* expression marks the ANR and is crucial for the specification of the rostral areas of the telencephalon (E. Meyers *et al*., 1998). *Shh* expression maintains *Fgf8* expression in the commissural plate (integral part of the telencephalon medium) by inhibiting the repressor activity of GLI3. *Fgf8* expression itself activates *Nkx2.1* expression in the ventral telencephalon, which in turn induces *Shh* expression in the rostral ventral telencephalon to specify the medial ganglionic eminence (MGE) fate (L. Sussel *et al*., 1999; E. Storm *et al*., 2006; Y. Ohkubo *et al*., 2002). *Fgf8* expression from the ANR regulates *Wnt8b* and *Bmp4* expression in the dorsal midline in a dosage-dependent manner (E. Storm *et al*., 2006; E. Storm *et al*., 2003). BMP and WNT activity in turn restrict *Fgf8* and *Shh* expression to the ventral forebrain (Y. Ohkubo *et al*., 2002) (Figure 1.4).

The proper formation of these opposing morphogen gradients and their correct spatial and temporal expression pattern are responsible for regulating each others' expression. This regulated interaction between the different morphogens promotes regular forebrain formation and patterning.

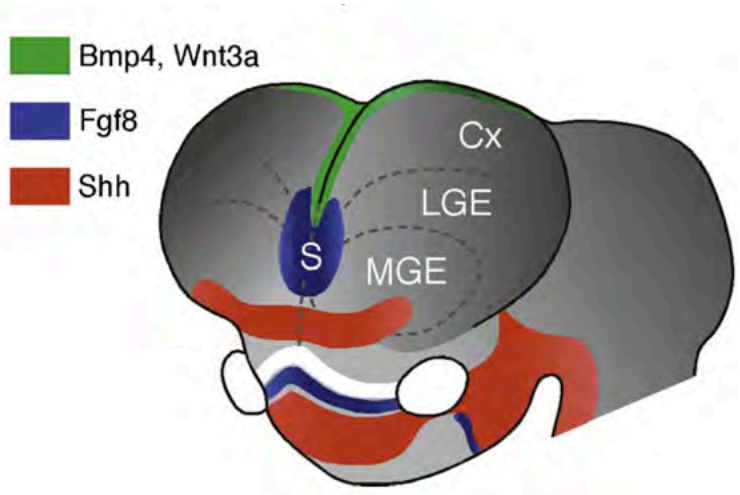

Figure 1.4: Patterning centers during forebrain development at E10.5. Expression of *Bmp4* and *Wnt3a* marks the dorsal midline, while *Fgf8* expression establishes the ANR and *Shh* expression displays the ventral signaling center. Cx, cortex; LGE, lateral ganglionic eminence (striatum); MGE, medial ganglionic eminence; S, septum. (R. Hoch *et al*., 2009)

1.1.2 The sonic hedgehog pathway

Formation of the forebrain requires correct dorso-ventral patterning, which is controlled by a set of secreted morphogens including sonic hedgehog (SHH) protein from ventral signaling sources. SHH acts as a classical morphogen during development: SHH protein spreads from a localized signal source and forms a gradient that patterns fields of responsive cells in a concentration- and signal duration-dependent manner (J. Hooper *et al*., 2005); if SHH is genetically or environmentally perturbed, severe brain malformations are the consequence.

The mature SHH protein is synthesized as a precursor that undergoes a series of post-translational modifications in which the precursor protein is auto-catalytically cleaved (J. Porter *et al*., 1995). This cleavage results in the generation of a 19 kDa active N-terminal fragment that is palmitoylated at the N-terminus. A cholesterol moiety is attached at the C-terminus forming the mature processed SHH protein with two lipid modifications (SHH-Np) (R. Pepinsky *et al*., 1998). Both lipid moieties are crucial for SHH movement or signaling activity. In recent studies, different variants of SHH-Np proteins were purified from stably transfected neural cell lines, and it was demonstrated that the C-terminal cholesterol is sufficient for multimerization and membrane tethering of hedgehog proteins, whereas the N-terminal palmitate is required for multimerization but also specifically for inducing signaling activity (J. Feng *et al*., 2004). The multimeric complexes with the lipid moieties embedded in the core, in analogy to micelles, are supposed to promote long-range signaling (X. Huang *et al*., 2007a; X. Huang *et al*., 2007b).

The release of active SHH-Np from producing cells requires the multi-pass transmembrane protein, dispatched homolog 1 (Disp1) (T. Caspary *et al*., 2002; Y. Ma *et al*., 2002).

In the absence of SHH, patched homolog 1 (Ptch1), the SHH receptor, maintains Smoothened (Smo), another transmembrane protein, in an inactive state, and the intracellular signaling cascade of the morphogen is blocked. Binding of SHH-N to Ptch1 inactivates Ptch1 and results in the release of the inhibitory effect on Smo and activation of downstream SHH target genes through glioma-associated oncogene (Gli) proteins (P. Ingham *et al*., 2001). In vertebrates, three *Gli* genes have been identified. In general, GLI1 acts primarily as an activator, GLI2 as both an activator and repressor and GLI3 mostly as a repressor (A. Ruiz i Altaba *et al*., 2003).

Recent studies demonstrated that primary cilia, relatively large protrusions of the cell membrane encountered in almost every cell of multicellular organisms, which serve as sensory organelles, appear to be an important structure in vertebrate hedgehog signaling (Figure 1.5). In the absence of SHH, Ptch1 represses not only the activity of Smo but also the translocation of Smo to the primary cilium of the SHH target cell. In these cells, protein kinase A (PKA) promotes the proteasome-dependent degradation of the Gli transcription factors (GLI2 and GLI3). The truncated forms of these proteins (GliR) translocate to the nucleus and repress the transcription of SHH signaling targets. Suppressor of fused (Sufu) maintains any remaining full-length Gli protein in an inactive state. SHH signal reception removes Ptch1 from the primary cilium, thereby allowing Smo accumulation in the primary cilium (K. Corbit *et al*., 2005; L. Milenkovic *et al*., 2009). Smo inhibits the proteolytic processing of Gli proteins, which are also concentrated in the cilia, primarily at the tip (C. Haycraft *et al*., 2005). Consequently, Smo promotes Gli activity and blocks the formation of Gli transcriptional repressor forms by interacting with suppressor of fused (Sufu) and protein kinase A (PKA). Activated Gli proteins (GliA) translocate to the nucleus to activate target gene expression. How Ptch1 is internalized upon binding of SHH and how it promotes localization of Smo in the cilium is still under investigation. Ongoing studies also identified several additional cell surface-expressed molecules that also bind to SHH, including hedgehog-interacting protein 1 (Hhip1), which blocks pathway activation (J. Jeong *et al*., 2005), as well as Cdo, Boc (cell surface Ig/fibronectin superfamily members) and growth arrest-specific protein 1 (Gas1), which enhance pathway activation (B. Allen *et al*., 2007; D. Martinelli *et al*., 2007; T. Tenzen *et al*., 2006).

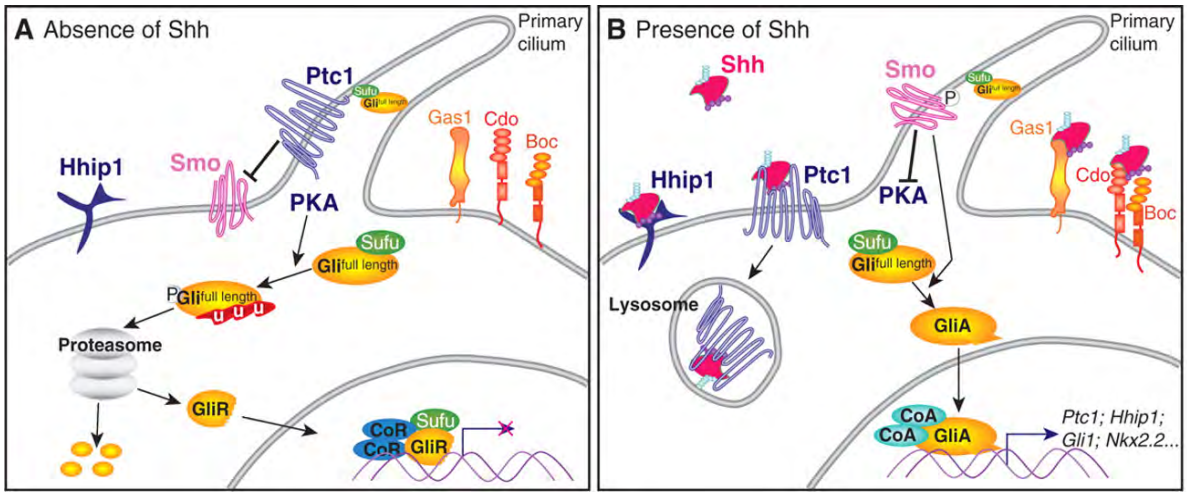

Figure 1.5: Model of SHH signaling in the primary cilium. Upon SHH binding to its receptor Ptch1 (Ptc1), Smo is released and transported to the ciliary tip, where it activates the SHH signaling pathway. (V. Ribes *et al*., 2009)

Ongoing studies try to analyze how SHH signaling promotes the positional identities of distinct neuronal subtype progenitors throughout the developing neural tube. So far the spatiotemporal dynamics of cellular responses to morphogens are believed to depend on the changes of the morphogen gradient itself, the dynamics of its signal transduction, the downstream interactions between target genes, or a combination of all three (E. Kutejova *et al*., 2009).

The concentration profile of a morphogen is determined by the morphogen's diffusion coefficient, and by its production and degradation rates. After the onset of morphogen production, the gradient needs some time to be established and to reach its steady state. The SHH gradient shows an increasing amplitude while development continues, probably because the number of SHH producing cells also increases. As a consequence, cells located in the ventral midline in the developing neural tube (overlying the notochord, the signaling source of SHH protein for the developing neural tube) are exposed to higher concentrations of SHH and for a longer period of time than cells located in more dorsal areas (V. Ribes *et al*., 2010).

Additionally, the gradient is shaped by SHH binding proteins, which influence the dynamics of the SHH signal transduction. Cdo, Boc, and Gas1 enhance SHH signaling but are transcriptionally downregulated (B. Allen *et al*., 2007; D. Martinelli *et al*., 2007; T. Tenzen *et al*., 2006). Gas1 and Cdo are believed to sensitize cells to the initial low concentration of the SHH gradient. The SHH dependent inhibition of Gas1

and Cdo is important to keep this sensitization only temporary (V. Ribes *et al*., 2010). In contrast Ptch1 and Hhip1 inhibit SHH signaling in a negative feedback loop and are transcriptionally upregulated by SHH signaling (P. Chuang *et al*., 2003; J. Jeong *et al*., 2005). The upregulation of Ptch is necessary for the temporal adaptations of cells to SHH signaling in regulating the duration of the signal and it leads to desensitization of cells to SHH signaling. As a consequence higher levels of SHH are required to neutralize Ptch1 (E. Kutejova *et al*., 2009).

The SHH pathway is also controlled by the interaction of downstream target genes. In midline cells of the caudal neural tube an initial activation of the SHH pathway and a following downregulation of the SHH signal is necessary to induce floor plate development. It is reported that SHH in this specific area first induces the expression of the transcription factor *FoxA2*, which then induces the expression of *Shh* itself but also leads subsequently to extinction of SHH signaling within these cells. The inhibition of SHH signaling may be caused by the regulation of components of the SHH signal transduction pathway (V. Ribes *et al*., 2010).

These spatiotemporal dynamic characteristics of the SHH pathway were mostly analyzed in the developing neural tube, but there is growing evidence for similar mechanisms in the developing brain. A nice model for the sequential temporal response to SHH signaling in the telencephalon is the development of the medial and lateral ganglionic eminences (the MGE and LGE). The initial inductive event is defined by SHH protein from the axial mesendoderm, patterning the overlying telencephalic neuroepithelium. SHH protein activates its own expression and the expression of *Nkx2.1*, which marks the developing MGE around E9.5. At E10.5, *Gsx2* expression appears as a consequence of SHH signaling and marks the developing LGE. The positive regulation of the SHH pathway within the LGE is coupled with the negative regulation of SHH signaling in the MGE, probably caused by Nkx2.1 mediated down-regulation of Gli2 (V. Sousa *et al*., 2010). These studies indicate that SHH functions through dynamic changes in temporal competence not only in the posterior developing neural tube but also in the developing forebrain.

1.2 Holoprosencephaly

Defects in the complex genetic network of forebrain development described above lead to holoprosencephaly (HPE). HPE is a developmental disorder and the most common forebrain abnormality in humans, affecting 1 in 16,000 live births (E. Roach *et al*., 1975) and 1 in 250 fetuses (E. Matsunaga *et al*., 1977). The etiology of HPE includes genetic and environmental causes. Environmental risk factors include maternal diabetes, maternal alcoholism, and prenatal exposure to drugs (M. Cohen *et al*., 2002). As genetic causes for HPE, an autosomal-dominant trait in patients, mutations in the following genes have been identified: *SHH*, *PTCH1*, *GLI2*, teratocarcinoma-derived growth factor 1 (*TDGF1* or *CRIPTO*), TGF-β-induced factor homeobox (*TGIF*), forkhead box H1 (*FOXH1*), zinc finger protein of the cerebellum 2 (*ZIC2*), *SIX3*, and *DISP1* (M. Muenke, and M. Cohen, 2000; M. Cohen, 2006; C. Dubourg *et al*., 2007; R. Krauss, 2007; M. Hayhurst, 2003; M. Muenke, and P. Beachy, 2000; E. Roessler *et al*., 2009).

In HPE the cerebral hemispheres fail to separate along the midline due to defects in midline induction. HPE includes a wide spectrum of malformations of face and brain structures (D. Wallis *et al*., 1999). Based on the severity of the defect, HPE is sub-grouped into three forms: alobar, semilobar and lobar HPE.

Alobar HPE is the most severe form. In alobar HPE, the brain consists of a single spherical forebrain structure with a single ventricle, lacking corpus callosum and olfactory bulbs. The brain malformations are accompanied by severe midline facial anomalies. Most affected individuals are not viable.

Semilobar HPE is a moderate form of the disease with partially separated cerebral hemispheres and a single ventricular cavity.

Lobar HPE is the least severe form. The cerebral hemispheres develop close to normal, and midline craniofacial defects are often absent or mild. However the ventricles still appear dysmorphic due to absence of the septum pellucidum (midline structure of the lateral ventricles).

Additionally, a middle interhemispheric variant of HPE (MIH) is also observed in humans. In MIH, the posterior frontal and parietal lobes of the brain are not well separated (A. Lewis *et al*., 2002).

Different mouse models with defects in four distinct morphogen pathways (nodal, sonic hedgehog, fibroblast growth factors, and bone morphogenetic proteins) can be grouped in alobar HPE, semilobar HPE, and MIH, and may serve as a model to identify the mechanisms leading to HPE in patients (M. Hayhurst *et al*., 2003; E. Monuki, 2007; X. Geng *et al*., 2009).

Mutations in the Nodal signaling pathway are often associated with alobar HPE. Additionally, alterations occurring in early developmental stages in the mouse around E6.5 - E8.5 and affecting the prechordal plate also often lead to alobar HPE. Such patterning defects during early developmental processes can be caused not only by mutations in the Nodal signaling pathway, but also by lack of *Zic2* expression, mutations in BMP signaling pathway components (like chordin and noggin), or by disruption of *Shh* expression (L. Lowe *et al*., 2001; J. Chu *et al*., 2005; D. Bachiller *et al*., 2000; A. Petryk *et al*., 2004; C. Chiang *et al*., 1996).

Mutations within the BMP pathway often result in semilobar HPE or MIH (E. Monuki, 2007). In MIH, dorsal telencephalic patterning centers are affected and fail to develop dorsal midline structures but do not alter dorso-ventral patterning of the telencephalon. Reduced *Zic2* expression levels result in a defective telencephalon roof plate (T. Nagai *et al*., 2000) and therefore affect the BMP and WNT signaling centers, which are important for development of dorsal midline structures.

Alterations in the SHH- and FGF signaling pathways often lead to semilobar HPE. Changes taking place during or after neural tube closure between E8.5 – E10.5 disrupt the formation of rostral (secreting FGF8) and ventral (producing SHH) telencephalic patterning centers and cause semilobar HPE. Impaired *Six3* and *Cdo* expression lead to reduced levels of ventral *Shh* expression in the forebrain and, consequently, to impaired ventral specification (X. Geng *et al*., 2008; Y. Jeong *et al*., 2008; W. Zhang *et al*., 2006). Reduced levels of *Fgf8* expression cause disturbed rostral midline formation (E. Storm *et al*., 2006; G. Gutin *et al*., 2006).

Another protein implicated in forebrain development and in HPE when defective is LRP2 (low density lipoprotein receptor related protein 2), a member of the low-density lipoprotein receptor gene family of multifunctional endocytic receptors. Loss of LRP2 function in mice leads to alobar or semilobar HPE-like

phenotypes, implicating this receptor in early CNS patterning processes. An important role for LRP2 in CNS development in humans was recently confirmed by Kantarci *et al*., who identified *LRP2* mutations in six families with Donnai-Barrow syndrome and in one family with facio-oculo-acoustico-renal syndrome (S. Kantarci *et al*., 2007). Donnai-Barrow syndrome (DBS) is an autosomal recessive disorder associated with agenesis of the corpus callosum, congenital diaphragmatic hernia, facial dysmorphology, ocular anomalies, sensorineural hearing loss, and developmental delay. The facio-oculo-acoustico-renal (FOAR) syndrome is typically characterized by proteinuria and macrocephaly but lacks agenesis of the corpus callosum. All affected individuals showed mutations in conserved residues of both *LRP2* alleles. The similarity of phenotypes suggested that these alterations result functionally in a null mutation. Therefore, DBS and FOAR syndromes represent the first human phenotype associated with mutations in *LRP2* and can be regarded as the same syndrome (S. Kantarci *et al*., 2007).

In addition, in the beginning of this year, microforms of HPE have also been described in patients with deletion within the *LRP2* gene locus (J. Rosenfeld *et al*., 2010) underlining the importance of the gene in the etiology of HPE not only in mice but also in humans. Microforms of HPE are characterized by milder craniofacial anomalies in the absence of neurological defects.

The structure and function of LRP2 in mice will be discussed in detail in the following sections.

1.3 The low-density lipoprotein receptor gene family

The low-density lipoprotein (LDL) receptor gene family (Figure 1.6) consists of a group of multifunctional, closely related cell surface receptors that bind and endocytose ligands with diverse biological functions (A. Nykjaer *et al*., 2002).

The LDL receptor gene family originated early in metazoan evolution, and its orthologues are found in multicellular organisms ranging from invertebrates like *Caenorhabditis elegans* (*C. elegans*) (J. Yochem *et al*., 1999) and *Drosophila melanogaster* (M. Wherli *et al*., 2000) to vertebrates like zebrafish (*Danio rerio*) (McCarthy *et al*., 2002), mouse (*mus musculus*) (M. Gafvels *et al*., 1994; M. Brown *et al*., 1998) and human (T. Südhof *et al*., 1985).

The core of the gene family consists of the low-density lipoprotein receptor (LDLR), the LDLR related protein 1 (LRP1), LRP1B and LRP2 (megalin, gp330), the very low-density lipoprotein receptor (VLDLR), the apolipoprotein E receptor-2 (APOER2, LRP8), the multiple epidermal growth factor repeat containing protein 7 (MEGF7, LRP4), Yolkless, and the receptor-mediated endocytosis-2 (RME-2). Distant members of the family that are not included in the core family because of a different domain organization are the low-density lipoprotein receptor related proteins 5 and 6 (LRP5 and LRP6) and the sorting protein related receptor containing LDLR class A repeats (SORLA) (Figure 1.6).

All members of the gene family share common structural and functional motifs. The extracellular domain is composed of complement-type repeats. These repeats are the ligand binding sites. At the carboxyl terminal site they are followed by ß-propellers, which are important for the pH-dependent release of ligands in endosomes. The β-propellers are flanked by epidermal growth factor type repeats. A module consisting of complement-type repeats and β-propellers may exist as single (e.g. LDLR) or multiple (e.g. LRP2) copies in the receptors. In the more distantly related receptors (LRP5, LRP6, and SORLA) the module is either inverted (LRP5/6) or combined with structural elements (such as fibronectin type III domains) that are not present in the other receptors (SORLA).

A single transmembrane domain anchors the receptors to the plasma membrane (P. May *et al*., 2003).

The cytoplasmic domain is highly variable in the different receptors but usually contains one or more asn-pro-any amino acid-tyr (NPxY) motifs. The NPxY motifs localize the receptors to clathrin coated pits at the cell surface, specialized regions for endocytosis (W. Chen *et al*., 1990; A. Bansal *et al*., 1991). They may also bind phosphotyrosine binding (PTB) domain containing adaptor proteins. In addition, Yxxϕ or a distal di-leu motif may contribute to receptor endocytosis (Y. Li *et al*., 2001a). Accessorily, the cytoplasmic domain can contain protein interaction motifs that interact with adaptor and scaffold proteins. Furthermore the domain can be modified by phosphorylation (Y. Li *et al*., 2001b). For the human VLDLR, phosphorylation was reported to regulate ligand-binding (R. Sakthivel *et al*., 2001) whereas phosphorylation of LRP1 controls endocytosis (Y. Li *et al*., 2001a).

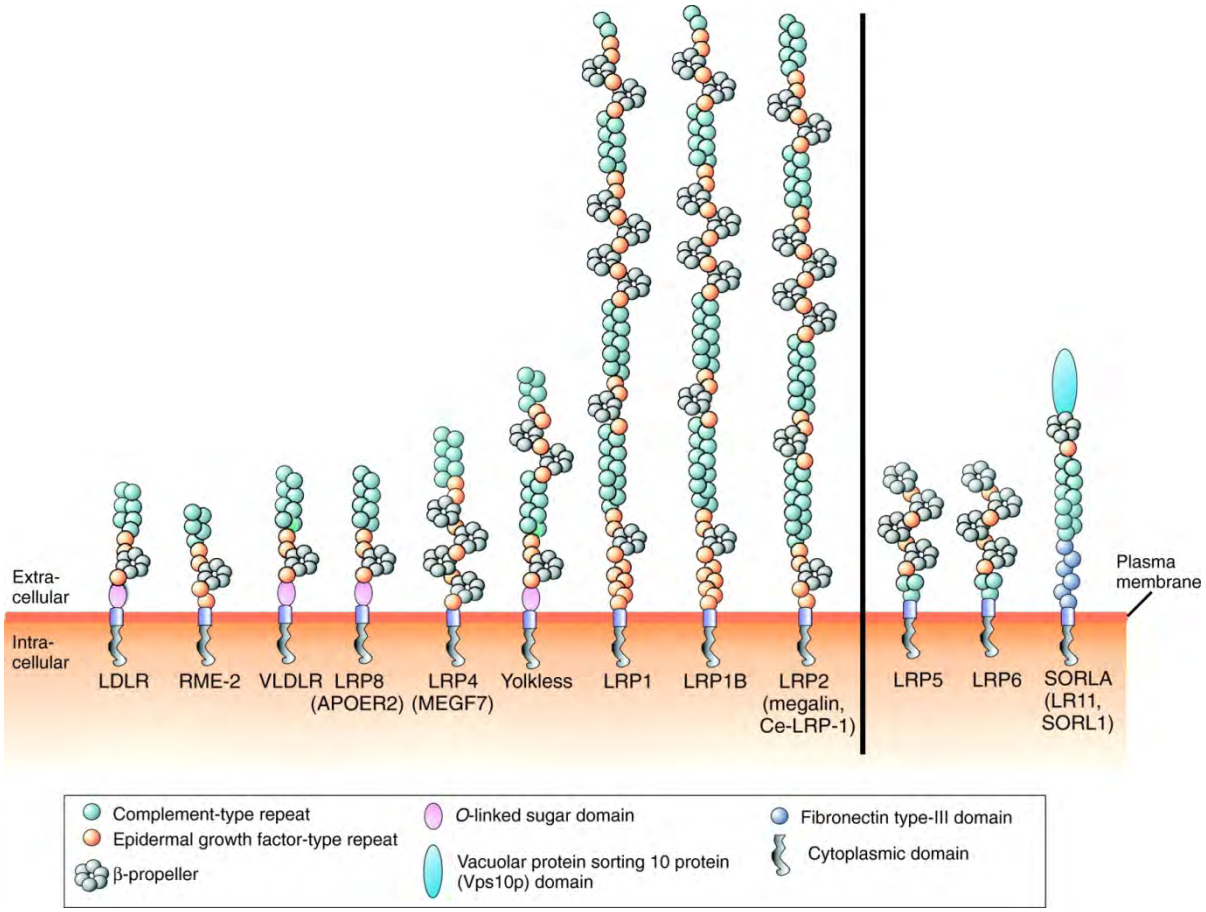

Figure 1.6: The LDL receptor gene family. The structural organization of the LDL receptor gene family is depicted. Receptors on the left are considered core members of the protein family. Receptors on the right are more distantly related. APOER2, apolipoprotein E receptor-2; Ce, *C. elegans*; LDLR, low-density lipoprotein receptor; LRP, LDL receptor-related protein; MEGF7, multiple epidermal growth factor-type repeat containing protein 7; RME-2, receptor-mediated endocytosis-2; SORLA, sortilin-related receptor with A-type repeats; VLDLR, very low- density lipoprotein receptor. (T. Willnow *et al*., 2007)

Two ligands, receptor associated protein (RAP) and the apolipoprotein (apo) E bind to all members of the LDL receptor gene family. ApoE has to associate with lipids or lipoproteins to be recognized by members of the LDL receptor gene family (R. Mahley *et al*., 1988). The binding of apoE on lipoproteins to the respective receptors results in the receptor-mediated removal from the circulation and plays an important role in regulation of the systemic lipid metabolism. RAP functions intracellularly as a molecular chaperone. It facilitates receptor folding in the endoplasmic reticulum and prevents premature ligand interaction with the receptors

during their trafficking through the secretory pathway (G. Bu, 1998). Because RAP inhibits ligand interaction with the receptors, the recombinant protein is commonly applied as a competitive inhibitor in receptor binding assays (G. Bu, 1998).

The prototype of the gene family is the LDL receptor that mediates cellular uptake of cholesterol-rich lipoproteins. Its significance for systemic cholesterol homeostasis is underscored by pathological features in patients with familial hypercholesterolemia caused by an inheritable LDL receptor gene defect, which results in the inability of affected individuals to clear cholesterol-rich lipoproteins from circulation (J. Goldstein *et al*., 2001).

Like the LDL receptor, other members also bind lipoproteins and mediate their uptake into cells. Therefore, a general role in regulation of lipoprotein metabolism had been anticipated for all receptors in the gene family. While this hypothesis could be confirmed for some (e.g., LRP1), recent findings revealed that most receptors not only bind lipoproteins, but many functionally diverse ligands including proteases, complexes of proteases and inhibitors, complexes of vitamins with carrier proteins, and extracellular signaling molecules (J. Herz *et al*., 2002). Intriguingly, the binding of different molecules to the LDL receptor-related proteins (LRPs) especially during development not only results in the uptake of the ligands but also influences many cellular activities, as will be discussed in the next section.

1.3.1 Multiple roles of the LDL receptor-related proteins during embryonic development

In mature organisms, members of the LDL receptor gene family mainly function as clearance receptors. In contrast, during embryonic development LRPs often act in signal transduction pathways. Consequently, mutations within these receptors in animal models (Tab. 1.1) and in humans (Tab 1.2) result in a variety of different phenotypes affecting the embryonic as well as the adult organism (reviewed in T. Willnow *et al*, 2007).

For example, disruption of the *Lrp1* gene in the mouse causes lethality of affected embryos around mid-gestation (J. Herz *et al*., 1993), a defect likely attributed to abnormal development of the liver (A. Roebroek *et al*., 2006).

Homozygous *Lrp4* (*Megf7*)-deficient mice have defects in late embryogenesis that affect limb formation and result in polysyndactyly caused by a malformed apical ectodermal ridge (AER), an important structure of the developing limb bud. The AER secretes several factors like FGFs, BMPs, wingless-related MMTV integration site proteins (WNTs), and SHH. The AER is required for the coordination of growth and patterning. It is possible that LRP4 suppresses canonical Wnt signaling during limb development (E. Johnson *et al*., 2005). In addition, it was reported that LRP4 is a functional receptor for agrin. Agrin is a motor neuron-derived ligand that stimulates MuSK, a receptor tyrosine kinase that is expressed in skeletal muscle. This interaction between motor neurons and muscle fibers plays a critical role in synaptic differentiation. It is hypothesized that LRP4 self-associates and forms an agrin-independent complex with MuSK. Agrin binding to LRP4 may alter the conformation of this complex, reorienting adjacent MuSK molecules and promoting *trans*-phosphorylation and stimulating synaptic differentiation (N. Kim *et al.*, 2008).

APOER2 and VLDLR act as cellular receptors for reelin. Reelin is a large extracellular protein, synthesized and secreted in the cerebral cortex. Binding of reelin to APOER2 and VLDL induces cytoplasmic Disabled homolog 1 (Dab1) phosphorylation, which in turn regulates neuronal migration (G. D'Arcangelo *et al*., 1999; T. Hiesberger *et al*., 1999).

LRP5 and LRP6 have been reported to bind WNT proteins and act as co-receptors for Frizzled (Fzd), the known WNT receptor. WNT signaling plays important roles during embryonic development such as axis formation and nervous system patterning. In the absence of Wnt stimulation, β-catenin is sequentially phosphorylated by casein kinase 1α (CK1) and glycogen synthase kinase 3 (GSK3) within a protein complex that is assembled by the scaffolding protein axin, and is thereby ubiquitinated and degraded. Upon Wnt stimulation, β-catenin phosphorylation and degradation are inhibited, resulting in accumulation of β-catenin and β-catenin-dependent transcriptional activation (H. Clevers, 2006; C. Logan *et al*., 2004). Binding of Wnt activates LRP6 by inducing GSK3 and CK1 mediated phosphorylation of the LRP6 intracellular domain (G. Davidson *et al*., 2005; X. Zeng *et al*., 2005). The phosphorylated LRP6 intracellular domain provides docking sites for axin (K. Tamai *et al*., 2004). The association of the axin complex with the phosphorylated LRP6 is believed to lead to inhibition of β-catenin phosphorylation and activation of β-catenin signaling (B. Mao *et al*., 2001).

These examples illustrate that LRPs are not only cargo receptors but also cell surface proteins with distinct functions in signal transduction pathways during embryonic development. Next, the specific role for LRP2 in the adult mouse and during development, as well as its implication in HPE will be described.

Receptor	Expression	Organism	Phenotype	References
LDL receptor	Vertebrates	Rabbit (Watanabe heritable hyperlipidemic, WHHL)	Hyper-cholesterolemia	(Tanzawa *et al*., 1980
		Mouse (targeted gene disruption)	Hyper-cholesterolemia	(Ishibashi *et al*., 1993)
VLDL receptor	Vertebrates	Mouse (targeted gene disruption)	Dysplastic cerebellum, reduced adipose tissue mass	(Trommsdorff *et al*., 1999)
		Chicken (restricted-ovulator	Impaired vitellogenesis, female sterility	(Bujo *et al*., 1995)
Yolkless	Insects	*Drosophila* (yolkless)	Impaired vitellogenesis, female sterility	(Schonbaum *et al*., 1995)
RME-2	Nematodes	*C. elegans* (rme-2 null)	Impaired yolk deposition, reduced embryonic viability	(Grant *et al*., 1999)
APOER2 (LRP8)	Vertebrates	Mouse (targeted gene disruption)	Dysplastic hippocampus and cerebellum	(Trommsdorff *et al*., 1999)
LRP4 (MEGF7)	Vertebrates	Mouse (targeted gene disruption)	Impaired limp formation, polysyndactyly, neuromuscular junction defects	(Johnson *et al*., 2005; Simon-Chazottes *et al*., 2006; Weatherbee *et al*., 2006);
		Cattle (mulefoot disease)	Syndactyly	(Drögemuller *et al*., 2007; Duchesne *et al*., 2006; Johnson *et al*., 2005)
LRP5	Vertebrates and insects	Mouse (target gene disruption)	Low bone mass, hypercholesterolemia, impaired insulin secretion	(Fujino *et al*., 2003; Kato *et al*., 2002)
LRP6	Vertebrates and insects	Mouse (targeted gene disruption)	Abnormal body axis	(Pinson *et al*.,2000)
		Xenopus (null mutant)	Impaired dorsal axis and neural crest formation	(Tamai *et al*., 2000)
		Drosophila (arrow null)	Inhibition of Wingless-dependent patterning	(Wherli et al., 2000)
LRP1	Vertebrates	Mouse (targeted gene disruption)	Embryonic lethality	(Herz *et al*., 1992; Roebroek *et al*., 2006)
LRP1B	Vertebrates	Mouse (target gene disruption)	Unknown	(Marschang *et al*., 2004)
LRP2 (*Ce*-LRP1)	Vertebrates and invertebrates	Mouse (targeted gene disruption)	Holoprosen-cephaly, impaired maturation of reproductive organs, renal dysfunction	(Willnow *et al*., 1996; Nykjaer *et al*., 1999; Hammes *et al*., 2005)
		Rat (induced autoimmune disease)	Glomerular nephritis (Heymann nephritis)	(Raychowdhury *et al*., 1989)

		C. elegans (ce-lrp1 null)	Molting defect, larval growth arrest	(Yochem *et al*., 1999)
SORLA (LR11; SORL1)	Vertebrates and invertebrates	Mouse (target gene disruption)	Alzheimer's disease	(Andersen *et al*., 2005)

Table 1.1: Loss of function models of the LDL receptor family. Highlighted receptors are those for which loss-of-function is associated with developmental defects. (T. Willnow *et al*., 2007)

Receptor	Mutation	Disease	References
LDL receptor	Loss-of-function (familial, autosomal dominant)	Familial hypercholesterolemia (impaired clearance of LDL)	(Goldstein *et al*., 2001)
VLDL receptor	Loss-of-function (familial, autosomal dominant)	Autosomal recessive cerebellar hypoplasia (ataxia, mental retardation)	(Boycott *et al*., 2005)
LRP5	Loss-of-function (familial, autosomal recessive)	Osteoporosis-pseudoglioma syndrome (reduced bone mass)	(Gong *et al*., 2001)
	Gain of function (familial, autosomal dominant)	High-bone-mass trait (increased osteogenic activity)	(Little *et al*., 2002)
LRP6	Missense mutation (familial autosomal dominant)	Autosomal dominant early coronary artery disease (hyperlipidemia, hypertension, diabetes)	(Mani *et al*., 2007)
LRP1B	Loss-of-function (sporadic)	Esophageal squamous cell carcinoma, non-small cell lung cancer	(Liu *et al*., 2000; Sonoda *et al*., 2004)
LRP2	Loss-of-function (autosomal recessive)	Donnai-Barrow syndrome (proteinuria, brain malformations, diaphragmatic hernia)	(Kantarci *et al*., 2007)
		Microform of HPE	(J. Rosenfeld *et al*., 2010)
SORLA	Polymorphisms (sporadic)	Alzheimer's disease	(Andersen *et al*., 2005; Lee *et al*., 2007; Rogaeva *et al*., 2007)

Table 1.2: Human diseases of the LDL receptor family (adapted and modified from T. Willnow *et al*., 2007)

1.4 LRP2

1.4.1 The structure of LRP2

LRP2 is the largest member of the LDL receptor gene family. The extracellular domain is composed of four clusters of cysteine-rich complement type repeats which are separated by 17 EGF repeats and 8 β-propellers (YWTD-containing domains) (Figure 1.7). The intracellular domain contains two NPxY-motifs and one NPxY-like motif, which are important for internalization and receptor sorting. The receptor intracellular domain also contains one potential SH2-binding domain, one dileucine repeat (important for endocytosis), four potential SH3-domain binding sites, several potential PKC-phosphorylation sites, as well as a PDZ-binding motif.

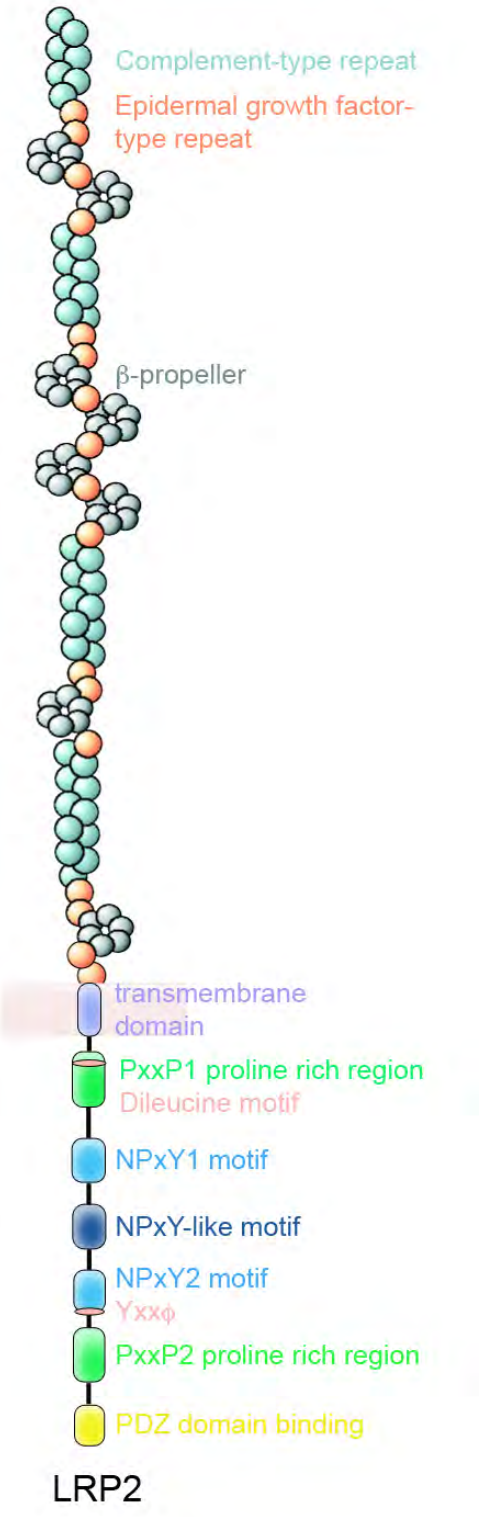

Figure 1.7: Structure of LRP2. The extracellular domain is composed of clusters of four complement-type repeats separated by EGF repeats and β-propellers. The intracellular domain contains 2 proline rich regions, 2 NPxY motifs and 1 NPxY-like motif as well as a PDZ binding domain, a dileucine motif and an Yxxϕ motif.

1.4.2 Expression pattern of LRP2

In the adult mouse, LRP2 is expressed in a variety of polarized epithelia where it facilitates transfer of ligands across compartments. Primarily, LRP2 is found in proximal tubule cells in the kidney and in type II pneumocytes and Clara cells in the lung. To a lesser extent, expression is also found in ependymal cells in the brain, in the epididymis, in the uterus, oviduct and inner ear as well as in the mammary epithelia, thyroid follicular cells and the ciliary body of the eye (G. Zheng *et al*., 1994; Kounnas *et al*., 1994; S. Lundgren *et al*., 1997; O. Van Praet *et al*., 2003; S. Argraves *et al*., 2004).

During embryonic development LRP2 expression is first evident at E3.5 in the primitive endoderm (PrE) (F. Gerbe *et al*., 2008). These cells will line the blastocoel cavitiy and will give rise to extraembryonic endoderm, which forms the yolk sac. At E6.0, LRP2 is additionally expressed in the developing neuroectoderm (C. Drake *et al*., 2004). At later embryonic stages it can be found most prominently in the choroid plexus, ependyma, metanephric tubules, ear, thyroid, pericardium, and intestine (M. Kounnas *et al*., 1994).

1.4.3 The role of LRP2 in adult mice

LRP2 is a multifunctional clearance receptor that binds a set of diverse ligands. These ligands represent three major classes of molecules: (1) proteases and protease/inhibitor complexes, (2) lipoproteins, and (3) vitamins or hormones bound to carrier proteins (reviewed in E. Christensen *et al*., 1995).

Similar to the clearance of cholesterol via lipoproteins, LRP2 also mediates the uptake of carrier-bound steroids. In contrast to the precursor cholesterol, cholesterol-derived steroid hormones such as vitamin D metabolites, sex steroids and glucocorticoids are not transported by lipoprotein particles but by specific plasma proteins in the circulation.

In the renal proximal tubules in the kidney, LRP2 is one of the most important receptors for protein reabsorption. The receptor is expressed on the brush border surface of proximal tubules facing the glomerular filtrate (R. Orlando *et al*., 1993; E. Christensen *et al*., 1995). Main ligands reabsorbed by LRP2 from the primary urine are 25-(OH) vitamin D_3 bound to its plasma carrier vitamin D-binding protein (DBP)

(A. Nykjaer *et al*., 1999), retinol (vitamin A) complexed with the retinol-binding protein (E. Christensen *et al*., 1999) and vitamin B_{12} bound to the carrier transcobalamin (H. Birn *et al*., 2002),

The physiological relevance of LRP2 in retrieval of filtered metabolites is best described for 25-(OH) vitamin D_3, the main vitamin D metabolite present in the circulation. 25-(OH) vitamin D_3 is an inactive precursor that needs to be converted into 1,25-$(OH)_2$ vitamin D_3, the active hormone that regulates the systemic calcium homeostasis. Conversion of 25-(OH) vitamin D_3 into 1,25-$(OH)_2$ vitamin D_3 takes place in the renal proximal tubules. Receptor-mediated uptake of 25-(OH) vitamin D_3/DBP complexes by LRP2 from the lumen of the renal tubules prevents urinary excretion of the metabolites and delivers them to the cells, where the precursor is converted into the active hormone (A. Brown *et al*., 1999). The physiological relevance of LRP2 for renal reabsorption processes is underscored by the phenotypes seen in mice with induced receptor gene defects. *Lrp2*$^{-/-}$ mice suffer from low-molecular-weight proteinuria. As a consequence of the inability to retrieve 25-(OH) vitamin D_3/DBP complexes from the primary urine, plasma levels of 25-(OH) vitamin D_3/DBP and 1,25-$(OH)_2$ vitamin D_3 are decreased, resulting in plasma vitamin D deficiency and in bone calcification defects (J. Hilpert *et al*., 2002; J. Leheste *et al*., 2003; A. Nykjaer *et al*., 1999).

In several tissues, like in renal proximal tubules, LRP2 is co-expressed with the receptor cubilin. Cubilin is unusual inasmuch as this endocytic receptor lacks a cytoplasmic as well as a transmembrane domain. Rather, the amino-terminal region of LRP2 attaches cubilin to the plasma membrane (M. Kristiansen *et al*., 1999). Thus, LRP2 and cubilin form a dual-receptor complex, where cubilin also binds ligands, but endocytosis is mediated by LRP2. This co-receptor complex was shown not only to bind DBP (A. Nykjaer *et al*., 1999) but also albumin (H. Birn *et al*., 2000) and transferrin (R. Kozyraki *et al*., 2001). Patients with defects in the cubilin gene also exhibit low-molecular-weight proteinuria and excrete ligand/carrier complexes such as 25-(OH) vitamin D_3/DBP (A. Nykjaer *et al*., 2001).

Recycling of the two receptors LRP2 and cubilin requires Disabled-2 (Dab2), a cytoplasmic adaptor for LRP2. The interaction between Dab2 and the intracellular domain of LRP2 regulates endocytosis of the receptor, as Dab2 binds to the cytoplasmic domain of LRP2 and the clathrin adaptor protein adaptin to promote efficient endocytosis of LRP2 and its ligands. Lack of Dab2 expression results in

impaired tubular endocytosis and in excretion of DBP in mutant mice (S. Morris *et al*., 2002).

In the kidney, LRP2 also mediates lysosomal degradation of parathyroid hormone (PTH) (J. Hilpert *et al*., 1999). When PTH binds to its receptor, which is also expressed on the tubular surface, the activity of the receptor increases calcium levels in the blood circulation. PTH binding to LRP2 counteracts the activity of the PTH receptor and therefore plays a role in regulating calcium homeostasis (J. Hilpert *et al*., 1999).

As described above, LRP2 is the first receptor described to mediate endocytic uptake of steroid hormones (here vitamin D metabolites in the kidney). This uptake pathway contrasts with the dogma posed by the free hormone hypothesis that steroid hormones solely enter target cells by unspecific diffusion through the plasma membrane. Intriguingly, LRP2 is also expressed in a number of other steroid-responsive tissues in the adult organism, in particular in the male and female reproductive organs (epididymis, ovaries, uterus) (G. Zheng *et al*., 1994). This observation suggests that the receptor-mediated uptake of steroids may not be restricted to vitamin D_3 metabolites in the kidney but extend to the uptake of sex steroid hormones in reproductive organs. This hypothesis was recently confirmed by analysis of *Lrp2*$^{-/-}$ mice. Apart from bone disease as a consequence of hypovitaminosis D (A. Nykjaer *et al*., 1999), adult *Lrp2*$^{-/-}$ mice suffer from anomalies in genital maturation consistent with insensitivity to androgens and estrogens (A. Hammes *et al*., 2005). *Lrp2*$^{-/-}$ female mice fail to induce opening of the vagina cavity during puberty. *Lrp2*$^{-/-}$ males suffer from testicular maldescent (cryptorchidism). The underlying defect is a failure in inducing regression of the cranial suspensory ligament (CSL) which normally ensures the descent of the testis to the bladder neck and finally into the scrotum. The CSL tethers the gonads to the dorsal body wall in the early embryo and normally dissolves in males during later embryonic development (from E14.5 onwards) upon androgen induction. In the absence of androgens, as in females, the CSL resides, fixing the ovaries in a position close to the caudal pole of the kidney. Regression of the CSL could not be rescued in *Lrp2*$^{-/-}$ embryos by giving exogenous androgens, indicating an insensitivity to sex steroids as the cause of the defects observed in this mouse model. The ability of LRP2 to endocytose androgens and estrogens bound to carrier proteins was also confirmed in cell culture experiments (A. Hammes *et al*., 2005).

1.4.4 The role of LRP2 during embryonic development

The group of Thomas Willnow demonstrated in previous experiments a critical role for LRP2 in embryonic development. Loss of receptor expression in LRP2-deficient mice results in forebrain abnormalities with conditions associated with HPE. Loss of LRP2 leads to impaired separation of the developing forebrain hemispheres along the midline resulting in enlarged and fused lateral ventricles. In addition, facial abnormalities such as a shortened snout and ocular abnormalities can be observed in LRP2 mutant mice at E18.5 (T. Willnow *et al*., 1996) (Figure 1.8 A + B). In coronal sections of E18.5 LRP2 mutant mice, enlarged brain ventricles are visible compared with proper developed brain ventricles in the control mice (Figure 1.8 C + D). The ventricular system can even fuse to a holosphere as demonstrated in horizontal sections of *Lrp2*$^{-/-}$ mouse brains at E18.5 compared with *Lrp2*$^{+/+}$ mouse brains (Figure 1.8 E + F). The onset of the HPE phenotype becomes evident as early as mid-gestation. LRP2-deficient embryos at E10.5 show much smaller telencephalic vesicles and clearly impaired subdivision of the forebrain hemispheres. (Figure 1.8 G + H). The neuroepithelial wall thickness in the rostral forebrain is reduced in *Lrp2*$^{-/-}$ embryos compared with wild type embryos (T. Willnow *et al*., 1996; R. Spoelgen *et al*., 2005). Most of the embryos homozygous for the gene defect on C57/Bl6 x 129SVEmcTer background die shortly after birth probably due to respiratory insufficiency (T. Willnow *et al*., 1996).

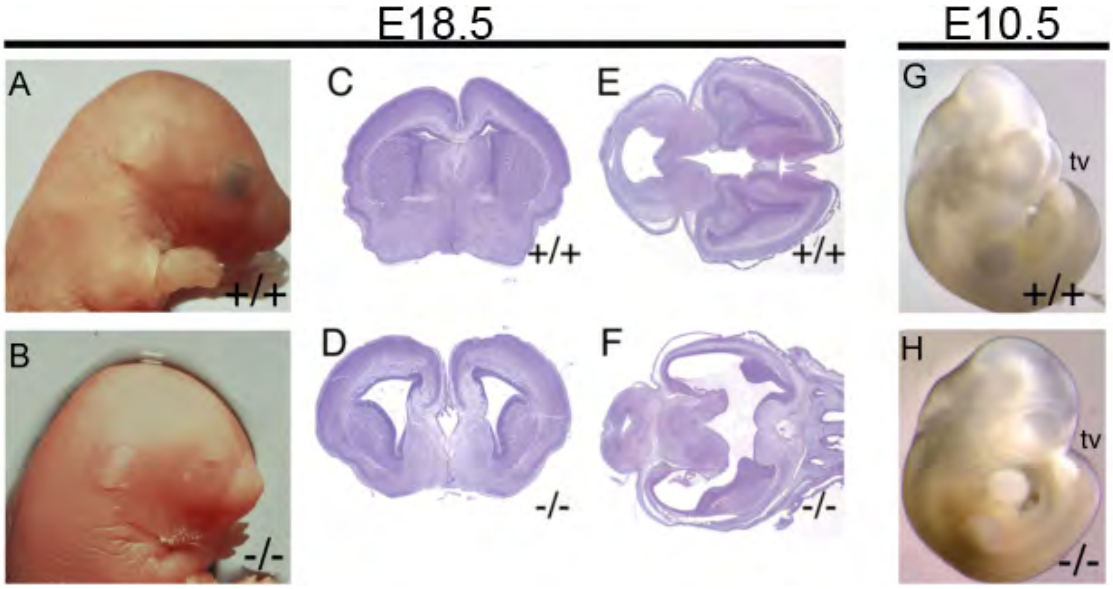

Figure 1.8: Neuroanatomy of LRP2-deficient neonates and embryos. (A, B) Cranio-facial abnormalities, including smaller eyes and a shorter snout in *Lrp2*$^{-/-}$ neonates in comparison to the wild type control. (C, D) Coronal H+E stained sections through the rostral brain of E18.5 embryos, demonstrating enlarged ventricles in the LRP2-deficient mice. (E, F) Horizontal sections through the rostral brain of E18.5 embryos, depicting a fused brain ventricular system forming a holosphere in *Lrp2*$^{-/-}$ mice in comparison to control mice. (G, H) Lateral view of E10.5 *Lrp2*$^{-/-}$ and *Lrp2*$^{+/+}$ embryos, showing reduced telencephalic vesicles (tv) in the LRP2-deficient embryo in comparison to the control. (Adapted from R. Spoelgen *et al*., 2005)

Analyzing the forebrain abnormalities in detail, it was shown that LRP2 deficiency in the early neuroepithelium leads to changes in the expression and activity of the three key morphogens in forebrain patterning, BMP4, SHH, and FGF8 (Figure 1.9) (R. Spoelgen *et al*., 2005). LRP2 deficiency leads to an increase in *Bmp4* expression in the rostral dorsal neuroepithelium, weaker and dorsally shifted *Fgf8* expression and loss of *Shh* expression in the ventral telencephalon (Figure 1.9).

These findings identify LRP2 as an important factor for proper forebrain patterning. In the following chapter potential mechanisms of LRP2 function in the correct establishment of morphogen gradients during development will be described.

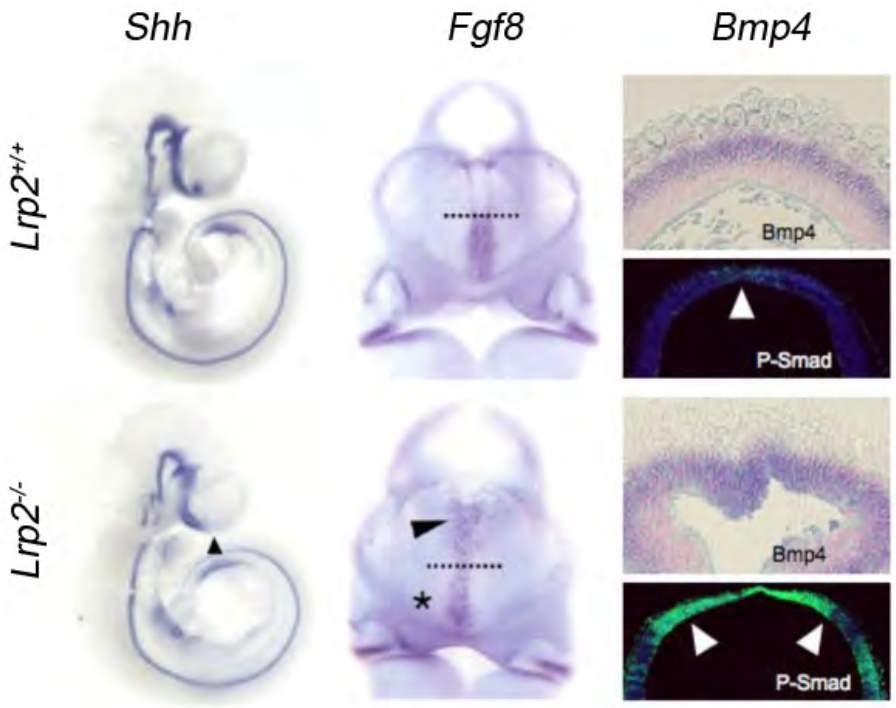

Figure 1.9: Analysis of *Shh*, *Fgf8,* and *Bmp4* expression and pathways in E10.5 embryos. (*Shh*) Lateral view of whole-mount ISH for *Shh*, indicating expression in preoptic area of *Lrp2*$^{+/+}$ embryos but not in *Lrp2*$^{-/-}$ embryos (arrowhead). (*Fgf8*) A frontal view of the head demonstrates a reduction of *Fgf8* expression in the ventral telencephalon (asterisk) and an extension from the commissural plate (dotted line) into more dorsal regions of the midline (arrowhead) in *Lrp2*$^{-/-}$ embryos. (*Bmp4*) Coronal sections highlight increased *Bmp4* expression in the dorsal telencephalon in *Lrp2*$^{-/-}$ embryos, and consequently higher levels of phospho-Smad, a mediator of BMP4 signaling. (Adapted from R. Spoelgen *et al*., 2005)

1.4.5 Possible signaling functions of LRP2 during development

As described above, LRP2 can bind many ligands, two of which may be particularly relevant for a role of this receptor in forebrain patterning, namely BMP4 and SHH.

A role for LRP2 in regulation of the BMP pathways is supported by data obtained from BIAcore assays, where our lab demonstrated specific binding of BMP4 to LRP2, while the related factor BMP5 did not bind (R. Spoelgen *et al*., 2005). In this scenario, LRP2 may act as a clearance receptor and restrict the BMP4 gradient to dorsal regions in the developing neural tube. Loss of receptor in mutant mice may result in enhanced and ventrally extended BMP4 signals, secondarily repressing

Shh. Additional support for the hypothesis that LRP2 acts as a clearance receptor for BMP4 comes from a recent study by our group. In this study the important role of LRP2 during adult neurogenesis was investigated (C. Gajera *et al*., 2010). It was demonstrated that loss of LRP2 activity results in increased activity of the BMP2/4 pathway in the subependymal zone (SEZ) in the adult mouse brain, a tissue that normally expresses this receptor.

An alternative hypothesis on how LRP2 may affect morphogen gradient formation and signaling in the forebrain came from a study in which it was shown that SHH-N binds to LRP2 (R. McCarthy *et al*., 2002). In this study, the lab of Scott Argraves demonstrated direct binding of SHH-N to LRP2 *in vitro* in BIAcore assays and in cell culture. In cell culture, McCarthy *et al.* also demonstrated the binding of SHH-N to LRP2 in BN16 cells but also LRP2 mediated endocytosis of SHH-N. Similar to the internalization of thyroglobulin, the transcobalamin-vitamin B_{12} complex, and the retinol-binding protein complex by LRP2, internalized SHH-N seemed to bypass lysosomal degradation, probably because the LRP2-SHH-N interaction is resistant to dissociation at low pH. Rather, receptor-mediated uptake is believed to target SHH-N to specific cellular compartments or to the basolateral surface for release, a process proposed to extend the signaling range of the morphogen (R. McCarthy *et al*., 2003). Recently, a potential role for LRP2 as SHH-N receptor was substantiated *in vivo* by the same lab (C. Morales *et al*., 2006). In this study, the authors showed that endocytosis of SHH-N by LRP2 in efferent duct epithelial cells of the epididymis leads to lysosomal degradation. This process is supposed to shape the gradient of SHH *in vivo* and is different to the internalization of SHH-N in endoderm-like cells, where the same investigators showed in their earlier study that SHH-N internalized by LRP2 is not degraded in lysosomes. Trafficking of SHH-N internalized via LRP2 is therefore differentially regulated in diverse cell types and needs further investigation concerning its role in gradient formation and delivery to Patched1 for signaling. In this scenario, loss of LRP2 activity in mutant mice may result in loss of ventral SHH activity and in subsequent extension of BMP4 signals in the dorsal neural tube.

Regardless of whether LRP2 may act as a receptor for BMP4 and/or SHH-N, independent studies in mice and in nematodes suggest the intriguing possibility that the intracellular domain of LRP2 might have a role in signaling activity. This

hypothesis is supported by a study on the *Caenorhabditis elegans* homolog of LRP2, *Ce*-LRP-1 (A. Grigorenko *et al*., 2004). In this study, the authors showed that expression of the soluble cytoplasmic *Ce*-LRP-1 domain partially rescues the molting defects induced by RNAi mediated knockdown of *Ce-Imp-2*. *Ce*-IMP-2 is a presenilin-related intramembrane protease involved in regulated intramembrane proteolysis (RIP) of surface receptors.

Recently, regulated intramembrane proteolysis (RIP) has been described as a novel but highly conserved mechanism in cell signaling (M. Brown *et al*., 2000; S. Urban *et al*., 2002). In this proteolytic processing event, the cytoplasmic domain of type-I transmembrane proteins is released from the membrane. RIP processing usually requires two sequential proteolytic events, carried out by distinct proteases. The first cleavage can occur in the lumen of the endoplasmic reticulum (ER), in a post-ER compartment or at the cell surface (M. Brown *et al*., 2000; R. Rawson, 2002; M. Medina *et al*., 2003). This initial ectodomain-shedding event is typically performed by proteases of the ADAM (a disintegrin and metalloprotease) family (C. Blobel, 2000; T. Tousseyn, 2006). It is reported that extracellular calcium influx or protein kinase C activators induce ectodomain shedding by activating membrane-associated metalloproteinases (S. Dethlefsen *et al*., 1998; U. Steinhusen *et al*., 2001; P. May *et al*., 2002; R. Carey *et al*., 2005; J. Cowan *et al*., 2005). Additionally, specific ligands can induce the ectodomain proteolysis of type-I membrane receptors at the cell surface, an essential step in controlling the function of these receptors (Y. Kawano *et al*., 2000; J. Mumm *et al*., 2000; W. Zhou *et al*., 2000). This initial cleavage event shortens the ectodomain, allowing the second cleavage event to take place. The second cleavage is intramembranous and is mediated by the γ-secretase protease complex, which releases the active cytoplasmic domain of the cleaved receptors.

Evidence for RIP of LRP2 has been provided before. Zou and colleagues demonstrated γ-secretase activity in the brush border of rat kidney, where also LRP2 is localized. Furthermore, they identified the extracellular domain of LRP2 on the microvillar surface, while the cytosolic domain was found in the dense apical tubules and coated pits, suggesting that LRP2 in rat kidney undergoes RIP including metalloprotease-mediated ectodomain shedding and γ-secretase-mediated intramembrane proteolysis (Figure 1.10) (Z. Zou *et al*., 2004).

A few years later, the same lab showed that the membrane-bound LRP2 COOH-terminal fragment (MCTF), stably expressed in opossum kidney proximal

tubule cells (OKP), was constitutively processed by γ-secretase. The transfected MCTF as well as the transfected soluble LRP2 intracellular domain (MICD) in OKP cells mediated the reduction of *Lrp2* expression itself and of the *Na^+/H^+ exchanger* (*Nhe3*) (Y. Li *et al*., 2008). These studies support evidence for a potential role of the LRP2 ICD in signaling. Whether or not this activity has any relevance for the function of the receptor in forebrain development was unclear.

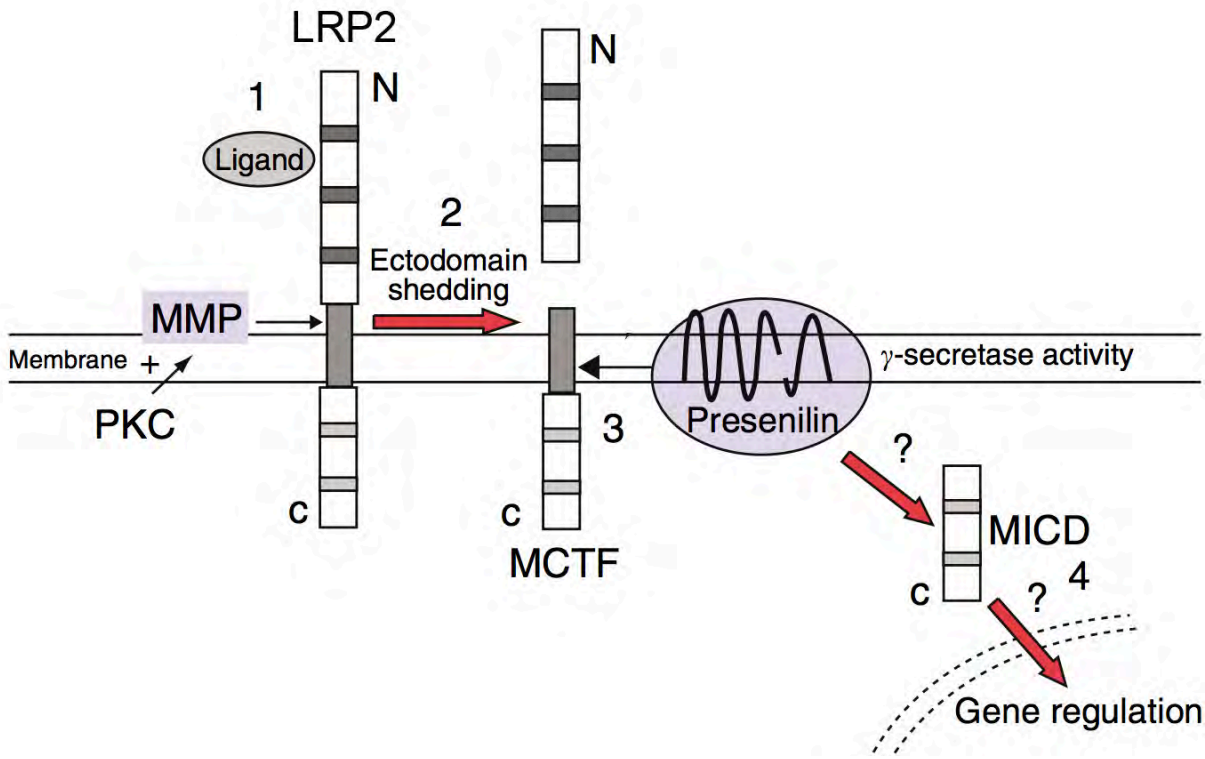

Figure 1.10: Proposed model of the LRP2 signaling pathway. Metalloprotease (MMP) activity, activated by ligand binding (1) and regulated by protein kinase C, results in ectodomain shedding (2) of LRP2, producing a membrane bound C-terminal fragment of the receptor (MCTF). MCTF is substrate for γ-secretase activity in the membrane. The soluble C-terminal intracellular domain of LRP2 (MICD) is released into the cytosol (3). The intracellular domain of LRP2 may translocate to the nucleus where it acts as a transcriptional regulator (4). (Adapted from D. Biemesderfer, 2006)

2. Aim

Defects in early forebrain development lead to a fatal disorder, defined as HPE, in which the cerebral hemispheres fail to separate along the midline due to defects in midline induction. HPE is the most common forebrain malformation in human embryos. LRP2, a member of the LDLR gene family, is a candidate gene for HPE in humans and mice. Recent studies in mice have identified the receptor as a novel genetic factor that affects dorsal midline separation and ventral neuronal cell fate specification in the developing forebrain. LRP2-deficient mouse embryos are characterized by an imbalance of dorsal and ventral morphogen pathways that critically regulate patterning of the neural tube.

The aim of my project was to characterize the molecular mechanisms underlying the function of LRP2 in early forebrain development and the reasons for patterning defects and HPE in receptor-deficient mice. In particular, I aimed at substantiating current hypotheses proposing a role for the receptor in BMP4 and SHH morphogen gradient formation and signaling. In addition, I investigated a possible function of the intracellular domain of LRP2 (ICD) in signaling pathways controlling forebrain patterning. From these studies I hoped to gain insight on an important novel pathway, that is crucial for normal brain development and that, when altered, results in neurodevelopmental disorders in patients.

3. Material & Methods

3.1 Animal Experiments

3.1.1 Mouse Husbandry

Mice were kept at standard conditions according to the German animal protection act. The wild type mice used in this study were of a mixed genetic background (*129SvEmcTer and C57BL/6N*).

The generation of *Lrp2*$^{-/-}$ mice has been described before (T. Willnow *et al*., 1996). The role for LRP2 during forebrain development was analyzed in receptor-deficient embryos and somite-matched control littermates (*Lrp2*$^{+/+}$ or *Lrp2*$^{+/-}$) on a hybrid (*129SvEmcTer x C57BL/6N*) background.

The generation of *Lrp2*$^{+/TglCD}$ mice is described in the result part 4.1.1 of this study. A role for the ICD of LRP2 was analyzed in mice heterozygous for the transgene and in age-matched control littermates on a hybrid (*129SvEmcTer x C57BL/6N*) background. In the meanwhile the mouse line was also backcrossed on a pure *C57BL/6N* background.

Timed matings were set up in the evening to obtain embryos at different stages of development. The presence of a vaginal plug in the morning was considered as day E0.5 (embryonic day). Embryos were harvested by sacrificing pregnant mice according to the German animal protection act, staged by counting the somites and further processed.

3.2 Microbiological Methods

3.2.1 Culture media

Medium	Composition
LB	10 g/l bacto-tryptone, 5 g/l bacto-yeast extract, 10 g/l NaCl; pH 7.2
SOC	20 g/l bacto-peptone, 5 g/l bacto-yeast extract, 0.5 g/l NaCl, 0.17 g/l KCl, 0.95 g/l MgCl2, 3.6 g/l glucose; pH 7.0
LB-Agar	LB-medium containing 15 g/l agar

3.2.2 Transformation of bacteria with DNA

Electro-competent *E. coli* XL1Blue or DH5α cells were transformed with purified plasmid DNA or directly with DNA-ligation reactions. An aliquot of electro-competent XL1Blue or DH5α cells was thawed on ice. 10 ng of plasmid DNA (or 2 µl of the ligation reaction) were mixed with 40 µl of electro-competent XL1Blue or DH5α cell suspension and electroporated at 1.8 kV.

The cell suspension was transferred from the cuvette to a 2.0 ml tube, mixed with 1 ml of SOC medium and incubated at 37°C for 30 min. Cells were then collected (2500 x g; 5 min; RT) and re-suspended in 100 µl of LB medium and plated on a LB agar plate containing the appropriate selective agent.

3.2.3 Preparation of GST-SHH-N protein

A single colony of BL21 cells containing pSh1-GSTK (kindly provided by Jeremy Barth, Argraves lab, (R. McCarthy *et al*., 2002)) was used to inoculate 50 ml LB-medium with 100 µg/ml ampicillin (Biomol, Germany) and incubated overnight at

37°C. The next day the culture was diluted 1:100 into 1 l fresh pre-warmed LB-medium containing 100 µg/ml ampicillin and was grown at 37°C until the OD A_{600} reached 0.5. Then 500 µl of 20% IPTG was added in 1 l and incubated additionally 5 hrs at 25°C. Afterwards the culture was centrifuged at 2500 x g for 15 min at 4°C. The pellet was completely re-suspended in 10 ml of ice-cold GST-sonication buffer (15% sucrose, 50 mM Tris, 50 mM EDTA, 1 mM PMSF, 0.1% lysozyme, pH 8.0). Finally 10 ml of GST-sonication buffer was added and the re-suspended cells were incubated on ice for 30 min. Then 1/20 of 10% Triton X-100 was added and the cells were stirred. Afterwards the cells were sonicated on ice for 3 min in short bursts. After centrifugation at 12000 x g for 30 min at 4°C the supernatant was filtered and DTT was added to a final concentration of 1 mM. At the end 4 volumes of buffer A (10 mM Tris, 1 mM PMSF, 150 mM NaCl, 1 mM DTT, pH 7.5) were added and the protein solution was ready to be filtered over the glutathion-agarose column from Sigma-Aldrich (G4510).

For this 350 mg of the lyophilized powder were re-constituted in 50 ml deionized H_2O overnight at 4°C. In the next step the column was washed with 10 volumes of H_2O and then with buffer A. Finally the protein solution was added to the column. Affinity chromatography was performed, by using the Biologic LP chromatography system (Bio Rad). After the column was washed with 190–350 ml buffer B (10 mM Tris, 150 mM NaCl, pH 7.5), the protein of interest was eluted using 350-400 ml buffer E (10 mM Tris, 25 mM glutathion, 150 mM NaCl, pH 7.5). The different fractions from the elution were tested in SDS-PAGE and coomassie-staining. Fractions of interest were dialyzed in 1 l dialysis buffer (150 mM NaCl, 10 mM Tris, 2 mM $CaCl_2$, 2 mM $MgCl_2$, pH 7.5 – 7.8) overnight at 4°C.

3.2.4 Cryopreservation of bacteria

1 ml of an overnight culture of *E. coli* XL1Blue or DH5α was mixed with 1 ml of 100% glycerol and immediately frozen at -80°C.

3.3 Molecular biology methods

3.3.1 Isolation of plasmid DNA from bacteria

5 ml of LB medium were inoculated with a single colony of *E. coli* XL1Blue or DH5α picked from a LB agar plate containing the appropriate selection marker. The LB culture was grown overnight at 37°C with vigorous shaking. The next day the cells were harvested by centrifugation (14000 x g; 5 min; RT). The pellet was re-suspended in resuspension buffer (50 mM Tris-HCl, 10 mM EDTA, 100 µg/ml RNase A; pH 8.0) and subsequently lysed by adding an equal volume of lysis buffer (200 mM NaOH, 1% SDS (w/v)). The solution was mixed cautiously with an equal volume of neutralization buffer (3.0 M K-acetate; pH 5.5) and incubated on ice for 15 min. Cellular debris and genomic DNA were removed by centrifugation of the solution (14000 x g; 20 min; 4°C). The supernatant containing the plasmid DNA was transferred to a new reaction tube and the DNA collected by adding 10 % volume of 3 M LiCl and 2.5 volume of 100% isopropanol followed by centrifugation (14000 x g, 30 min, 4°C). The pellet was washed once with 70 % ethanol and re-suspended in 50 µl of sterile water. The purified plasmid DNA was stored at -20°C.

3.3.2 Isolation of genomic DNA from tissue samples

Tissue for isolating genomic DNA was obtained by subjecting adult mice to a tail biopsy. Yolk sac tissue was used to isolate DNA for genotyping mouse embryos. DNA was isolated by incubating the tissue with proteinase K in tail buffer (10 mM Tris-HCl, 0.3 M Na-Acetate, 0.1 mM EDTA, 1% SDS (w/v); pH 7.0) at a final concentration of 0.5 mg/ml overnight at 52°C. Proteins were removed by extracting with an equal volume of phenol/chloroform/isoamylalcohol (25:24:1) followed by centrifugation (14000 x g; 5 min; RT) to separate the phases. The upper, aqueous DNA containing phase was mixed with 2.5 volumes of 100% ethanol. The precipitate was collected by centrifugation (14000 x g, 10 min, 4°C) washed once with 70%

ethanol and re-dissolved in TE-buffer (10 mM Tris-HCl, 1 mM EDTA; pH 8.0). Isolated genomic DNA was stored at 4°C.

3.3.3 Isolation of total RNA from tissue samples

Total RNA was isolated with the TRIZOL® reagent from Invitrogen, USA. Tissue samples were homogenized in 1 ml of TRIZOL® reagent per 50-100 mg of tissue and incubated for 5 min at RT. 0.2 ml of chloroform were added to the homogenate per 1 ml of TRIZOL® reagent. Samples were shaken vigorously by hand for 15 seconds and incubated at RT for 3 min. The phases were separated by centrifugation (12000 x g; 15 min; RT). Following centrifugation, the upper aqueous phase was transferred to a fresh tube and precipitated by adding 0.5 ml of isopropanol per 1 ml of TRIZOL®. The RNA was collected by centrifugation (12000 x g, 10 min, 4°C) and washed once with 1 ml of 70% ethanol per 1 ml TRIZOL®. The pellet was air-dried for 5-10 min, re-dissolved in RNase-free water and stored at -80°C. For TaqMan® experiments the RNA was re-dissolved and incubated with DNase I for 20 min at 37°C (100 µg total RNA were incubated with 10 Units DNase I from Ambion). Finally the RNA was purified using the RNeasy Mini Kit from Qiagen, Germany according to the manufacturers instructions.

3.3.4 DNA and RNA concentration determination

The concentration of DNA and RNA samples was determined spectrophotometrically at a wavelength of 260 nm (OD260) since the concentration of DNA and RNA is a direct function of the optical density at this wavelength. For DNA, an OD260 of 1.0 equals a concentration of 50 µg/ml of double stranded DNA, for RNA an OD260 of 1.0 equals a concentration of 40 µg/ml of RNA.

DNA quality measurement was done, by measuring the OD280, because proteins absorb UV-light maximally at this wavelength. Pure DNA solutions have an OD260:OD280 ratio of 1.8. A lower ratio indicated contamination of the sample with proteins.

Riboprobes were measured using the NanoDrop® ND-1000 spectrophotometer. 1 µl of RNA solution was used to measure RNA concentration, utilizing optic fiber connectors.

3.3.5 Enzymatic digest of DNA

The appropriate amount of DNA was incubated with the corresponding restriction enzyme(s) and buffer at a ratio of 0.5 U enzyme/µg DNA. The digest was incubated at 37°C for 2 hrs to overnight. All restriction enzymes were obtained from New England Biolabs, USA. After incubation, the digest was either column purified or subjected to gel electrophoresis to isolate the fragment of interest.

3.3.6 Agarose gel electrophoresis of DNA and RNA

DNA and RNA fragments were separated according to their molecular weight on 0.8-2.0% agarose gels in TAE buffer (40 mM Tris, 1 mM EDTA, 20 mM glacial acetic acid, pH 8.0). Ethidium bromide was added to the gel at a final concentration of 0.5 µg/ml to facilitate visualization of the DNA or RNA fragments after electrophoresis.

3.3.7 Isolation of DNA from agarose gels

Polymerase chain reaction (PCR) products or DNA digests were separated by length on 0.8-1.2% agarose gels containing ethidium bromide. By exposing the agarose gel to UV-light, the DNA was visualized and bands of interest were cut from the gel. The DNA was extracted using the High Pure PCR Product Purification Kit from Roche, Switzerland. The gel slice was incubated with binding buffer (3 M guanidine-thiocyanate, 10 mM Tris-HCl, 5% ethanol (v/v); pH 6.6) at a ratio of 300 µl buffer/100 mg agarose at 52°C until the gel slice was completely dissolved. The sample was transferred to a filter column and subjected to centrifugation (14000 x g, 1 min, RT). The filter column was washed two times with 500 µl washing buffer (2

mM Tris-HCl, 20 mM NaCl, 80% ethanol (v/v); pH 7.5) and the DNA was eluted with 50 µl elution buffer (10 mM Tris-HCl; pH 8.5) and stored at -20°C.

3.3.8 Ligation of PCR-products in the pGEM-T® Easy Vector

Ligation of PCR products with the pGEM-T® Easy Vector (Promega, USA) was done according to the manufacturers instructions: 5-10 ng of the PCR-product or digested DNA were incubated with 5 µl 2X Rapid Ligation Buffer, 15 ng of pGEM-T Easy vector and 3 U of T4 DNA-ligase. The volume of the reaction setup was adjusted to 10 µl with H_2O and incubated at 16°C overnight. The next day 2 µl of the ligation reaction was used to transform electro-competent *E. coli* Xl1Blue or DH5α.

3.3.9 Ligation of a DNA-fragment in a target vector

50 ng of vector DNA were mixed with the appropriate amount of insert DNA according to the equation:

$$mass_{insert}(ng) = 5 \times mass_{vector}(ng) \times length_{insert}(bp) / length_{vector}(bp)$$

After addition of 2 µl ligation buffer (400 mM Tris-HCl, 100mM MgCl2, 100 mM DTT, 5 mM ATP, pH 7.8), 1 U of T4 DNA ligase (Fermentas, Germany) and water to a final volume of 10 µl, the mixture was incubated at 16°C overnight. The next day, 2 µl of the ligation reaction were used to transform electro-competent *E. coli* Xl1Blue or DH5α.

3.3.10 Polymerase chain reaction (PCR)

PCR reaction using Taq DNA polymerase from Invitrogen:

The following components were added to a 0.5-ml microcentrifuge tube on ice:

DNA:	50-100 ng
dNTPs:	0.2 mM
forward primer:	0.2 µM
reverse primer:	0.2 µM
PCR buffer (200 mM Tris-HCl, 500 mM KCl, pH 8.4):	1x
MgCl2:	1.5 mM
water :	not applicable
Taq DNA polymerase (Invitrogen, UK, 5 U/µl):	2 Units

PCR reaction using Phusion DNA polymerase from Finnzymes:

The following components were added to a 0.5-ml microcentrifuge tube on ice:

DNA:	50-100 ng
dNTPs:	0.2 mM
forward primer:	0.5 µM
reverse primer:	0.5 µM
Phusion HF buffer contains 7.5 mM MgCl2:	1x
water:	not applicable
Phusion DNA polymerase (Finnzymes, FIN, 2U/µl):	2 Units

The tube was placed into a thermocycler (MJ Reasearch, USA) and the reaction was started by the first cycle of denaturation at 94°C for 3 min for the Taq polymerase and at 98°C for 30 sec for the Phusion polymerase. The primers were allowed to anneal at the specific T_M (T_M – 3 degrees for Taq polymerase and T_M + 3 degrees for the Phusion polymerase) for 30 sec and DNA synthesis was carried out at 72°C for 1 min/kb for the Taq polymerase and 15-30 sec/kb for the Phusion polymerase. For the following cycles (35 - 40) the reaction mix was denatured at 95°C for 45 sec for the Taq polymerase and at 98°C for 10 sec for the Phusion

polymerase, annealed at the specific T_M for 30 sec and elongated at 72°C for 1 min/kb for the Taq polymerase and 15-30 sec/kb for the Phusion polymerase. This was followed by a final elongation step at 72°C for 10 min for the Taq polymerase and at 72°C for 7 min for the Phusion polymerase. The reaction mix was then chilled to 10°C. The amplification products were analyzed by agarose gel electrophoresis.

3.3.11 Genotyping of mice

Polymerase chain reaction (PCR) was used to genotype the *Lrp2*$^{-/-}$ as well as the *Lrp2*$^{+/TgICD}$ or *Lrp2*$^{TgICD/TgIDC}$ animals.

The primer pair BPA/G21 amplified a 300 bp fragment that was specific for the mutant allele of *Lrp2* and primer pair G20/G21 amplified a 200 bp fragment specific for the wild type allele of *Lrp2*.

The primer pair WT tail forw/KI tail rev3 amplified a 400 bp fragment that was specific for the knock-in allele of the LRP2 ICD and primer pair WT tail forw/WT tail rev amplified a 200 bp fragment specific for the wild type allele of *Lrp2*.

Genotyping of *Lrp2*$^{-/-}$ mice:

The following components were added to a 0.5-ml microcentrifuge tube on ice:

DNA:	50-100 ng
dNTPs:	0.25 mM
forward primer:	0.3 µM
reverse primer:	0.3 µM
PCR buffer (10 mM Tris-HCl, 50 mM KCl, 1,5 mM $MgCl_2$, 0.001% (w/v) gelatine, pH 8.3):	1x
Triton X-100 (v/v)	0.01%
water :	not applicable
AmpliTaq Gold DNA polymerase (Applied B., USA, 5U/µl):	2 Units

During the first cycle the reaction mix was denatured at 95°C for 10 min, primers were allowed to anneal at 60°C for 1 min and DNA synthesis was carried out at 72°C for 1 min. For the following 35 cycles the reaction mix was denatured at 95°C

for 45 sec, annealed at 60°C for 45 sec and elongated at 72°C for 45 sec. This was followed by a final elongation step at 72°C for 10 min. The reaction mix was then cooled down to 4°C and analyzed by agarose gel electrophoresis.

Genotyping of *Lrp2*$^{+/TgICD}$ and *Lrp2*$^{TgICD/TgICD}$ mice:

The following components were added to a 0.5-ml microcentrifuge tube on ice:

DNA:	50-100 ng
dNTPs:	0.2 mM
forward primer:	0.2 µM
reverse primer:	0.2 µM
PCR buffer (200 mM Tris-HCl, 500 mM KCl, pH 8.4):	1x
water :	not applicable
Taq DNA polymerase (Invitrogen, UK, 5 U/µl):	2 Units

During the first cycle the reaction mix was denatured at 95°C for 3 min. For the following 37 cycles the reaction mix was denatured at 95°C for 30 sec, annealed at 50°C for 40 sec and elongated at 72°C for 45 sec. The reaction mix was then cooled down to 4°C and analyzed by agarose gel electrophoresis.

3.3.12 Mouse specific primer sequences

Primer identifier	Sequence (5'-3')
BPA	GATTGGGAAGACAATAGCAGGCATGC
G20	GACCATTTGGCCAGCCAAGG
G21	CATATCTTGGAAATAAAGCGAC
WT tail forw	GAAGGAACGGCGAGGCCCG
WT tail rev	GCGCTCAGCCGGAGCAGCTC
KO tail rev3	CAATATAATATACCCTGATTGCC
Shortarm_forw2	CTGTAGGAGACGCTGTCTGGCATG
Shortarm_rev2	CGCGGAGACGGCCCCGGGCCTCGCCG
LA1_forw	CTGGAATTTGCAGCGTAGACTGC
LA1_rev	CAGAGTGAAAGCTACATGTTATC
LA2_forw	CAGCTGATGAGTGATGTAATGG
LA2_rev	CAGCTGATGAGTGATGTAATGG
PspOMI_Flag_Megtail	GGGCCCATGGACTACAAAGACCATGACGGTGATTATAA AGATCATGACATCGATTACAAGGATGACGACGATGACAA GCACTACAGGAAAACTGGCTC
BamHI_Megtail_rev	GGATCCCTATACATCAGAGTCTTCCTTCACAAGGTTTG
SondeSouthern_forw	GCTTGGTCCACAGAACCCAC
SondeSouthern_rev	CCACTATCCCATCGCAATCCC
WSA169_forw	GGGCTGGCAAGCCACGTTTGG
WSA228_rev	GGGAGCTGCATGTGTCAGAGG

3.3.13 Southern blotting

For Southern blotting 1% agarose gels were used. Genomic DNA was digested with 20 U of the specific enzyme overnight at 37°C. DNA was loaded on the gel and resolved at 80 V for approximately 6 hrs in TAE buffer. Following, the gel was washed in H_2O and subsequently transferred to 0.4 M NaOH for 30 min at RT to denature the double stranded DNA into single stranded. The transfer of the electrophoresis-separated DNA to a positive loaded nylon membrane was performed in 0.4 M NaOH overnight using capillary action. Therefore the gel was placed on 2 pieces of Whatman paper, the nylon membrane was put on the gel followed again by 2 Whatman papers and a pack of paper cloths. Before the transfer, the membrane and the Whatman paper were equilibrated in 0.4 M NaOH. Then pressure was applied to the gel to ensure even contact between the gel and the membrane. The 2 pieces of Whatman papers under the gel reached a reservoir with 0.4 M NaOH and

therefore the DNA was transferred to the membrane following the buffer transfer by capillary action to the overlying pack of paper cloths. After the transfer the membrane was baked at 80°C for 10 min and transferred DNA was permanently attached to the membrane by exposure to ultraviolet radiation (0.010 Joule, Crosslinker, Bio-Link). Then the membrane was pre-hybridized in rapid-hyb buffer (GE Healthcare, UK) for 1 hr at 65°C. Finally the radioactive labelled probe, which was denatured before was added. The specific probe was labelled using the Prime-It II Random Primer Labelling Kit from Stratagene. In a hybridization volume of 20 ml 0.5 ng/µl of the specific DNA probe was labelled using 0.1 U/µl of Exo–Klenow polymerase, 1 x random 9-mer primers, 1 x dCTP-buffer and 1 x ^{32}P-dCTP. Hybridization was performed overnight and the next day the membrane was washed 4 times in washing buffer I (2 x SSC, 0.1% SDS) and 2 times in washing buffer II (0.1 x SSC, 0.5% SDS) for 5 min at 65°C. To visualize the DNA fragments the membrane was exposed for 12 hrs to an imaging plate (Fuji) and analyzed using the FLA 3000-2R Radioluminographie Scanner (Fuji).

3.3.14 Sequencing of DNA

DNA sequencing was performed by using BigDye Terminator v3.1 Cycle Sequencing Kit (Applied Biosystems, USA), according to manual instructions:

purified DNA	2µl
sequencing primer (10 µM)	0.25 µl
5 x BigDye buffer	2 µl
water	4.75 µl
BigDye reaction mix	1 µl

The tubes were placed in a thermal cycler and the following program was started:

Initial denaturation:	96°C for 1 min	
Denaturation:	96°C for 10 sec	} 30 cycles
Primer Annealing:	55°C for 5 sec	
Elongation:	60°C for 4 min	
Stop reaction:	10°C for ever	

After amplification, the DNA was purified with Sephadex G-50 (Amersham Pharmacia, UK), sequenced (ABI PRISM 377 DNA Sequencer) and, subsequently, analyzed by Lasergene DNA Star SeqMan Version 7.0.0.

3.3.15 Reverse transcription

Generation of cDNA from RNA was done using the First-Strand cDNA Synthesis SuperScript™ II RT Kit (Invitrogen, UK). 2µg of total RNA were incubated with 1.0 µl dNTP Mix (10 mM) and 1 µl random hexamers (50 ng/µl). The volume was filled with H_2O to 10 µl. The sample was denatured for 5 min at 65°C and then placed on ice for at least 1 min. 4 µl of 5x First-Strand buffer, 2 µl of 0.1 M DTT and 1 µl of RNaseOUT (40 U/µl) were added and mixed gently. Following, 1 µl of SuperScript II RT (200 U/µl) was added and annealed for 10 min at 25°C. cDNA synthesis was performed for 50 min at 42°C. The reaction was inactivated for 15 min at 70°C and cDNA was stored at -20°C.

3.3.16 TaqMan Real-time PCR

As template in TaqMan Real-time PCR 10 ng of cDNA, synthesized from total RNA from adult mouse kidneys, was used (see 3.3.3 Isolation of total RNA from tissue samples and 3.3.15 Reverse transcription). The cDNA, specific for different genotypes, was mixed with 5 µl qPCR™ Mastermix from Eurogentec, Germany and with 0,5 µl specific primer probe mix. As primer probe mix TaqMan® Gene Expression Assays for *Lrp2* (Mm01328171_m1) and *Nhe3* (Mm01352473_m1) were ordered from Applied Biosystems, USA. The PCR reaction was performed in a 384 well plate using the 7900 HT Fast Real-Time PCR System. The thermal cycler protocol accorded to standard conditions:

stage 1	50°C	2 min
stage 2	95°C	10 min
stage 3 x50 cycles	95°C	15sec
	60°C	1min

Data were collected using the Sequence Detection System 2.3 (Applied Biosystems, USA) and analyzed with the Comparative CT Method described in: USER Bulletin2 of

the ABI Prism 7700 Sequence Detection System. Values for *Lrp2* and *Nhe3* were measured in triplicates and normalized to ß$_2$-*microglobulin* (Mm00437762_m1) expression determined in parallel in the respective samples.

3.3.17 Gene expression profiling

Gene expression profiling was performed on total RNA from kidneys of adult mice (3 animals per genotype) using the Mouse Genome 430 2.0 probe array (Affymetrix) according to the manufacturer's protocols. Readings from the quantitative scannings were analyzed using R/Bioconductor. In detail, the arrays were normalized using the RMA algorithm and differential expression analysis was performed using the limma package.

3.3.18 *In vitro* transcription of digoxigenin-labelled RNA

Digoxigenin (DIG)-labelled probes for in situ hybridization (ISH) were generated using the DIG labeling Kit (Roche, Switzerland). 1 µg of linearized template plasmid-DNA was incubated with transcription buffer (40 mM Tris-HCl, 6 mM MgCl2, 10 mM dithiothreitol, 2 mM spermidine; pH 8.0), 1 mM ATP, 1 mM GTP, 1 mM CTP, 0.65 mM UTP, 0.65 mM DIG-11-UTP, 40 U RNA polymerase and 20 U RNase inhibitor. The volume of the reaction was adjusted to 20 µl and incubated for 2 hrs at 37°C. Template DNA was removed by incubating the reaction setup with 20 U DNase I at 37°C for 15 min. The RNA was purified using the RNeasy Mini Cleanup Kit (Qiagen, Germany).

3.3.19 *In situ* probes

Gene name	Probe	Restr.-site	Promotor
bone morphogenetic protein 4	*Bmp4*	*EcoRI*	SP6
fibroblast growth factor 8	*Fgf8*	*BamHI*	T7
glioma-associated oncogene homolog1	*Gli1*	*NotI*	T3
glioma-associated oncogene homolog3	*Gli3*	*HindIII*	T7
homeobox expressed in ES cells 1	*Hesx1*	*BamHI*	T3
homeobox protein Nkx-2.1	*Nkx2.1*	*EcoRI*	T3
noggin	*noggin*	*NotI*	T7
patched1	*Ptch1*	*SalI*	T3
sonic hedgehog	*Shh*	*HindIII*	T3
sine oculis homeobox homolog 3	*Six3*	*XbaI*	T7

3.3.20 *In situ* hybridization (ISH) on whole-mount mouse embryos

Mouse embryos were dissected in PBS and fixed overnight in 4% (PFA) in PBS. After fixation the embryos were dehydrated through a series of graded methanol solutions: 25%, 50%, 75% and 100% methanol in PBS, containing 0.1% Triton X- 100 (PBT) for 10 min each and stored at -20°C until use. For ISH, embryos were rehydrated through a series of graded methanol solutions (reverse of above) and E10.5 old embryos were punctured (eyes, hindbrain, heart) to facilitate penetration of solutions. Specimens were washed two times for 10 min in PBT and bleached in PBT containing 6% H_2O_2 for 1 hr at 4°C. After washing with PBT for 5 min, the embryos were permeabilized with 10 µg/ml proteinase K in PBT for 20 min (E10.5), 15 min (E9.5), 10 min (E9.0), 5 min (E8.5), 3 min (E8.0) and 1 min (E7.5) at RT. The proteinase K digest was stopped, by washing with 2 mg/ml glycine in PBT for 5 min, followed by two additional washes in PBT. Next, the embryos were re-fixed with 4% PFA containing 0.2% glutaraldehyde for 20 min at RT, and washed twice with PBT for 5 min. The embryos were then incubated with pre-hybridization solution (750 mM NaCl, 75 mM Na_3Citrate, 50% formamide, 50 µg/ml heparin, 100 µg/ml yeast tRNA, 0.1% Triton X-100; pH 4.5) for 3 hrs at 65°C. After pre-hybridization the embryos were incubated overnight at 65°C with the DIG-labelled RNA probe in fresh

pre-hybridization buffer at a final concentration of 1 µg/ml. The next day, the embryos were washed extensively in a series of buffers of increasing stringency: 2 times for 30 min at 65°C with wash-solution I (600 mM NaCl, 60 mM Na_3Citrate, 50% formamide, 1% SDS; pH 4.5), 2 times for 30 min at 65°C with wash-solution II (300 mM NaCl, 30 mM Na3Citrate, 50% formamide; pH 4.5) and 3 times for 10 min at RT with Tris buffered saline, containing 1% Tween (TBST; 140 mM NaCl, 2.7 mM KCl, 2.5 M Tris-HCl, 1% Tween; pH 7.5). After washing, the embryos were blocked with TBST containing 10% sheep serum for 3 hrs at RT, and were finally incubated with an anti-digoxigenin-alkaline-phosphatase (anti-DIG-AP, Fab fragments) conjugate at a dilution of 1:2000 overnight. The anti-DIG-AP was pre-absorbed with embryo-powder (3 mg/ml) in TBST at a dilution of 1:400 for 3 hrs at 4°C before use. Un-specifically bound antibody was removed the next day by three brief washes for 5 min, 5 washes for 1 hr at RT and a single wash overnight at 4°C, all in TBST. The next day, embryos were washed 3 times for 10 min in staining buffer (NTMT, 100 mM NaCl, 100 mM Tris-HCl, 50 mM $MgCl_2$, 0,1% Triton X-100; pH 9.5) before they were incubated with NTMT containing 1.88 mg/ml nitro blue tetrazolium chloride (NBT) and 0.94 mg/ml 5-Bromo-4-chloro-3-indolyl phosphate (BCIP). BCIP is the AP-substrate, which reacts further after the de-phosphorylation to give a dark- blue indigo dye as an oxidation product. NBT serves herein as the oxidant and gives also a dark-blue dye. The staining reaction was stopped by washing the embryos 3 times for 10 min at RT in NTMT, followed, by 4 hrs incubation in PBT pH 5.3 at RT. The embryos were re-fixed in 4% PFA containing 0.1% glutaraldehyde (GTA) for 20 min at RT. To decrease background the stained embryos were dehydrated and rehydrated through a series of graded methanol solutions: 25%, 50%, 75% and 100% methanol in PBT and cleared by incubating in 25%, 50%, 70% and 80% glycerol in PBS for 5 min each at RT. The embryos were stored at 4°C in the dark.

3.3.21 Preparation of membrane protein extracts

To specifically enrich membrane or membrane-associated proteins from mouse kidney, the sample was smashed in liquid N_2 using a mortar until a fine powder of the kidney was produced. 1 ml of sucrose buffer (250 mM sucrose, 10 mM TEA, including protease inhibitor cocktail tablets from Roche (1 tablet complete in 50 ml)

was added to one half of the kidney and the samples were incubated on ice for 10 min. To solubilize the nuclei, the samples were subjected 2 times to ultrasound for 20 sec at an intensity of 60 (Bandelin Sonopuls). Afterwards the cellular debris was removed by a centrifugation step at a low g-force (1500 x g, 10 min, 4°C). The supernatant was used in an additional centrifugation step at a medium g-force (14000 x g, 45 min, 4°C). The pellet was re-suspended in 500 µl NP40 buffer (150 mM NaCl, 50 mM Tris-HCl pH 7,4, 2 mM EDTA, 1% Nonidet-P40 (NP40, US Biological) and presented the membrane fraction. Finally, the supernatant was ultracentrifuged at a high g-force (130000 x g, 60 min, 4°C) to pellet the vesicle fraction. The pellet was re-suspended in 250 µl of NP40 buffer presenting the vesicle fraction, while the supernatant was taken as cytoplasmic fraction. Membrane, vesicle and cytoplasmic fractions were stored at -80°C until use. For western blotting, 150 µg of membrane and vesicle extracts were applied to a 5% (full-length LRP2) or 15% (soluble ICD) SDS-polyacrylamide-gel.

3.3.22 Determination of the protein concentration

The procedure is based on the formation of a complex between the dye Brilliant Blue G, and the basic and aromatic amino acids of the proteins in solution. The protein-dye complex causes a shift in the absorption maximum of the dye from 465 nm to 595 nm. The assay was prepared by diluting 1 ml Bradford reagent (Bio-Rad, CA) with 2 µl protein solution. The absorbance spectrum of the sample was recorded at 595 nm. The protein concentration was calculated as follows:

$$OD959\ nm/0{,}042 = x\ \mu g/\mu l$$

3.3.23 SDS polyacrylamide gel electrophoresis of proteins

Proteins were separated depending on their molecular weight on continuous or 4-20% gradient gels (for separation of proteins of high and low molecular weight at the same time) containing 10-15% polyacrylamide (PA). If not stated otherwise, 12,5 ng/µl or 3,1 µg/µl of protein or 20 µl of urine were mixed with sample buffer (62.5 mM

TrisHCl, 10% glycerol, 2% SDS, 0.01 mg/ml bromphenol blue, pH6.8), incubated for 5 min at 95 °C (not in case of urine samples) and resolved at 80-100 V (2-10 V/cm) in SDS-PAGE running buffer (950 mM glycine, 1% SDS, 125 mM Tris-HCl pH 8.4). After electrophoresis the gels were either subjected to western blotting or to coomassie brilliant blue staining.

3.3.24 Western blotting

After gel electrophoresis, proteins were transferred to a nitrocellulose membrane (Hybond-C, Amersham, UK). The membrane was probed with antibodies specific to the target protein. The setup in one gel holder cassette was as follows: one fiber pad (Bio-Rad, CA), two Whatman paper, gel, nitrocellulose membrane, two Whatman paper, one fiber pad. The assembled case was inserted in the case holder (Bio-Rad, CA) and put into the transfer chamber (Bio-Rad, CA), which was filled with transfer buffer (25 mM Tris-HCl, 192 mM glycine, pH 8.4). The transfer took 2 hours at 80 V. After the transfer, proteins were blocked with blocking solution (133 mM NaCl, 2.7 mM KCl, 25 mM Tris, 5% dry milk, pH 7.4) for 1 hour at RT with shaking. The primary antibody was applied in blocking buffer and the membrane was incubated with the primary antibody solution at 4°C overnight on a rocking platform. The next day, the primary antibody was removed and the membrane was washed 3 times 10 min in wash buffer (133 mM NaCl, 2.7 mM KCl, 25 mM Tris, pH 7.4) prior to 1 hour exposure to peroxidase-conjugated secondary antibody (dilution: 1:2000 in blocking buffer). After washing (2 x 10 min with wash buffer and 1 x 10 min with wash buffer-T (133 mM NaCl, 2.7 mM KCl, 25 mM Tris, 1% NP40, 1% triton-X, pH 7.4), the membrane was incubated with detection solution (Super Signal West Pico Stable Peroxide/Luminol Enhancer solution, Pierce, USA). Bands were detected using a CCD-camera (Fujifilm LAS-1000/ Intelligent Dark Box, Fujifilm, Japan).

3.3.25 Antibodies for Western blotting

Antibody	Dilution	Provided by
rabbit anti-Flag	1:750	Sigma-Aldrich
mouse anti-Flag	1:500	Sigma-Aldrich
guinea pig anti-LRP2	1:500	Willnow Lab
rabbit anti-DBP	1:1000	DAKO
rabbit anti-RBP	1:1000	Bio Trend
rabbit anti-GST	1:1000	Sigma-Aldrich
rabbit anti-SHH	1:1000	Santa Cruz
mouse anti-Na/K ATPase	1:5000	Millipore
mouse anti-Dab2	1:500	BD Transduction Laboratories

3.3.26 Coomassie brilliant blue staining of SDS-PAGE-gels

Coomassie brilliant blue staining is based on the binding of the dye coomassie brilliant blue R250, which binds non-specifically to proteins. For staining, the gel was incubated with coomassie blue staining solution (0.025% coomassie brilliant blue R250, 40% (v/v) methanol, 7% (v/v) acetic acid) for 4 hrs. The next day, the gel was transferred to de-staining solution I (40% (v/v) methanol, 7% (v/v) acetic acid), incubated for 30 min and transferred to de-staining solution II (7% (v/v) acetic acid, 5% (v/v) methanol). De-staining solution II was changed several times until the background was clear. The stained gel was imaged and dried to preserve.

3.3.27 Co-immunoprecipitation

Chinese hamster ovary (CHO) cells were transiently co-transfected with expression constructs for flag-tagged TgICD and murine Disabled 2 isoform b (Open Biosystems, UK). After 48 hours, cells were washed and lysed in lysis buffer (50 mM Tris-HCl, 150 mM NaCl, 1% NP40, 1% Triton-X, 1 x protease inhibitor cocktail, pH 8.0) on ice. Co-immunoprecipitations were performed using anti-flag antiserum

(Sigma-Aldrich, USA), and protein G-coupled Sepharose beads (Pierce, USA) according to standard protocols. Briefly, 2 µl antibody was mixed with the antigen in 1 ml immunoprecipitation buffer (IP) (25 mM Tris, 150 mM NaCl, pH 7.2), and 1 x protease inhibitor cocktail for 1 hour at room temperature. 20 µl of settled immobilized protein G was added to the antibody/antigen sample and further incubated 2 hours at room temperature. The beads were collected by centrifugation (1 min, 8000 x rpm, RT) and washed 6 x with 500 µl IP buffer. The protein-complex was eluted by incubating the beads with 30 µl of SDS-sample buffer (62.5 mM Tris-HCl, 10% glycerol, 2% SDS, 0.01 mg/ml bromphenol blue, pH 6.8) for 5 min at 95°C. Finally, the sample was resolved by SDS-PAGE.

3.4 *Ex vivo* model systems

3.4.1 Cephalic explant preparation

To prepare cephalic explants heads from E9.5 mouse embryos are cut at the level of rhombomeres (r) r4/ r5. The otic vesicle is taken as a caudal reference. Then, the neural tube is opened along the dorsal midline (roof plate) by cutting in a caudal to rostral direction, to the level of the *lamina terminalis.* To unfold the tissue, the floor plate at the level of the cephalic flexure is also cut. Thus, the neural tube appears like an “open book”. The cephalic explants are transferred to sterile petri dishes and placed (ventricular part facing up) on floating polycarbonate membrane filters of 0.4 µm pore size (culture plate insert, Millipore, USA) with 10% fetal bovine serum in DMEM culture medium with and without 200 nM SAG (Smo agonist; Alexis Biochemicals, USA). Explants are generally maintained for up to 24 hours in an incubator at 37°C, with 5% CO_2 and 95% humidity. Following the cephalic explants were fixed overnight in 4% PFA in PBT at 4°C. The next day the cephalic explants were washed and dehydrated through a series of graded methanol solutions: 25%, 50%, 75% and 100% in PBT, for 10 min each and stored at -20°C until use.

3.4.2 Whole embryo culture preparation

Whole embryo cultures were performed from E7.0 to E7.5 old embryos. The embryos were isolated from the uterus with the intact yolk sac and were incubated in whole embryo culture serum (WEC, Harlan Laboratories) for 24 hrs with and without 200 nM SAG (Alexis Biochemicals, USA) in an incubator at 37°C, with 5% CO_2 and 95% humidity. After incubation the embryos were fixed in 4% PFA in PBT overnight at 4°C. The next day the embryos were washed and dehydrated through a series of graded methanol solutions: 25%, 50%, 75% and 100% in PBT, for 10 min each and stored at -20°C until use.

Whole embryo cultures that were incubated with 5 µg/ml GST-SHH-N or 2,5 µg/ml recombinant SHH-N (R&D systems, UK) were kept in culture for 2 hrs in

DMEM supplied with 1.5% BSA. To allow the proteins to reach the neuroepithelium of the embryos, the yolk sac and the amnion was opened in this set of experiments. After culturing, the embryos were washed and fixed in 4% PFA in PBT for 15 min at 4°C, subsequently processing of the embryos is described in 3.5.3 Cryosections.

3.5 Histology

3.5.1 Paraffin sections

For paraffin sections tissue samples were fixed overnight in 4% PFA in PBS at 4°C. After fixation the samples were washed two times in PBT and then dehydrated through a series of graded methanol/PBT solutions for 10 min each step: 25%, 50%, 75%, and 100% methanol. The samples could be stored at -20°C until they were needed. The samples were transferred to 100% ethanol for 30 min at room temperature. Following, the samples were incubated for 2 hrs in Roti-Histol® (Roth, Gemany). The samples were pre-infiltrated with paraffin for 2 hrs at 67°C and finally infiltrated with fresh paraffin overnight at 67°C. The next day, the samples were embedded in paraffin using molds and stored at 4°C until use. If not otherwise stated, sectioning was done at 10 µm on a rotary microtome (Leica, Germany). Slides were stored at 4°C until further processing.

3.5.2 Plastic sections

Samples were embedded in Technovit 7100 (Heraeus Kulzer, Germany) according to the manufacturer's instructions. Embryos were used after ISH on whole-mount mouse embryos. Following, the re-fixation in 4% PFA containing 0.1% glutaraldehyde (GTA) for 20 min at RT, the embryos were dehydrated for 2 hrs in 70%, 80%, 90% and 100% ethanol in PBS. Then the embryos were pre-infiltrated with 50% ethanol/50% Technovit 7100 (v/v) for 2 hrs at RT. Next, samples were infiltrated with Technovit 7100 containing 1% (w/v) hardener I for 2 hrs at RT. Finally specimens were embedded in Technovit 7100 containing 1% hardener I and 6% (v/v) hardener II. After polymerisation, samples were cut at 10 µm on a rotary microtome (Leica, Germany). Slides were stored at 4°C until further processing.

3.5.3 Cryo sections

Specimens were fixed for 15 min at 4°C in 4% PFA and incubated in 30% sucrose/PBS until the tissue was descending. In the next step embryos were transferred to Tissue-Tek® OCT (Sakura, Japan) and cooled down on dry ice. The samples were then dissected at 10 µm on a rotary cryotome (Leica, Germany). Slides were stored at -80°C until further processing.

3.5.4 Counterstaining of sections

Plastic sections were counterstained using orange G (Sigma-Aldrich, USA), staining the cytoplasma of tissues. The sections were incubated for 30 sec with orange G staining solution (0.5% (w/v) orange G in ethanol), rinsed with tap water for 2 min, dried and mounted with Histo-clear® (Roth, Germany).

3.5.5 Immunohistochemistry on paraffin sections

The slides were removed from 4°C and allowed to equilibrate at RT for 10 min. After equilibration the slides were deparaffinized 3 times for 3 min in Roti-Histol® (Roth, Gemany). Afterwards the sections were rehydrated through a series of graded ethanol/H_2O solutions for 3 min each step: 100%, 96%, 90%, 70%, 50%, H_2O. Next the sections were post-fixed in 1% PFA in PBS for 20 min at RT and subsequently washed 2 times in PBS. To block endogenous peroxidase activity the slides were incubated for 3 min in 3%H_2O_2 and 10% methanol in H_2O. After 2 times washing in PBS for 5 min at RT, the sections were blocked in blocking solution (10% goat serum, 10% donkey serum, 0.1% Triton X-100, 0.05% Tween in PBS) for 1 hr at RT. The slides were drained for a few seconds and incubated with the primary antibody rabbit-anti-LRP2 (1:2000) (provided by Joachim Herz, University of Texas, USA) in blocking solution overnight at RT. The next day the sections were washed 3 times for 5 min in PBS at RT. Thereafter sections were incubated with the peroxidase-conjugated secondary antibody (1:100) (Sigma-Aldrich, USA) for 1h at 37°C in blocking solution. Then the sections were washed 3 times in PBS at RT. After

washing the sections were incubated with a peroxidase anti-peroxidase antibody (PAP) (1:200) (Sigma-Aldrich, USA) for 1 hr at 37°C in blocking solution. Following 3 times washing in 0.1 M TrisHCl pH7.5 the sections were stained using the DakoCytomation Kit (Dako North Amerika Inc, USA) for 5 min. The staining reaction was stopped, by washing the sections in H_2O and subsequently dehydration through a series of graded ethanol/H_2O solutions for 3 min each step: 50%, 70%, 90%, 96%, 100%. For analysis the sections were mounted with Roti®-Histokit II (Roth, Germany). Confocal images were made with a 40x oil immersion objective on a Leica Laser Scanning Microscope (TCS SP2, Leica, Germany).

3.5.6 Immunohistochemistry on cryo sections

The slides were removed from the -80°C freezer and allowed to equilibrate at RT for 10 min. After equilibration, the slides were washed 1 time in TBS (50 mM Tris-HCl, 150 mM NaCl; pH 7.4) for 5 min, 1 time in TBS containing 0.1% Triton X-100 (TBST) for 5 min and for an additional time in TBS for 5 min. Sections were then blocked for 1 hr at RT with TBS containing 10% donkey serum, 1% BSA and 0.3% Triton X-100. After blocking the slides were washed once in TBS for 5 min and then incubated with the primary antibody: sheep-anti-LRP2 (1:5000) (provided by Olivier Devuyst, University catholique de Louvain), and rabbit-anti-SHH (1:25) (Santa Cruz Biotechnology, USA, H-160) or rabbit-anti-GST (1:250) (Sigma-Aldrich, USA, G7781), in TBST at RT overnight. The next day, the slides were washed 1 time for 5 min with TBS, 1 time for 5 min with TBST and 1 time for 5 min with TBS at RT. Sections were stained with Alexa488- and Alexa555-conjugated secondary antibodies raised in donkey (dilution 1:2000, Molecular Probes (USA)) in TBS for 2 hrs at RT. Finally, the slides were washed 3 times in TBS for 5 min and then incubated for 10 min with DAPI (1:8000) (Roche 5 mg/ml) in TBS. Afterwards the sections were washed in TBS for additional 3 times for 5 min at RT. The sections were mounted with Dako Fluorescent Mounting Medium. Confocal images were made with a 40x oil immersion objective on a Leica Laser Scanning Microscope (SPE, Leica, Germany).

3.6 Cell biology methods

3.6.1 Primary proximal tubular culture

Proximal tubular cultures (PTCs) were prepared as described previously (S. Terryn *et al*., 2007). Briefly, renal cortices were dissected visually in ice-cold dissection solution (DS) (HBSS with 10 mmol/l glucose, 5 mmol/l glycine, 1 mmol/l alanine, 15 mmol/l HEPES, pH 7.4 and osmolality 325 mosmol/kg H_2O) and sliced into pieces of 1mm wide. The fragments were transferred to collagenase solution (DS with 0.1 % (wt/vol) type-2 collagenase and 96 µg/ml soybean trypsin inhibitor (Th. Geyer, Germany) at 37°C and digested for 30 min. After digestion, the supernatant was sieved through two nylon sieves (pore size 250 µm and 80 µm). The longer proximal tubule fragments remained in the 80 µm sieve and were re-suspended by flushing the sieve in the reverse direction with warm DS (37°C) containing 1 % bovine serum albumin (BSA; wt/vol). The proximal tubules present in the BSA solution were centrifuged for 5 min at 170 g, washed, and then re-suspended into the appropriate amount of culture medium (1:1 DMEM/F12 with 1 % heat-inactivated FCS, 15 mmol/l HEPES, 2 mmol/l L-glutamine, 50 nmol/l hydrocortisone, 5 g/ml insulin, 5 g/ml transferrin, 50 nmol/l selenium, 0.55 mmol/l sodium pyruvate, 10 ml/l nonessential amino acids, 100 IU/ml penicillin and 100 g/ml steptomycin, pH 7.4 and osmolality 325 mosmol/kg H_2O). The proximal tubule fragments were seeded onto collagen-coated permeable PTFE-filter supports (Corning, USA) and left unstirred for 48 h at 37°C with 5% CO_2 and 95% humidity, after which the culture medium was changed for the first time. The medium was then replaced every 2 days. After 7 days, cell cultures were organized as a confluent monolayer. Confluent cell layer were incubated with 0,5 mg/ml fluorescein isothiocyanate-conjugated BSA for 15 min at 37°C. Thereafter fluorescence signals were determined in cell lysates and normalized for total protein in the samples.

3.6.2 Binding assay in BN16 cells

For the binding assay Brown Norway rat yolk sac carcinoma (BN16) cells were used. This cell line expresses LRP2 and for this reason the cell line is suitable to analyze ligand-binding to LRP2. BN16 cells were grown on glass coverslips coated with 0.1% gelatine in phosphate-buffered saline (PBS) (Invitrogen, UK) in 24 well plates. When the cell density reached 70% the cells were incubated in 1.5% BSA in serum free DMEM for 2 hrs to remove nonessential proteins that could block binding to LRP2. After this the medium was replaced with fresh 1.5% BSA (to stabilize the added proteins) in serum free DMEM supplied with 2.5 µg/ml rec SHH-N (R&D systems, UK) or 5 µg/ml GST-SHH-N with and without 100 µg/ml HisRAP. After 2 hrs of incubation the cells were washed in PBS and fixed like described in the next part.

3.6.3 Immunofluorescence microscopy

Cellular localization of proteins was detected by sequential scanning confocal immunofluorescence microscopy. BN16 cells treated with different proteins were grown on glass coverslips coated with 0.1% gelatine in phosphate-buffered saline (PBS) (Invitrogen, UK) and fixed with 3% formaldehyde (10 min, RT). After washing 2 times with PBS, the cells were permeabilized for 10 min in 0.25% Triton X-100/PBS. Thereafter, all unspecific protein binding sites were blocked with 5% not fat milk in PBS for 1 hour at room temperature and afterwards stained with primary antibodies: rabbit-anti-SHH (1:25) (Santa Cruz Biotechnology, USA, H-160) or rabbit-anti-GST (1:250) (Sigma-Aldrich, USA, G7781) over night at 4°C. The next day, the cells were washed twice with PBS and stained with Alexa555-conjugated secondary antibody (dilution 1:2000, Molecular Probes, USA) 2 hours at room temperature in the dark. After staining, the cells were washed 3 times for 10 min with PBS. Following, the cells were stained with DAPI (1:5000) (Roche 5 mg/ml) in PBS. After additional 3 washing steps the cells were mounted on object holder with Dako Fluorescent Mounting Medium. Confocal images were made with a 63x oil immersion objective on a Leica Laser Scanning Microscope (SPE, Leica, Germany).

3.7 Generation of knock-in mouse mutants

3.7.1 Knock-in vector construction

As a template to amplify the ICD of LRP2 in PCR (3.3.10 Polymerase chain reaction (PCR), embryonic brain cDNA was used (3.3.15 Reverse transcription). PCR reaction was carried out using Phusion DNA polymerase from Finnzymes. For the amplification of the long arm and short arm for homologous recombination, bacterial artificial chromosome (BAC) DNA, was used. The BAC construct contained mouse genomic DNA sequences homologous to the endogenous Lrp2 gene loci that were targeted in my knock-in approach. Four different BACs were used and ordered from geneservice, UK:

(1) bMQ-304N8
(2) bMQ-351C24
(3) bMQ328D18
(4) bMQ-53P18

BAC DNA was purified using the Large Construct Kit from Qiagen, Germany according to the manufacturers instructions: A starter culture for the four different BAC clones was incubated for ~8 hrs at 37°C with vigorous shaking in 5 ml LB medium with the antibiotic chloramphenicole (20 µg/ml). 1 ml of the starter culture was transferred to 500 ml selective LB medium and grown over night at 37°C. Then the bacteria were pelletised at 6000 x g for 15 min at 4°C. Afterwards the bacterial cells were re-suspended in 20 ml resuspension buffer (50 mM Tris-Cl, pH 8.0, 10 mM EDTA; 10 µg/ml RNase A). 20 ml of lysis buffer (200 mM NaOH, 1% SDS) were added, the lysate was mixed and incubated at RT for 5 min. Then 20 ml of chilled neutralization buffer (3 M potassium acetate, pH 5.5) were admixed and the lysate was incubated on ice for 10 min. After centrifugation at 20000 x g for 30 min at 4°C the supernatant containing BAC DNA was removed. The lysate was filtered. Then BAC DNA was precipitated by adding 0,6 volumes of isopropanol. After centrifugation at 15000 x g for 30 min at 4°C the supernatant was discarded and the DNA pellet was washed with 5 ml of 70% ethanol and centrifuged at 15000 x g for 15 min. The DNA was allowed to air-dry for 2-3 min and then re-dissolved in 9,5 ml buffer EX. In

the next step 200 µl adenosintriphosphate (ATP)-dependent exonuclease and 300 µl ATP solution were added to the dissolved DNA and incubated at 37°C for 60 min. 10 ml of buffer QS was admixed to the DNA solution and it was applied to the QIAGEN-tip, which was equilibrated before with 10 ml buffer QBT (750 mM NaCl; 50 mM MOPS, pH 7.0; 15% isopropanol; 0,15% Triton®, X-100). The QIAGEN-tip was washed 2 times with 30 ml buffer QC (1 M NaCl; 50mM MOPS, pH 7.0; 15% isopropanol). Finally the BAC DNA was eluted using pre-warmed (65°C) buffer QF (1,25 M NaCl; 50 mM Tris-Cl pH 8.5; 15% isopropanol). The eluted DNA was precipitated by adding 10,5 ml isopropanol. After mixing and centrifugation at 15000 x g for 30 min at 4°C the DNA pellet was washed with 5 ml of 70% ethanol and centrifuged at 15000 x g for 15 min. The BAC DNA pellet was air-dried and finally re-dissolved in 50 µl of TE buffer (10 mM Tris-CL, pH 8.0; 1 mM EDTA).

Following the purified BAC DNA was digested with BstEII or NdeI for amplification of the long arm and digested with BamHI or HindIII for amplification of the short arm. The restriction enzymes were selected to cut the BAC DNA several times excluding cutting within the sequence for long arm and short arm amplification. The DNA, digested with the specific enzymes, was pooled and used as template in PCR reactions (3.3.10 Polymerase chain reaction (PCR), PCR reaction using Phusion DNA polymerase from Finnzymes).

The different fragments of the knock-in vector were cloned into the vector pBSSK neoA (kindly provided by M. Gotthard lab), which was used for targeting of embryonic stem cells (ES cells, see 3.7.2 Electroporation of ES cells).

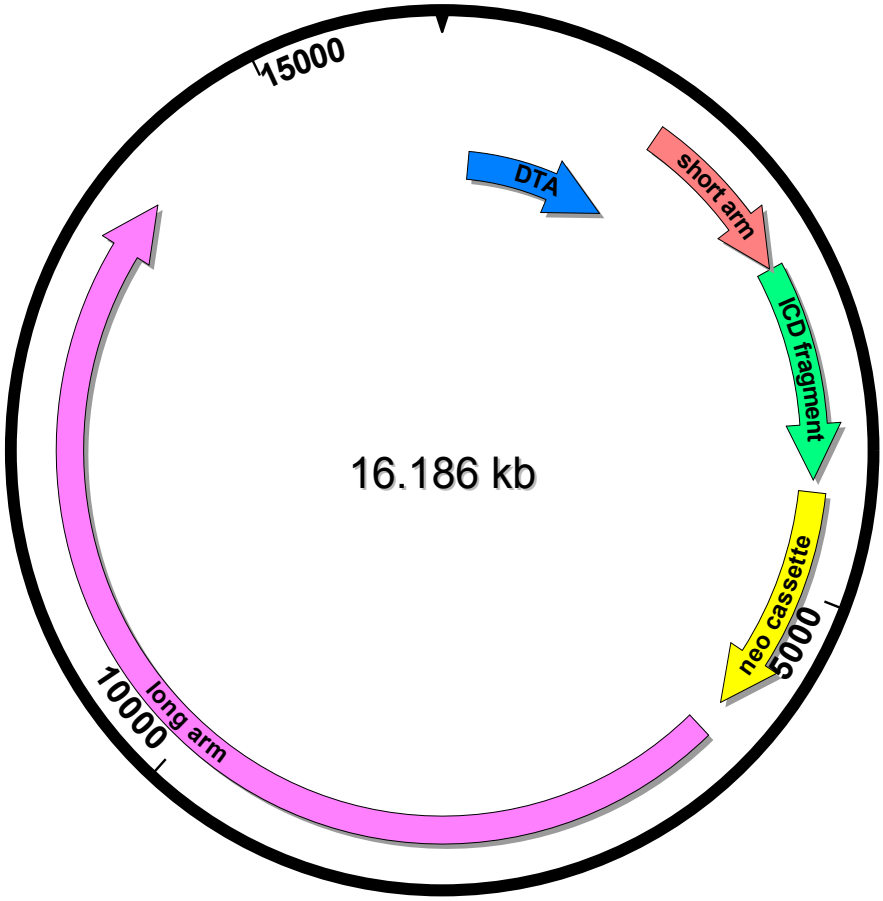

Figure 3.1: Construction of the knock-in targeting vector. The arrows indicate the different fragments inserted into the pBSSK neoA vector. Diphtheria toxin A (DTA, in blue) was inserted to ensure homologous recombination in the embryonic stem cells (ES cells). Non-homologous recombination would result in the production of the toxin and in the death of the cell producing it. The short arm (orange) is followed by the ICD fragment, encoding an intron of the rabbit ß-globin gene followed by three copies of the flag epitope, the intracellular domain (ICD) of LRP2, and a translation stop codon. NeoR was used as a marker to select for murine embryonic stem cells carrying the mini gene.

3.7.2 Cultivation of embryonic stem cells (ES cells)

ES cells were grown in petri dishes coated with 0.1% gelatine in PBS and inactivated feeder cells (neomycin (G418, Gibco®, Invitrogen, UK) resistant mouse fibroblasts, inactivated with mitomycin, (Sigma-Aldrich USA) at 5% CO_2 and 37°C. To split the cells, they were washed once in PBS and then treated with 0.25%

trypsin/EDTA (Invitrogen, UK) for 5 min at 37°C. The reaction was stopped by adding the double amount of ES cell medium. The cells were separated by pipetting up and down and were split until the desired cell density was reached.

ES cell medium:

5,58 g DMEM (Invitrogen, UK)
1,0 g Sodium Bicarbonate (Gibco, UK)
82,5 ml ES-FCS (Invitrogen, UK)
5,5 ml Penicillin/Streptomycin (Invitrogen, UK)
5,5 ml L-Glutamine (Invitrogen, UK)
5,5 ml Non essential amino acids (Invitrogen, UK)
3,8 µl 2-Mercaptoethanol (Sigma-Aldrich, USA)
55 µl murine LIF (Chemicon, USA)

ES cell freezing medium:

60 ml ES cell medium
20 ml ES-FCS
20 ml 20% DMSO (Sigma)

3.7.3 Electroporation of ES cells

800 µl (1 half of a 10 cm petri dish) ICp4 ES cells (inner cell mass, passage 4) (derived from mice from AB2.1 ES cells) were electroporated with 50 µg linearized knock-in construct vector DNA. The cells were electroporated with a pulse of 250 V and 5 µF. After electroporation the cells were seeded on a 10 cm petri dish coated with gelatine and feeder cells.

3.7.4 Isolation of ES cell clones

To select for positive ES cell clones 0.18 mg/ml geneticin (G418 = neomycin, Gibco®, UK) was added to the ES cell culture medium 2 days after electroporation. After 6-8 days cell clones were picked and transferred into a 96 well plate and incubated with 30 µl trypsin/EDTA (Invitrogen, UK) for 3 min at 37°C. To stop the reaction 70 µl of ES cell medium were added into each well. Afterwards by pipetting up and down cell clones were separated. Following, 100 µl of the ES cell clones were transferred into a 96 well plate coated with gelatine and feeder cells. Cells on the 96 well plate were split after 2–3 days 1:4 onto two 96 well plates coated with gelatine

and feeder cells and in two 96 well plates only coated with gelatine. ES cell clones, grown in gelatine coated 96 well plates were used to isolate genomic DNA for Southern blot analysis and ES cell clones, grown in feeder coated 96 well plates were frozen to use for expanding of positive cell clones after Southern blot analysis.

3.7.5 Freezing of ES cell clones

The ES cell clones in the 96 well plates were frozen at -80°C until positive ES cell clones were identified and used for injection into blastocysts. To freeze the ES cells they were washed once in PBS and then treated with 30 µl trypsin/EDTA (Invitrogen, UK) for 7 min at 37°C to ensure separating into single cells. To stop the reaction 70 µl ES cell medium was added in each well and the cells were separated, by pipetting up and down. Finally, 100 µl of ES cell freezing medium was added and cells were slowly frozen at -80°C.

3.7.6 Injection of ES cell clones into blastocysts

ES cell clones, which were tested positive in Southern blot analysis were thawed at 37°C and transferred into 24 well plates coated with gelatine and feeder cells with fresh ES cell medium. After 2 days the positive ES cell clones were expanded into 6 well plates. Before the injection the cells were trypsinized and washed 2 times with PBS. Finally, the cells were suspended in 250 µl ES cell medium and injected into blastocysts from C57BL6 mice. The injected blastocysts were transferred into the uterus of a pseudo pregnant foster mother to obtain chimeras. Germ line transmission of the modified gene was confirmed in offspring from the chimeras by Southern blot analysis.

4. Results

4.1 Studying signaling functions of the intracellular domain (ICD) of LRP2

4.1.1 Generation of a new mouse model expressing the ICD of LRP2

LRP2, a member of the low density lipoprotein receptor gene family, is a multifunctional cell surface receptor. Little is known about mechanisms that may control receptor expression and activity *in vivo.*

In a previous study it was shown that LRP2 is subjected to RIP, which links receptor-mediated endocytosis and intracellular signaling events (Z. Zou *et al*., 2004). In cell culture experiments in opossum kidney cells the COOH terminus of LRP2 down-regulates its own expression and the expression of the Na^+/H^+ *exchanger* (Y. Li *et al*., 2008). Furthermore, in *C. elegans*, the cytoplasmic domain of *Ce-LRP-1* (homolog of mammalian LRP2) partially suppressed the molting defect, which has been induced by knock down of *Ce-IMP-2* (homologues to presenilins, a part of the γ-secretase protease complex which deliberates the receptor intracellular domain) (A. Grigorenko *et al*., 2004).

To establish an *in vivo* model to explore the relevance of the mammalian LRP2 ICD in signal transduction processes, I generated a new mouse model, where a mini gene construct encoding the ICD of LRP2 was introduced into the *Lrp2* endogenous gene locus, to achieve expression under control of the endogenous *Lrp2* promoter.

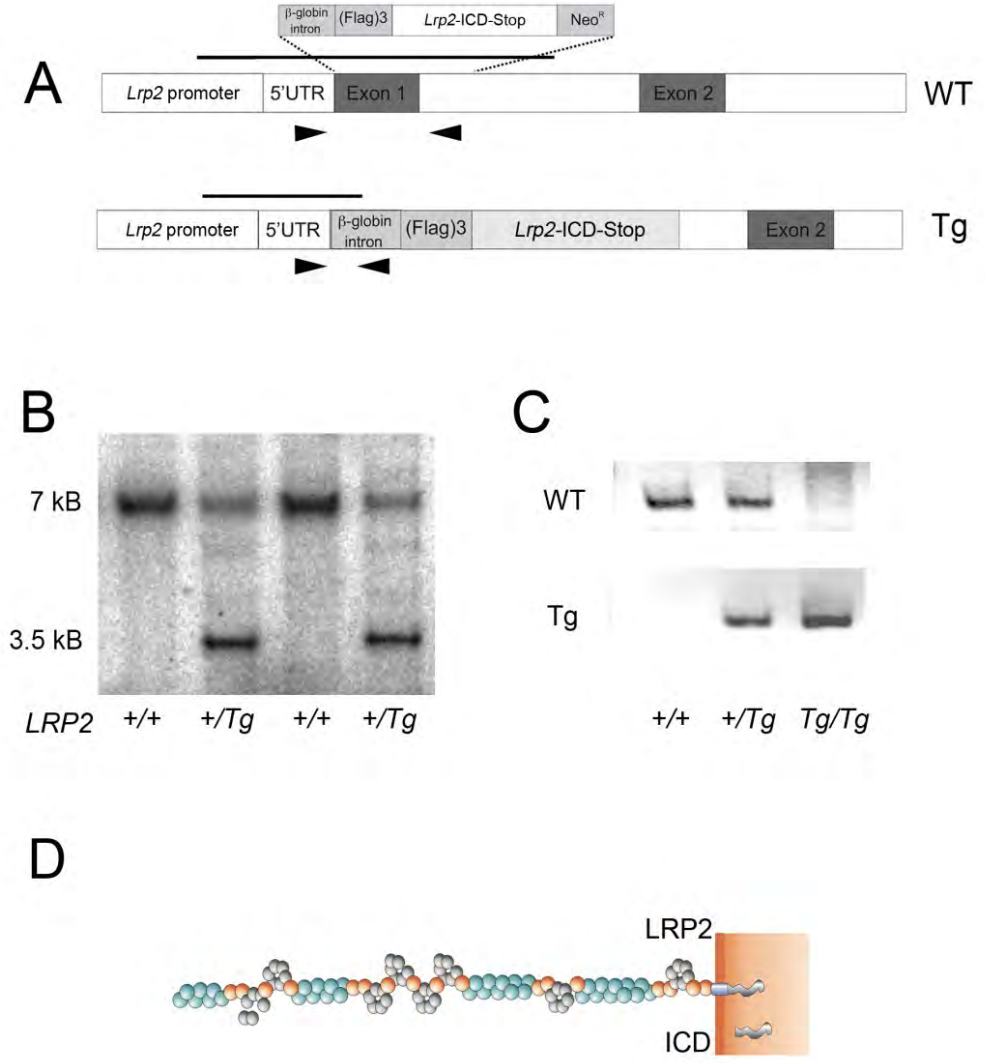

Figure 4.1.1: Generation of mice expressing the ICD of LRP2. (A) Genomic organization of the wild type (WT) and the targeted (Tg) *Lrp2* locus. Homologous recombination with a mini gene construct encoding an intron of the rabbit β-globin gene followed by three copies of the flag epitope, the ICD of LRP2, and a translation stop codon is indicated. Neo^R was used to select for murine embryonic stem cells carrying the mini gene. Arrows indicate the position of primer sequences used for PCR genotyping of wild type and targeted alleles. The solid lines above the gene regions highlight genomic DNA fragments diagnostic for both genotypes in Southern blots. (B) Southern blot analysis of genomic DNA from mice homozygous for the wild type allele ($Lrp2^{+/+}$) or heterozygous for the ICD transgene ($Lrp2^{+/TgICD}$). The positions of the 7 kB and 3.5 kB HindIII fragments indicative of the wild type and the targeted allele, respectively are shown. (C) PCR genotyping of E10.5 embryos from $Lrp2^{+/TgICD}$ breeding indicates the presence of littermates homozygous for the ICD transgene (*Tg/Tg*). (D) Structure of the full-length LRP2 and the soluble ICD. The soluble ICD encompasses amino acids 4448 to 4661 of the mouse LRP2 polypeptide (NM_001081088).

The mouse model expressing the soluble ICD of LRP2 instead of the full-length form of the receptor from the endogenous *Lrp2* locus (Figure 4.1.1 D) was generated by homologous recombination in murine embryonic stem cells and subsequent injection of targeted ES cell clones into blastocysts (Figure 4.1.1 A). Targeting of the wild type *Lrp2* locus results in expression of the flag-tagged soluble ICD under control of the endogenous *Lrp2* promoter. The blastocysts were injected into the uterus of pseudo pregnant foster mothers to obtain chimeras. Germ line transmission of the modified *Lrp2* gene was confirmed in offspring from the chimeras by Southern blot analysis (Figure 4.1.1 B). In HindIII digested genomic DNA hybridized with a probe from the *Lrp2* gene promotor, wild type animals show a 7 kB DNA fragment, whereas animals heterozygous for the ICD transgene are identified by a 3.5 kB DNA fragment. Breeding of $Lrp2^{+/TgICD}$ mice produced newborn littermates with all three possible genotypes: $Lrp2^{+/+}$, $Lrp2^{+/TgICD}$ and $Lrp2^{TgICD/TgICD}$ (Figure 4.1.1C). However, animals homozygous for the transgene and lacking a functional *Lrp2* gene ($Lrp2^{TgICD/TgICD}$) died perinatally as described previously for $Lrp2^{-/-}$ mice (Willnow *et al*., 1996).

4.1.2 Cellular localization of the LRP2 ICD in the kidney

Recent studies suggested a possible role for the LRP2 ICD in signal transduction pathways in rat kidneys and in opossum kidney proximal tubule cells (Z. Zou *et al*., 2004; Y. Li *et al*., 2008). In these studies it was reported that LRP2 is subjected to RIP and that the ICD is able to regulate its own gene expression and the expression of *Nhe3*. To test this hypothesis *in vivo*, I analyzed the role of LRP2 ICD in adult mouse kidneys.

LRP2 functions as a major scavenger receptor in the renal proximal tubules. In renal tissue extracts subjected to Western blot analysis, the wild type receptor was typically found in the membrane and vesicle fraction in line with localization of the receptor on the apical surface of proximal tubular cells and endocytic vesicles (Figure 4.1.2 A).

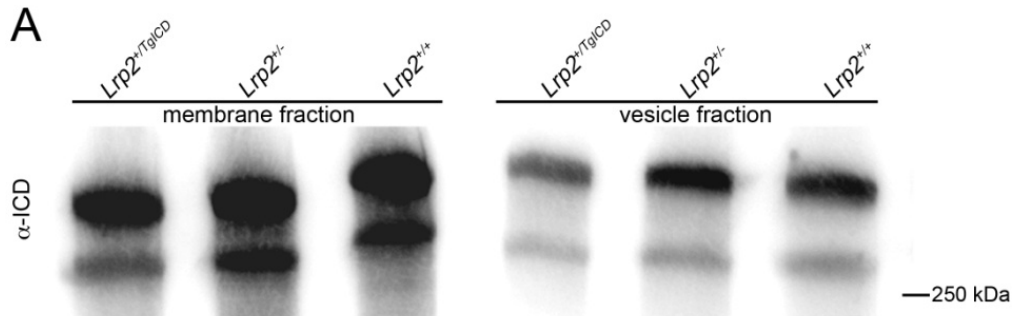

Figure 4.1.2 A: Detection of the full-length receptor LRP2. The wild type receptor LRP2 is detected in the membrane and vesicle fraction of *Lrp2*$^{+/+}$, *Lrp2*$^{+/-}$ and *Lrp2*$^{+/TgICD}$ kidney extracts using the anti-ICD antiserum, which recognizes the carboxyl terminal domain of the full-length receptor.

In contrast, Western blot analysis showed robust expression of the ICD in the cytosolic fraction of kidneys from adult *Lrp2*$^{+/TgICD}$ mice. In these Western blot experiments, I used antibodies directed against the Flag epitope as well as antibodies specifically recognizing the ICD of LRP2. The LRP2 ICD expressed in the mutant mice had the expected size of 26 kDa. The LRP2 ICD recombinant protein transiently expressed in HEK293 cells under the control of a CMV promoter was loaded as positive control for antibody specificity (Figure 4.1.2 B).

Immunohistological detection of the soluble ICD confirmed the data obtained in Western blot analyses. In adult kidney sections of *Lrp2*$^{+/+}$ and *Lrp2*$^{+/TgICD}$ mice the antibody against the cytoplasmic domain of LRP2 detected the wild type receptor on the apical surface of proximal tubular cells in *Lrp2*$^{+/+}$ mice. In *Lrp2*$^{+/TgICD}$ mice the antibody detected the apical wild type receptor, but in addition a diffuse signal, likely representing the soluble ICD in the cytoplasm. In *Lrp2*$^{-/-}$ kidney sections used as a control, neither the α-Flag nor the α-ICD antibody detected any specific signals (Figure 4.1.2 C). To test localization of the ICD in kidneys lacking a functional *Lrp2* gene copy (*Lrp2*$^{TgICD/TgICD}$) breeding of *Lrp2*$^{+/TgICD}$ mice were set up. The kidneys from E16.5 *Lrp2*$^{+/+}$ and *Lrp2*$^{TgICD/TgICD}$ embryos were analyzed for the localization of the full-length receptor, the ICD, and cubilin, the co-receptor to LRP2 in the kidney. In *Lrp2*$^{+/+}$ embryos the anti-ICD antibody localized the intracellular domain of the full-length receptor at the apical site of renal proximal tubule cells. In contrast, in *Lrp2*$^{TgICD/TgICD}$ embryonic kidneys no apical cell surface staining representative of the wild type receptor was seen. Rather, a diffuse cytoplasmic pattern indicative of the

ICD was apparent. As expected from data on LRP2-deficient mice (H. Birn *et al*., 2000), the apical localization of the co-receptor cubilin was not affected in homozygous *Lrp2*$^{TgICD/TgICD}$ embryos (Figure 4.1.2 D).

Taken together, these results demonstrated that I have successfully generated a novel mouse model exhibiting robust expression of the LRP2 ICD *in vivo*.

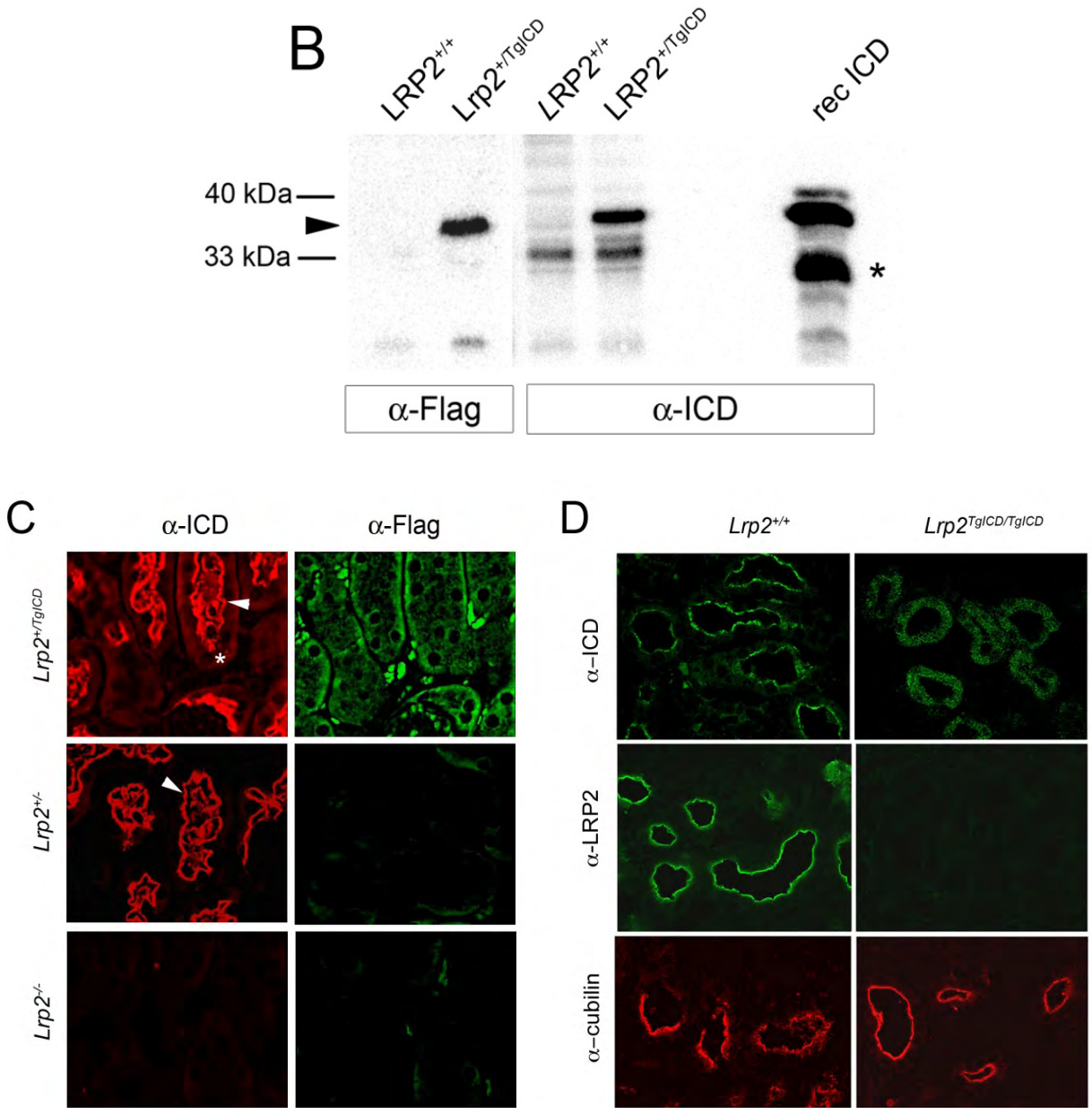

Figure 4.1.2 B-D: Detection of the soluble ICD. (B) Western blot analysis detects expression of the ICD (arrowhead) in cytosolic kidney extracts from adult *Lrp2*$^{+/TgICD}$ mice using both, antisera against the flag epitope (α-Flag) and the ICD (α-ICD). The recombinant ICD transiently expressed in HEK293 cells was used as a positive control (recICD). The asterisk marks a degradation product of recICD in HEK293 cell lysates. (C) Immunohistological detection of the cytoplasmic domain of LRP2 (α-ICD) or the flag-tagged ICD (α-Flag) in kidneys of adult *Lrp2*$^{+/TgICD}$, *Lrp2*$^{+/-}$ and *Lrp2*$^{-/-}$ mice. The anti-ICD antiserum recognizes the carboxyl terminal domain of the full-length receptor at the apical membrane of proximal tubular cells *in Lrp2*$^{+/-}$ and *Lrp2*$^{+/TgICD}$ mice (arrowheads). In addition, a diffuse cytoplasmic signal is seen in the *Lrp2*$^{+/TgICD}$ kidneys (asterisk). The anti-Flag antibody detects only the recombinant ICD in renal *Lrp2*$^{+/TgICD}$ tissue. Embryonic sections of mouse kidneys at embryonic day 16.5 were used for immunohistological detection of the ICD, full-length receptor, or the co-receptor cubilin (D). Anti-ICD antiserum recognizes the intracellular domain of the full-length receptor at the apical membrane of proximal tubular cells in *Lrp2*$^{+/+}$ embryos. In kidney sections of *Lrp2*$^{TgICD/TgICD}$ embryos, the antibody recognizes the soluble ICD, which displays a diffuse cytoplasmic pattern. An antiserum against full-length LRP2 detects the wild type receptor in *Lrp2*$^{+/+}$ but not the ICD in *Lrp2*$^{TgICD/TgICD}$ embryos. Localization of cubilin at the apical surface is not affected in proximal tubular cells expressing only the ICD (*Lrp2*$^{TgICD/TgICD}$). (Magnification: x63).

4.1.3 The soluble LRP2 ICD can bind to the intracellular adaptor protein Disabled-2

The cytoplasmic domain of LRP2 contains one potential SH2-binding domain, a dileucine repeat (important for endocytosis), four potential SH3-domain binding sites, as well as a PDZ-binding motif. Previous studies showed that Disabled-2 (Dab2) is a cytoplasmic adaptor protein that binds through its phosphotyrosine interaction domain to the cytoplasmic domain of the receptor in the kidney (A. Oleinikov, *et al*., 2000; J. Nagai *et al*., 2005). The interaction between LRP2 and the cytosolic adaptor protein Dab2 is known to be important for proper endocytosis of LRP2-ligand complexes. Former studies showed that in conditionally null *Dab2*$^{-/-}$ mice, the LRP2-mediated protein uptake is reduced (S. Morris *et al*., 2002). To confirm that the ICD expressed in the *Lrp2*$^{+/TgICD}$ mice is able to interact with

physiological ligands (such as Dab2), co-immunoprecipitation experiments were performed (Figure 4.1.3).

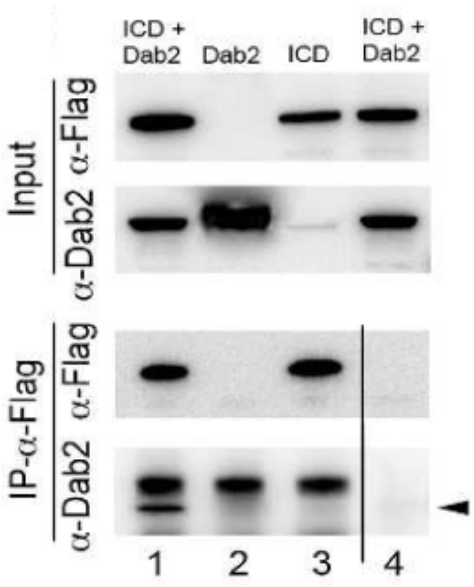

Figure 4.1.3: Co-immunoprecipitation of Dab2 and the ICD from Chinese hamster ovary (CHO) cells. The Input represents cell lysates from CHO cells transiently expressing murine Dab2 (lane 2), the flag-tagged ICD (lane 3), or both proteins (Lane 1 and 4). Detection of the ICD (α-Flag) and Dab2 (α-Dab2) in anti-Flag immunoprecipitates from the various CHO cell clones is indicated in panel IP. In cells with ICD (lane 1) co-immunoprecipitation of Dab2 was detected, using the α-Flag antiserum, but not in cells without ICD (lane 2). As negative control, non-immune IgG failed to precipitate ICD or Dab2 (lane 4).

Antibodies directed against the flag-tagged ICD (α-Flag) or Dab2 (α-Dab2) detected strong expression of Dab2 (lane 2), the ICD (Lane 3), or both proteins (lane 1 and 4) in the various CHO cell extracts used for co-immunoprecipitation (Input). In CHO cells expressing both proteins (lane 1) Dab2 was detected in anti-Flag immunoprecipitates (Figure 4.1.3 arrowhead), but not in cells expressing only Dab2 (lane 2) or the ICD (lane 3).

These results showed that the soluble ICD is able to bind cytoplasmic interaction partners as exemplified for Dab2.

4.1.4 The ICD has no effect on wild type receptor function in the adult kidney

Expression of a constitutively active ICD in *Lrp2*$^{+/TgICD}$ mice might have a dominant negative effect on the wild type receptor. For example, the ICD may sequester cytosolic adapter proteins that normally bind to the intracellular domain of

the full-length receptor and therefore alter its localization or endocytic function (M. Gotthard *et al*., 2000).

Immunohistochemistry experiments were carried out to analyze if the ICD influences wild type receptor localization, distribution of cubilin, and/or the uptake of LRP2 specific ligands such as vitamin D binding protein (DBP).

In mice heterozygous for the ICD transgene no difference in wild type LRP2 localization was detected (Figure 4.1.4 A). In adult kidney sections of *Lrp2*$^{+/-}$ and *Lrp2*$^{+/TgICD}$ mice wild type LRP2 localized apically at the brush border in proximal tubular cells. Also the co-receptor cubilin did not show any changes in expression or localization in kidneys of adult *Lrp2*$^{+/TgICD}$ mice (Figure 4.1.4 A). Equally, introducing one allele of LRP2 ICD had no effect on the uptake of DBP, which was localized in apical endosomes in *Lrp2*$^{+/-}$ and *Lrp2*$^{+/TgICD}$ mouse proximal tubule cells to a similar extent (Figure 4.1.4 A).

LRP2 is a key component for tubular retrieval of many low molecular weight plasma proteins from the glomerular filtrate (J. Leheste *et al*., 1999). Consequently, LRP2-deficient mice suffer from tubular reabsorption deficiency and urinary loss of filtered proteins (low molecular weight proteinuria) (J. Leheste *et al*., 1999). Western blot experiments were done to analyze if the ICD, expressed in *Lrp2*$^{+/TgICD}$ mice, inhibits ligand uptake by the wild type receptor. In contrast to *Lrp2*$^{-/-}$ mice, which show low molecular weight proteinuria and excrete DBP as well as retinol-binding protein (RBP) (Figure 4.1.4 B, lane 4), no receptor ligands were detected in urine of *Lrp2*$^{+/TgICD}$ and *Lrp2*$^{+/-}$ animals (Figure 4.1.4 B, lane 1-3 and 5). Also the urinary electrolyte profiles (Na^+, K^+, Cl^-, Ca^{2+}, phosphate, glucose, and pH) showed no difference between *Lrp2*$^{+/-}$ and *Lrp2*$^{+/TgICD}$ animals (Table 4.1.1).

Genotype	Na^+ (mmol/l)	K^+ (mmol/l)	Cl^- (mmol/l)	Ca^{2+} (mg/l)	Phosphate (mmol/l)	Glucose (g/l)	pH	Volume (ml)
Lrp2$^{+/-}$	88,67	99,25	98,17	46,25	52,48	0,14	6,5	1,94
Lrp2$^{+/TgICD}$	95,5	136,20	114,33	54,20	52,97	0,13	6,36	1,26

Table 4.1.1: Urinary electrolyte profiles. From each genotype 6 individual urine samples of adult *Lrp2*$^{+/-}$ and *Lrp2*$^{+/TgICD}$ mice were collected over night. The table shows mean values of ions and metabolites in the two genotypes. No significant changes were detected in the urinary profiles (Na^+, K^+, Cl^-, Ca^{2+}, phosphate, glucose, and pH).

To test the activity of the LRP2-cubilin pathway, primary proximal tubule (PTC) cell cultures were established. An obvious cytoplasmic signal for the flag-tagged ICD was detected in the cells from *Lrp2*$^{+/TgICD}$ kidneys but not in control kidneys (*Lrp2*$^{+/-}$ and *Lrp2*$^{-/-}$) (Figure 4.1.4 C). LRP2 is known to bind and mediate endocytosis of albumin (S. Moestrup *et al*., 1996). To quantify LRP2 endocytic activity, the albumin uptake was measured in *Lrp2*$^{+/TgICD}$, *Lrp2*$^{+/-}$ and *Lrp2*$^{-/-}$ proximal tubule cultures. As expected, a dramatic endocytic defect is seen in the PTCs from *Lrp2*$^{-/-}$ mice, which lack the wild type receptor and consequently fail to take up albumin. A comparable albumin uptake is observed in the PTCs from *Lrp2*$^{+/TgICD}$, *Lrp2*$^{+/-}$ and *Lrp2*$^{+/+}$ mice.

In conclusion, these results demonstrated that the ICD did not affect wild type LRP2 function in the proximal tubule of adult mouse kidneys.

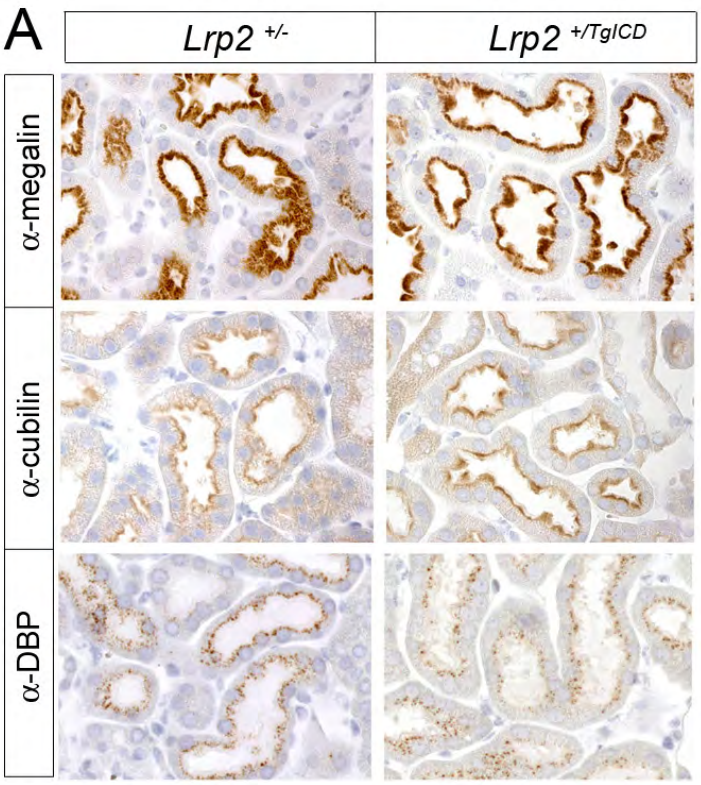
A
Lrp2 +/-
Lrp2 +/TgICD
α-megalin
α-cubilin
α-DBP

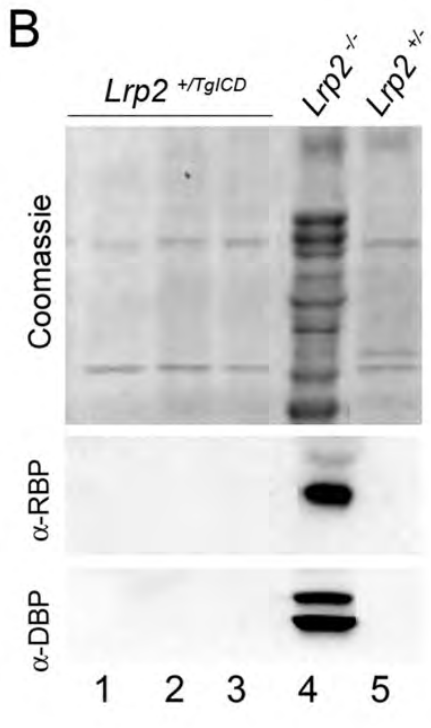
B
Lrp2 +/TgICD
Lrp2 -/-
Lrp2 +/-
Coomassie
α-RBP
α-DBP
1
2
3
4
5

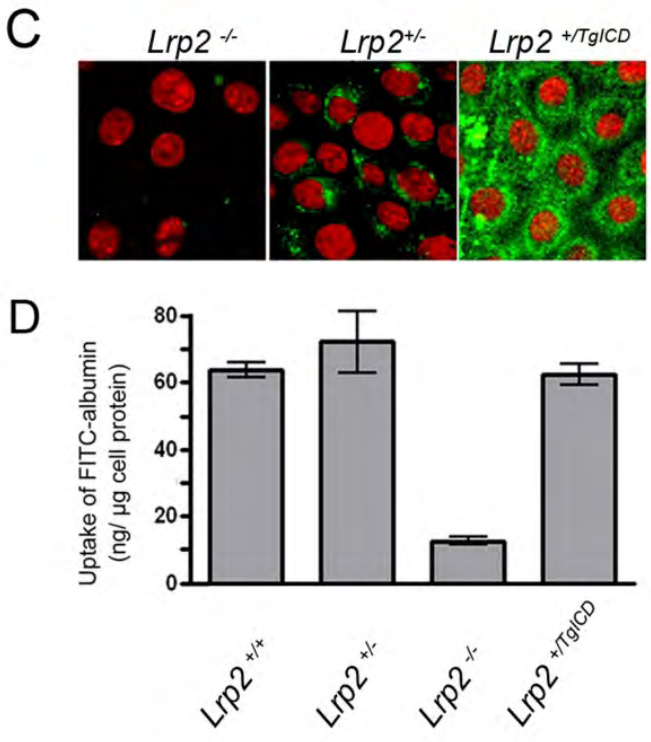
C
Lrp2 -/-
Lrp2+/-
Lrp2 +/TgICD
D
Uptake of FITC-albumin (ng/ µg cell protein)
80
60
40
20
0
Lrp2 +/+
Lrp2 +/-
Lrp2 -/-
Lrp2 +/TgICD

Figure 4.1.4: No effects of the ICD on functional *Lrp2* expression in renal proximal tubules. (A) Immunohistological detection of full-length LRP2, cubilin and vitamin D binding protein (DBP) on adult kidney sections from *Lrp2*$^{+/TgICD}$ and *Lrp2*$^{+/-}$ mice. No discernable differences were seen in the apical localization of the wild type receptor LRP2 and its co-receptor cubilin or in staining for DBP, localized in apical endosomes, between *Lrp2*$^{+/TgICD}$ and *Lrp2*$^{+/-}$ mice (magnification: x63). (B) Western blot analysis of *Lrp2*$^{+/TgICD}$, *Lrp2*$^{-/-}$ and *Lrp2*$^{+/-}$ animals demonstrated low-molecular weight proteinuria (Coomassie) as well as excretion of DBP and retinol-binding protein (RBP) in *Lrp2*$^{-/-}$ mice (lane 4) but not in *Lrp2*$^{+/TgICD}$ (lane 1-3) and *Lrp2*$^{+/-}$ (lane 5) mice. (C) In primary proximal tubule cell cultures the cytoplasmic flag-tagged ICD was detected using α-Flag antiserum in *Lrp2*$^{+/TgICD}$ cultures but not in *Lrp2*$^{-/-}$ and *Lrp2*$^{+/-}$ cultures. Nuclei were counterstained with DraQ5^{TM} (magnification: x63). (D) Similar rates of FITC-labelled albumin uptake were seen in cells from *Lrp2*$^{+/+}$, *Lrp2*$^{+/-}$ and *Lrp2*$^{+/TgICD}$ cultures in contrast with dramatically decreased uptake in *Lrp2*$^{-/-}$ cells. All values are mean $\pm$ SEM.

4.1.5 The ICD of LRP2 does not regulate gene expression in the adult kidney

Previous studies reported that LRP2 is subjected to RIP (Z. Zou *et al*., 2004). After metalloprotease-mediated ectodomain shedding followed by γ-secretase-mediated release of the cytosolic domain, the intracellular part of the receptor may play a role in signaling. In cell culture experiments using opossum kidney cells, overexpression of the soluble LRP2 intracellular domain resulted in a dramatic down-regulation of LRP2 itself and Na^+/H^+ exchanger 3 (Nhe3) on the level of both protein and transcript (Y. Li *et al*., 2008).

To investigate if the ICD also controls protein and mRNA expression *in vivo,* microarray and real time PCR (RT-PCR) analyse were performed. No significant alterations were found in global gene expression of adult kidney cells comparing renal expression profile of *Lrp2*$^{+/+}$and *Lrp2*$^{+/TgICD}$ mice (Figure 4.1.5 A). Also, no significant changes in levels of *Lrp2* and *Nhe3* transcripts or LRP2 protein were detected using quantitative RT-PCR and Western blot analyses (Figure 4.1.5 B)

These data argue that the soluble ICD is not able to act as a transcriptional regulator in proximal tubule cells.

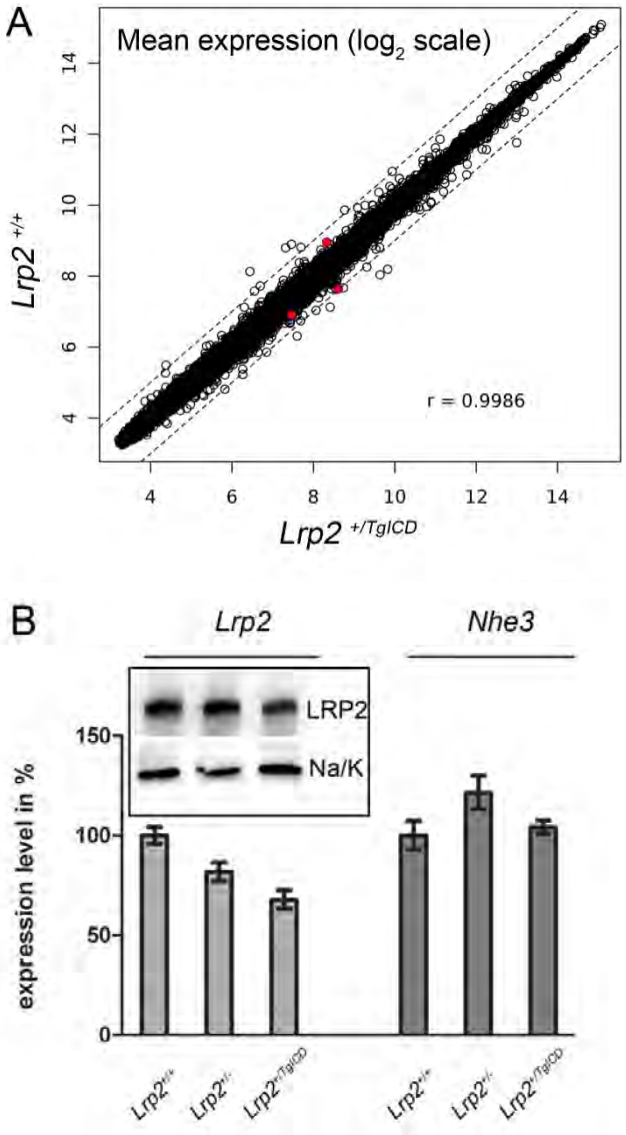

Figure 4.1.5: Analysis of the expression profile in the kidney of *Lrp2*$^{+/TglCD}$ mice. (A) Gene expression profiling of adult kidneys from *Lrp2*$^{+/+}$ and *Lrp2*$^{+/TglCD}$ animals using mouse whole genome arrays. Genome-wide mean expression levels (log_2 scale) are given for both genotypes. The dotted lines indicate 2-fold change in expression level and the red dots indicate significant changes (p-value < 0.05, adjusted for multiple testing with the Benjamini Hochberg correction). No statistically significant changes were observed for any gene at threshold fold change > 2 and corrected p-value < 0.05. Rather, the expression profiles of the two samples were highly correlated (Pearson's correlation coefficient r = 0.9986). (B) Quantitative RT-PCR on total RNA isolated from *Lrp2*$^{+/+}$, *Lrp2*$^{+/-}$ and *Lrp2*$^{+/TglCD}$ adult kidneys did not detect significant changes in the level of transcripts as internal control. Data are given as percent change in expression level compared to *Lrp2*$^{+/+}$ (set at 100%). Values are mean values ± SEM. The inset depicts Western blot analysis of LRP2 and Na/K ATPase (Na/K; loading control) in renal membrane extracts from *Lrp2*$^{+/+}$, *Lrp2*$^{+/-}$ and *Lrp2*$^{+/TglCD}$ mice. No change in the protein level of LRP2 was detected in the different genotypes.

4.1.6 The ICD of LRP2 fails to rescue the forebrain phenotype caused by loss of the full-length receptor

In *C. elegans* the knock-down of *Ce-imp-2,* which is required for proper embryonic development, was rescued by expression of the *Ce-lrp-1* intracellular domain (A. Grigorenko *et al*, 2004). *Ce-lrp-1* is the nematode orthologe of mammalian *Lrp2* and *Ce-imp-2* is the nematode orthologe of mammalian presenilins, subunits of the γ-secretase protease complex. This complex cleaves the intracellular domain of many membrane receptors following ectodomain shedding (S. Sisodia *et al*., 2002).

LRP2-deficient embryos suffer from impaired forebrain development as described previously (T. Willnow *et al*., 1996). To examine if the ICD can partially substitute for the activity of the full-length receptor during forebrain development, embryos of the three different genotypes: $Lrp2^{+/+}$, $Lrp2^{-/-}$ and $Lrp2^{TgICD/TgICD}$ were analyzed.

$Lrp2^{-/-}$ and $Lrp2^{TgICD/TgICD}$ mouse embryos showed a similar phenotypic appearance at E10.5 (Figure 4.1.6). In both genotypes the telencephalic vesicles failed to develop properly compared to wild types (arrows). Also, investigation of different marker genes showed similar defects in $Lrp2^{-/-}$ and $Lrp2^{TgICD/TgICD}$ embryos. Thus, expression of *Shh*, a key morphogen of ventral forebrain development, was lost in the preoptic area of $Lrp2^{-/-}$ and $Lrp2^{TgICD/TgICD}$ embryos at E10.5 (arrowheads) but showed normal expression in more caudal regions such as the diencephalon. In $Lrp2^{-/-}$ and $Lrp2^{TgICD/TgICD}$ embryos, *Nkx2.1,* a downstream target of SHH signaling, was also dramatically down-regulated in the preoptic area (arrowhead) at E9.5. FGF8 is an important morphogen for rostrally derived CNS structures. In $Lrp2^{-/-}$ and $Lrp2^{TgICD/TgICD}$ embryos the expression domain of *Fgf8* was shifted to more dorsal regions in the telencephalon (asterisk) but was reduced in the ventral telencephalon. Also in later embryonic stages $Lrp2^{TgICD/TgICD}$ embryos showed characteristics of HPE as demonstrated for $Lrp2^{-/-}$ embryos before (T. Willnow *et al*., 1996).

These findings indicated that the full-length LRP2 is required for proper forebrain development and that the ICD cannot rescue the forebrain phenotype of LRP2-deficient embryos.

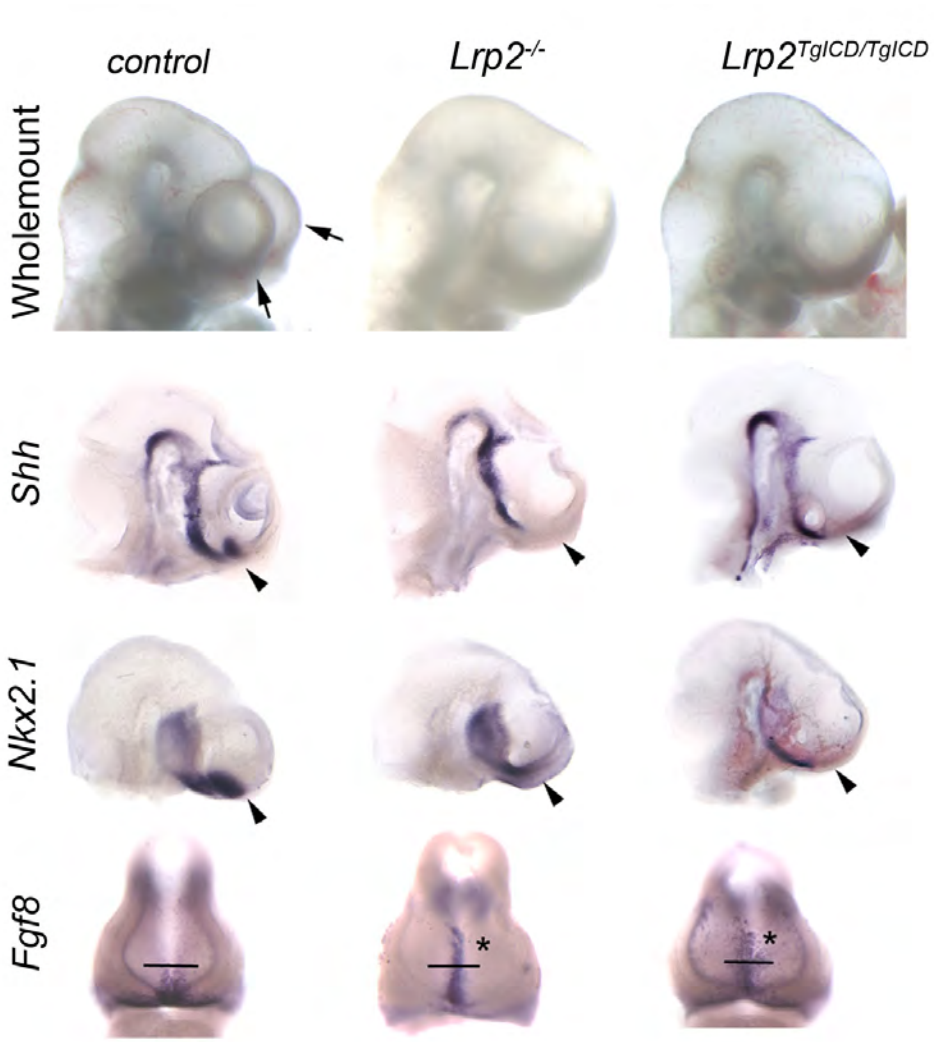

Figure 4.1.6: Features of holoprosencephaly in *Lrp2*$^{-/-}$ and *Lrp2*$^{TglCD/TglCD}$ embryos.
The telencephalic vesicles in the control embryos (*Lrp2*$^{+/+}$ and *Lrp2*$^{+/-}$*;* arrows) show proper development in comparison to the holoprosencephalic phenotype of *Lrp2*$^{-/-}$ and *Lrp2*$^{TglCD/TglCD}$ embryos at E10.5. *Shh* expression in the preoptic area is lost in the *Lrp2*$^{-/-}$ and *Lrp2*$^{TglCD/TglCD}$ embryos at E10.5 in comparison to strong expression in the wild type (arrowheads). *Nkx2.1* expression is significantly down-regulated in the ventral telencephalon (arrowheads) of *Lrp2*$^{-/-}$ and *Lrp2*$^{TglCD/TglCD}$ E9.5 embryos compared to the *Lrp2*$^{+/+}$ control embryo. The expression domain of *Fgf8* in the telencephalon of *Lrp2*$^{-/-}$ and *Lrp2*$^{TglCD/TglCD}$ embryos at E9.5 extends dorsally (asterisk) to the commissural plate (indicated by the line) and is reduced in the ventral region of the telencephalon (below the line) in comparison to the restricted and strong expression in the *Lrp2*$^{+/+}$ control embryo. (Whole mount in situ hybridization analyses)

4.2. Function of LRP2 during early forebrain development of the mouse

4.2.1 Expression pattern of LRP2 in the developing central nervous system (CNS) of the mouse

To investigate the role of LRP2 during forebrain development and to understand why loss of LRP2 function leads to HPE, I carried out a detailed expression analysis first (Figure 4.2.1).

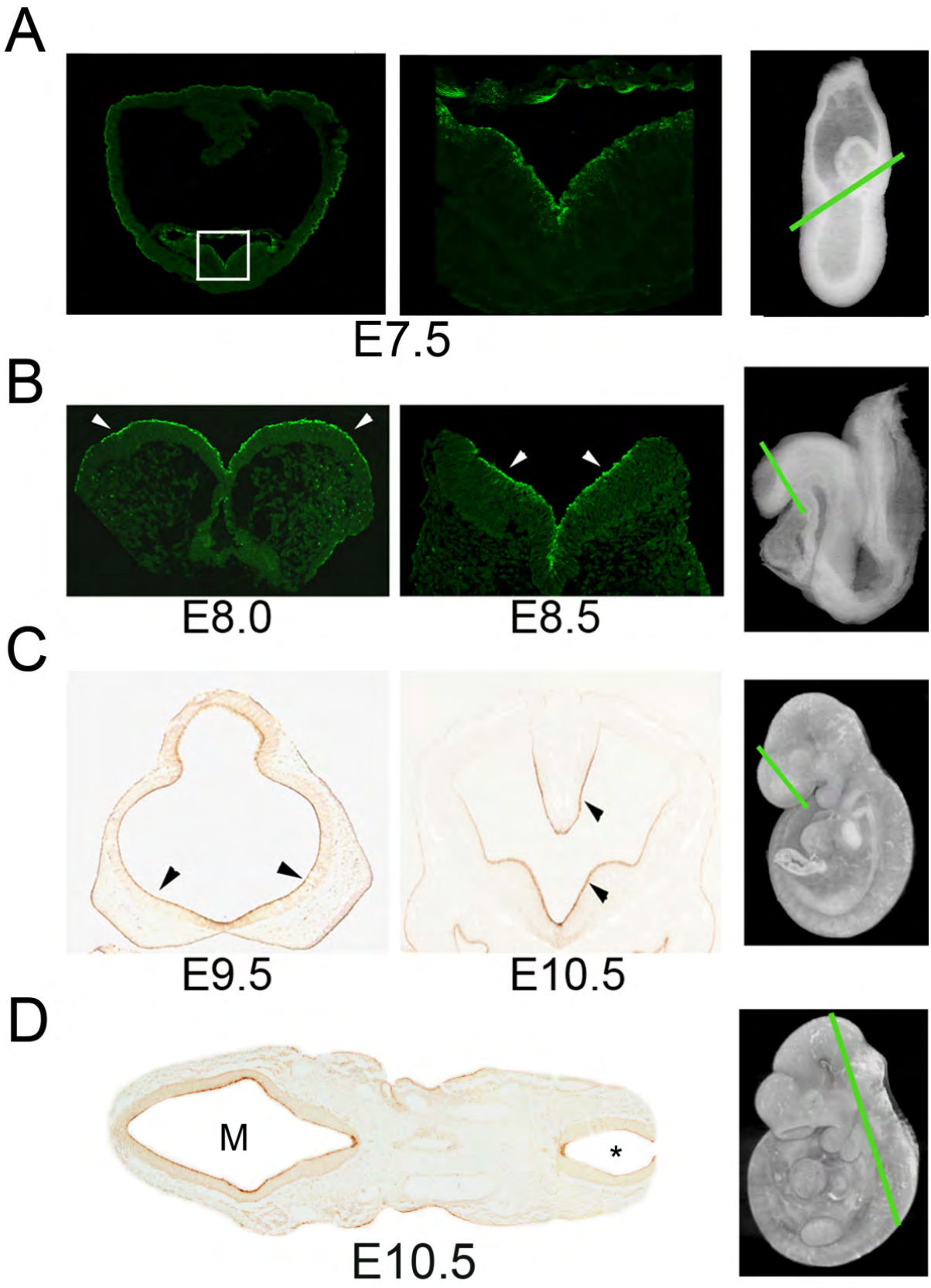
A
E7.5
B
E8.0
E8.5
C
E9.5
E10.5
D
M
*
E10.5

Figure 4.2.1: Neuroepithelial localization of LRP2 during forebrain development. (A) Transversal sections at E7.5, during neural plate formation, show robust expression of LRP2 on the apical surface of the neuroepithelium. The white square in the overview on the left (magnification: x10) indicates higher magnification of the neuroepithelium shown on the right (magnification: x63). (B) Coronal sections demonstrate that before neural tube closure at E8.0 - E8.5 LRP2 is uniformly expressed on the apical surface of the neuroepithelium (arrowheads; magnification: x40). (C) After neural tube closure LRP2 is mainly expressed in the ventral and dorsal region of the developing telencephalon starting at E9.5 (arrowheads) and clearly visible at E10.5 as displayed on coronal sections (arrowheads; magnification: E9.5 x20, E10.5 x5). (D) Throughout embryonic development LRP2 is expressed in the entire neural tube. Strong expression of LRP2, visible on coronal sections, is detected in the mesencephalon (M) as well as in the caudal neural tube (asterisk; magnification: x5). For reference, whole mount micrographs of the relevant embryonic stages indicating the plane of section by a green line are shown in each panel.

From early embryonic development E6.0 onwards, LRP2 is expressed on the apical surface of the developing neuroepithelium (C. Drake *et al*., 2004). At E7.5, I detected strong LRP2 expression on the apical side of the developing neural plate (Figure 4.2.1 A). Before the neural tube proceeds to closure, LRP2 is expressed uniformly along the entire length of the neural folds (Figure 4.2.1 B, arrowheads). After neural tube closure, the LRP2 expression domain centers in the ventral and dorsal midline region of the telencephalon starting from E9.5 on (Figure 4.2.1 C, arrowheads). Restriction of LRP2 immunoreactivity to the midline of the forming forebrain is even more pronounced on sections at E10.5. During embryonic development LRP2 is expressed along the entire neural tube from very rostral areas like the telencephalon (Figure 4.2.1 C) and mesencephalon (Figure 4.2.1 D; M) to caudal areas in the neural tube (Figure 4.2.1 D; asterisk).

4.2.2 LRP2 acts upstream of key morphogen pathways during forebrain development

Previous studies have reported that loss of LRP2 leads to a failure of proper forebrain development and consequently to HPE (T. Willnow *et al*., 1996; R. Spoelgen *et al*., 2005).

To uncover the underlying molecular defects of the HPE phenotype in *Lrp2*$^{-/-}$ mice I analyzed the expression of marker genes involved in early forebrain development. Remarkably, I found major changes in the expression and activity of key morphogens in all three forebrain patterning centers caused by LRP2 deficiency in the early neuroepithelium (Figure 4.2.2).

In detail, at E10.0 the telencephalic *Shh* expression just anterior to the optic recess was lost in *Lrp2* mutants compared to controls (arrowhead), whereas expression in more caudal regions of the forebrain were unaffected. As a control group I used both, *Lrp2*$^{+/+}$ or *Lrp2*$^{+/-}$ embryos, because there is no phenotype in embryos heterozygous for the receptor gene defect.

Fgf8 showed a dorsally shifted midline expression extending dorsally from the commissural plate in the telencephalon of *Lrp2*$^{-/-}$ embryos (asterisk), but also a reduction of expression in the ventral telencephalon (below the line) in comparison to control embryos at E9.5.

Finally, *Bmp4* expression was increased in the neuroepithelium of the dorsal telencephalon in *Lrp2*$^{-/-}$ E9.0 embryos (asterisk). *Bmp4* also showed a ventral shift in expression towards more rostral regions (arrowhead), sparing the region around the optic recess.

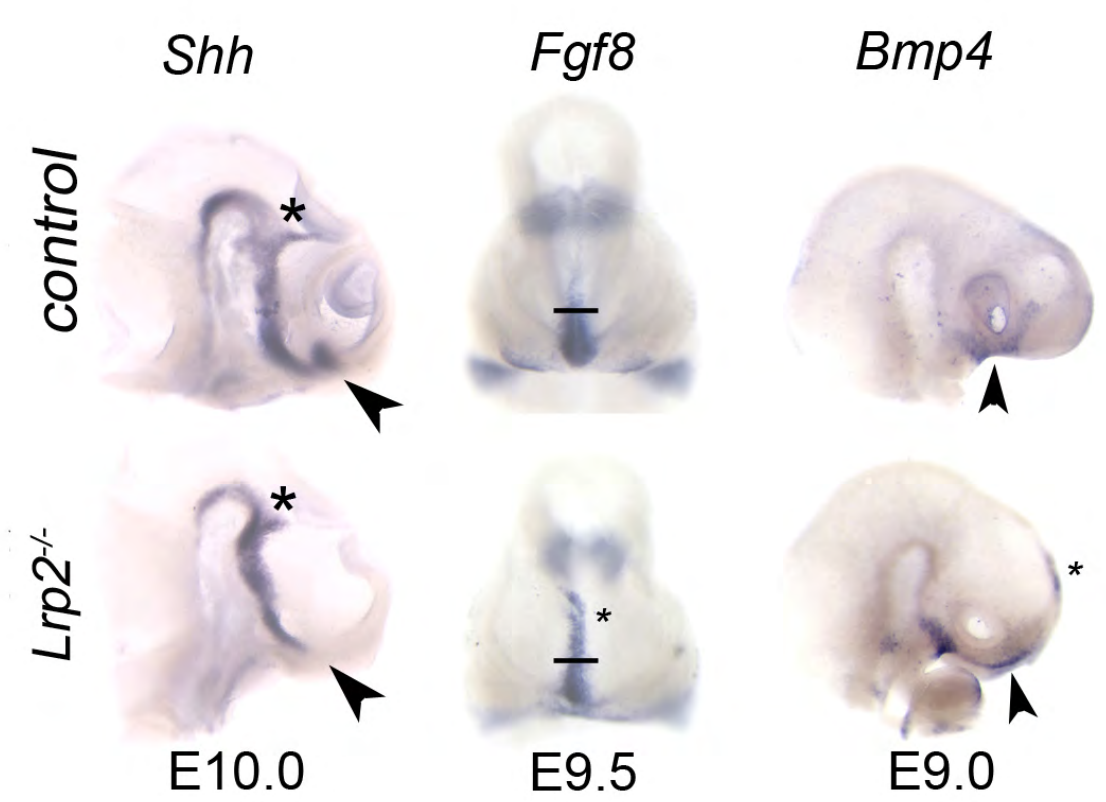

Figure 4.2.2: Analysis of *Shh*, *Fgf8,* and *Bmp4* expression in *Lrp2* mutant embryos. Whole-mount ISH for *Shh* in E10.0 embryos (lateral view) indicates expression in the ventral diencephalon as well as in the zona limitans intrathalamica (Zli, asterisk) and ventral telencephalon. Ventral telencephalic expression of *Shh* is visible in the control embryo (arrowhead) but not in the ventral telencephalic region anterior to the optic recess of *Lrp2*$^{-/-}$ embryos. At E9.5 the *Fgf8* expression domain, visible in frontal head aspects is reduced in the ventral telencephalon in the LRP2-deficient embryos (below the line) but extended into the dorsal region of the telencephalon (asterisk) in comparison to control embryos. In E9.0 embryos, *Bmp4* expression is increased in the rostral, dorsal telencephalon (asterisk) of *Lrp2*$^{-/-}$ embryos, but the ventral expression domain is shifted to more rostral regions in the telencephalon (arrowhead) compared with the expression pattern in the control embryo (lateral view).

The phenotype of LRP2 deficient embryos suggested a role for the receptor in early pattern formation of the developing rostral neural tube, potentially as a key factor for proper establishment of the three signaling centers marked by *Shh*, *Fgf8,* and *Bmp4* expression.

4.2.3 Downregulation of *Bmp4* levels in *Lrp2* mutants does not rescue the holoprosencephaly phenotype

Increase of *Bmp4* levels in *Lrp2* mutant embryos suggested that the receptor might act as negative regulator of the BMP4 pathway. If so, aberrant activity of this pathway in $Lrp2^{-/-}$ embryos should be rescued by partial ablation of BMP4 activity in the neural tube.

To test this hypothesis, I used the $Bmp4^{tm1blh}$ mouse, which has been obtained from Jackson laboratories in collaboration with Oleg Lyubinskiy. The *Bmp4* gene consists of two protein-coding exons. In this mouse model the first exon after amino acid position 7 is replaced by the MC1neo^{r} A+ cassette, and in the second exon a stop codon in all three reading frames is inserted. Therefore it is expected that neither a full-length nor a potentially dominant negative truncated protein will be expressed from the $Bmp4^{tm1blh}$ allele (G. Winnier *et al*., 1995). In former studies it was shown that having only one functional copy of *Bmp4* leads to developmental defects in a specific genetic background, demonstrating that a single copy of *Bmp4* cannot generate enough active protein, and that mice suffer from a haploinsufficient $Bmp4^{tm1blh}$ phenotype (R. Dunn *et al*., 1997). Previous studies also reported that decreasing the *Bmp4* dosage in animal models with mutations in BMP4 antagonists like noggin, suppresses the phenotype caused by these mutations, demonstrating that a rescue approach using the $Bmp4^{tm1blh}$ mouse line can indeed be successful (Stottmann *et al*., 2006). Conceptually, downregulation of *Bmp4* at the transcriptional level is now believed to play just as important a role as BMP4 antagonists such as noggin, chordin, gremlin, or follistatin (R. Stottmann *et al*., 2006). In line with this study, BMP4 levels were expected to decrease in LRP2-deficient mice by crossing them onto the heterozygous haploinsufficient $Bmp4^{tm1blh}$ background. According to my hypothesis, lower BMP4 levels should lead to a rescue from HPE in the $Lrp2^{-/-}$, $Bmp4^{tm1blh/+}$ mice.

The analysis of *Bmp4* transcript levels in $Lrp2^{+/+}$, $Bmp4^{tm1blh/+}$, and $Lrp2^{-/-}$, $Bmp4^{tm1blh/+}$ mice compared to levels in $Lrp2^{+/+}$ and $Lrp2^{-/-}$ mice uncovered a significant decrease of 50% of *Bmp4* transcript levels in mice haploinsufficient for *Bmp4* (Figure 4.2.3 A). In whole mount ISH experiments on embryos at E10.5, *Shh* expression was used as a read out for a possible rescue caused by decreased *Bmp4* transcript levels (Figure 4.2.3 B). Overall there was no change in *Shh* expression in embryos haploinsufficient for *Bmp4* comparing $Lrp2^{+/+}$ and $Lrp2^{+/+}$, $Bmp4^{tm1blh/+}$

embryos. Also, *Lrp2*$^{-/-}$, *Bmp4*$^{tm1blh/+}$ embryos showed the same phenotype as *Lrp2*$^{-/-}$ animals as ventral telencephalic expression of *Shh* was lost in the compound mutant (*Lrp2*$^{-/-}$, *Bmp4*$^{tm1blh/+}$) as well as in the single mutant (*Lrp2*$^{-/-}$).

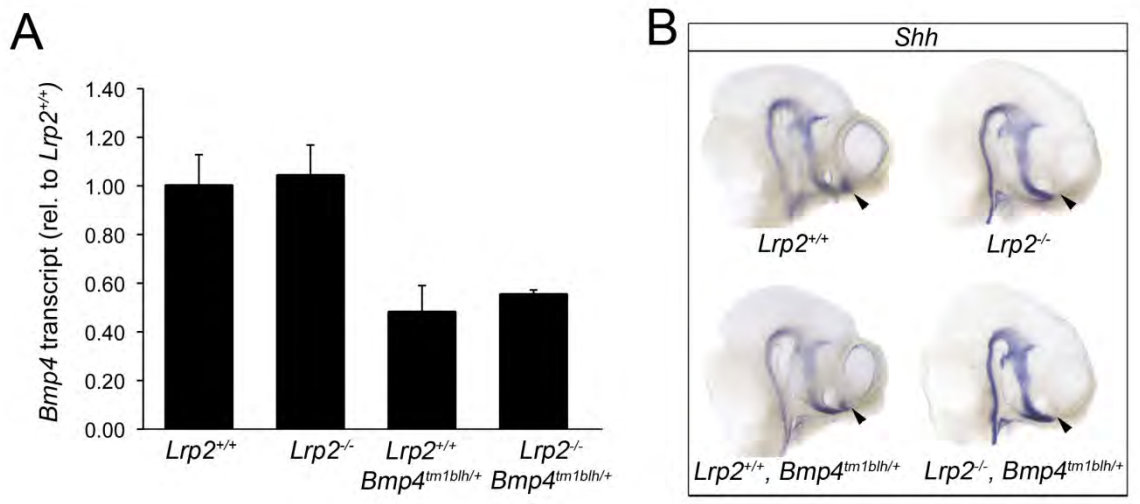

Figure 4.2.3: Analysis of *Bmp4* haploinsufficiency in *Lrp2* mutants (Figure provided by Oleg Lyubinskiy). (A) Real time PCR analysis of *Bmp4* RNA levels in E8.5 embryos. *Bmp4* RNA levels are reduced by 50% in haploinsufficient *Bmp4*$^{tm1blh/+}$ embryos in comparison to control embryos (*Lrp2*$^{+/+}$ and *Lrp2*$^{-/-}$ embryos). (B) Whole-mount *in situ* hybridization for *Shh* expression in E10.5 embryos (lateral view). Loss of *Shh* expression in the preoptic area of *Lrp2*$^{-/-}$ embryos is not rescued in *Lrp2*$^{-/-}$ embryos with reduced *Bmp4* levels (*Lrp2*$^{-/-}$, *Bmp4*$^{tm1blh/+}$ compound mutants).

My results demonstrated successful reduction of *Bmp4* transcript levels in *Lrp2*$^{-/-}$ embryos. However, reduced *Bmp4* levels did not rescue the LRP2-deficient phenotype, suggesting that the increased *Bmp4* expression in *Lrp2*$^{-/-}$ embryos at E9.0 may not be a primary event but a secondary consequence of other alterations (such as loss of *Shh*) during forebrain development in *Lrp2* mutant mice.

4.2.4 The onset of the phenotype in *Lrp2* mutants starts already before neural tube closure

At this point I decided to define more clearly the time point in development when the LRP2 null phenotype sets in. From these investigations I hoped to get a better insights into the primary events induced by receptor deficiency. I focused my analysis on embryonic stages between E6.5 and E8.5 at the transition from gastrulation to neurulation. In these stages, I investigated streak and neural plate formation in the LRP2-deficient embryos by ISH for specific markers of forebrain development.

First I analyzed gastrulation in E6.5 to E7.5 old embryos. At this stage, *Hesx1* marks the anterior visceral endoderm (AVE; arrowhead), which restricts the expression of posterior genes, thereby allowing the anterior epiblast to remain responsive to later neural induction and patterning (C. Lu *et al*., 2001). No difference was seen in *Hesx1* expression in E6.5 *Lrp2*$^{-/-}$ compared with control embryos (Figure 4.2.4 A).

In the early head fold stage at E7.5, *Six3* expression indicates establishment of the forebrain anlagen in the anterior epiblast overlying the anterior mesendoderm. I detected robust *Six3* expression in both genotypes (control and *Lrp2*$^{-/-}$) (arrowhead), indicating that the epiblast in *Lrp2*$^{-/-}$ embryos displays proper forebrain specific gene expression (Figure 4.2.4 A).

Bmp4 expression inhibits forebrain gene expression and forms a gradient from the proximal epiblast, allowing forebrain establishment in the anterior neural ectoderm (Y. Yang *et al*., 2006). In E7.5 old embryos I did not detect significant differences in *Bmp4* expression that shaped a gradient from the extraembryonic ectoderm (arrowhead) comparing control and mutant embryos (Figure 4.2.4 A).

Noggin expression marks the node, which promotes anterior gene expression and is required for normal development of the head primordial also by antagonizing *Bmp4* (S. Ang *et al*., 1994; J. Klingensmith *et al*., 1999). At E7.5, control and *Lrp2*$^{-/-}$ embryos showed the same expression pattern of *noggin* in the node and axial mesendoderm (AME; arrowhead) (Figure 4.2.4 A). The AME is formed from the node and migrates anteriorly to underlie the midline of the neural plate by headfold stage (late E7.5 to E8.0) (Y. Yang *et al*., 2006).

Since no changes in the expression of the key regulatory factors were detected in E6.5 to E7.5 old *Lrp2*$^{-/-}$ embryos in comparison to control littermates, I concluded that gastrulation proceeds normally in LRP2 deficient embryos. Accordingly, I turned my attention to slightly later embryonic stages (E8.0).

Starting with neurulation at E8.0, *Shh* expression marks the axial mesendoderm, including the notochord and prechordal plate (K. Aoto *et al*., 2009). These structures are underlying the neural plate that is developing into the neural tube. *Shh* expression in the notochordal and prechordal plate is believed to promote inductive signals for the overlying developing neural tube. In early E8.0 old *Lrp2*$^{-/-}$ embryos during head fold to somitogenesis transition, no differences were seen in *Shh* expression (Figure 4.2.4 B).

With the onset of neurulation, *Hesx1* expression marks the forebrain anlagen. In E8.0 embryos when the first somite is developing, *Hesx1* expression showed a comparable expression pattern in *Lrp2*$^{-/-}$ and control embryos (Figure 4.2.4 B).

During neurulation, *Six3* expression is important for proper forebrain development as it promotes inductive signals for telencephalic target genes. At E8.0 when somitogenesis has started, a severe reduction in *Six3* expression level was obvious in the neuroepithelium (arrowheads) and prospective forebrain tissue (asterisk) of *Lrp2*$^{-/-}$ embryos in comparison to the controls (Figure 4.2.4 B).

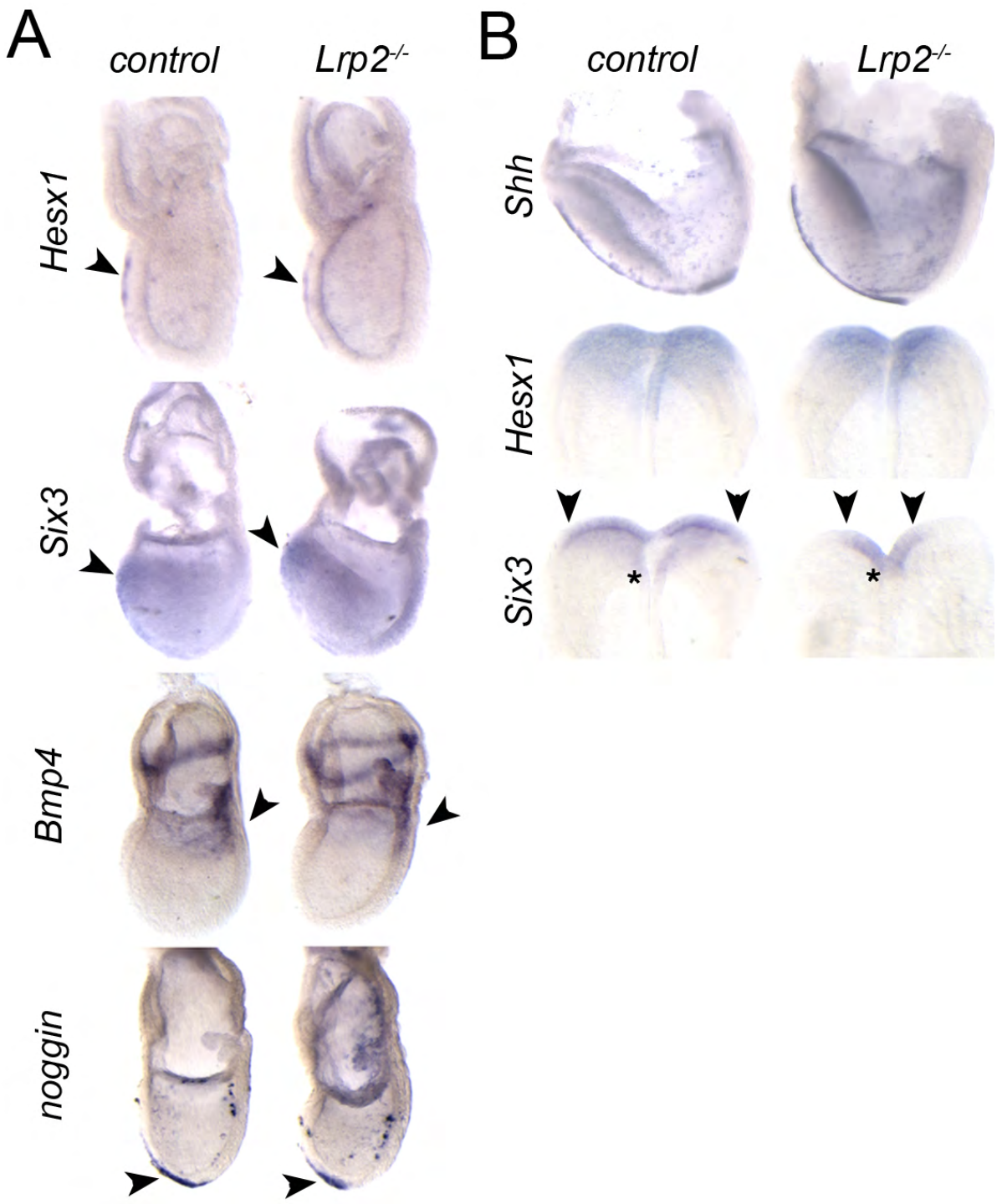
A
control
Lrp2-/-
Hesx1
Six3
Bmp4
noggin
B
control
Lrp2-/-
Shh
Hesx1
Six3
*
*

Figure 4.2.4: Early forebrain development in *Lrp2*$^{-/-}$ embryos. (A) Gastrula to head fold stages of *Lrp2*$^{-/-}$ and control embryos in whole-mount in situ hybridization (ISH). *Hesx1* expression in the AVE (arrowhead) is not changed in *Lrp2*$^{-/-}$ embryos in comparison to control embryos at E6.5. *Six3* is an early forebrain marker and its expression is comparable between control and *Lrp2*$^{-/-}$ embryos at E7.5 (arrowhead). *Bmp4* expression forms a gradient from the proximal epiblast and does not show any changes in *Lrp2*$^{-/-}$ compared to control embryos (arrowhead) at E7.5. *Noggin* expression, which marks the node and AME, exhibits an identical expression pattern in E7.5 control and *Lrp2*$^{-/-}$ embryos (arrowhead). (B) Late head fold to early somitogenesis stages (early E8.0) of *Lrp2*$^{-/-}$ and control embryos in whole-mount in situ hybridizations (ISH). Whole mount ISH for *Shh* does not display obvious changes in the expression pattern between control and *Lrp2*$^{-/-}$ embryos in the lateral view. *Hesx1* expression from a dorsal view is demonstrating the presence of forebrain anlagen in embryos of both genotypes, control and *Lrp2*$^{-/-}$. *Six3* expression is significantly reduced in the neuroepithelium (arrowheads) as well as in the future head region (asterisk) in LRP2-deficient embryos as compared with controls.

The results I obtained from the expression analyses of gastrula stages demonstrated unchanged expression pattern of different marker genes in mutants compared with control embryos. These findings demonstrated that *Lrp2*$^{-/-}$ embryos display normal axis formation and establishment of the forebrain anlagen. Especially the proper anterior-posterior axis formation points to the fact that the HPE phenotype of LRP2-deficient embryos likely develops later and is not caused by a mispatterned body plan.

Already before neural tube closure reduced *Six3* expression in neurulation stages at E8.0 highlight the phenotype onset in *Lrp2*$^{-/-}$ embryos. SIX3 a member of the sine oculis homeobox transcription factor gene family is closely associated with the SHH pathway. In the rostral diencephalon ventral midline (RDVM) a positive regulatory loop between *Six3* and *Shh* operates during patterning processes of the ventral forebrain (X. Geng *et al.*, 2008).

4.2.5 The SHH pathway is the primary pathway affected in *Lrp2*$^{-/-}$ embryos

To find out if the reduced *Six3* expression results from defects in the SHH pathway, I carried out a detailed expression analysis in E8.5 - E9.0 old control and *Lrp2*$^{-/-}$ embryos (Figure 4.2.5 A).

I identified significant changes in the SHH pathway in the mutant embryos. Already at E8.5, LRP2-deficient embryos showed severe defects in the expression pattern of *Shh*. Whereas in control embryos strong *Shh* expression was apparent in the notochord (bracket), the prechordal plate (asterisk) and in the overlying RDVM (dotted line), *Lrp2*$^{-/-}$ embryos showed a reduced *Shh* signal in the RDVM (structure above dotted line) at E8.5. Also at E9.0, expression around the optic stalk (bracket) was significantly reduced in the *Lrp2*$^{-/-}$ embryos in comparison to controls (Figure 4.2.5 A).

This altered *Shh* expression consequently led to altered expression of downstream targets of SHH signaling. For example, the expression of *Gli3*, a repressor for SHH signaling (A. Ruiz i Altaba *et al*., 2003), showed a diffuse gradient formation in the *Lrp2*$^{-/-}$ embryos at E8.5, while there was a more restricted gradient in the control embryos (compare arrowheads, Figure 4.2.5 A). In *Lrp2*$^{-/-}$ embryos, *Gli3* expression was even detectable in the neuroectoderm, which was spared in the control embryos (asterisk, Figure 4.2.5 A). This aberrant gradient formation in mutant embryos became even more pronounced at E9.0, as shown by a more widespread signal for *Gli3* in dorsal regions (arrowhead) and an extension of the signal into ventral regions of the telencephalon (asterisk) in *Lrp2*$^{-/-}$ embryos (Figure 4.2.5 A).

GLI1 acts as a positive mediator of SHH signaling, and SHH induces *Gli1* transcription (A. Ruiz I Altaba, 1999). Already at E8.5, *Gli1* showed significantly reduced expression levels in the neuroepithelium of *Lrp2*$^{-/-}$ embryos in comparison to somite-matched control embryos (Figure 4.2.5 A, arrowhead, seen in 3 individual *Lrp2*$^{-/-}$ embryos in comparison to their control embryos). This defect was still visible in E9.0 *Lrp2* mutants (Figure 4.2.5 A, asterisk) where less *Gli1* expression was visible in the ventral telencephalon of *Lrp2*$^{-/-}$ embryos in comparison to control embryos (Figure 4.2.5 A).

For *Patched1* (*Ptchl*), another downstream target of the SHH pathway, I couldn't detect any difference in the expression pattern at E8.5 between control and *Lrp2*$^{-/-}$ embryos. However, at E9.0 I observed a more diffuse expression pattern,

which reached dorsal areas of the telencephalon in *Lrp2*$^{-/-}$ embryos (expression in the *Lrp2* mutants continues above the line) in comparison to control embryos (Figure 4.2.5 A).

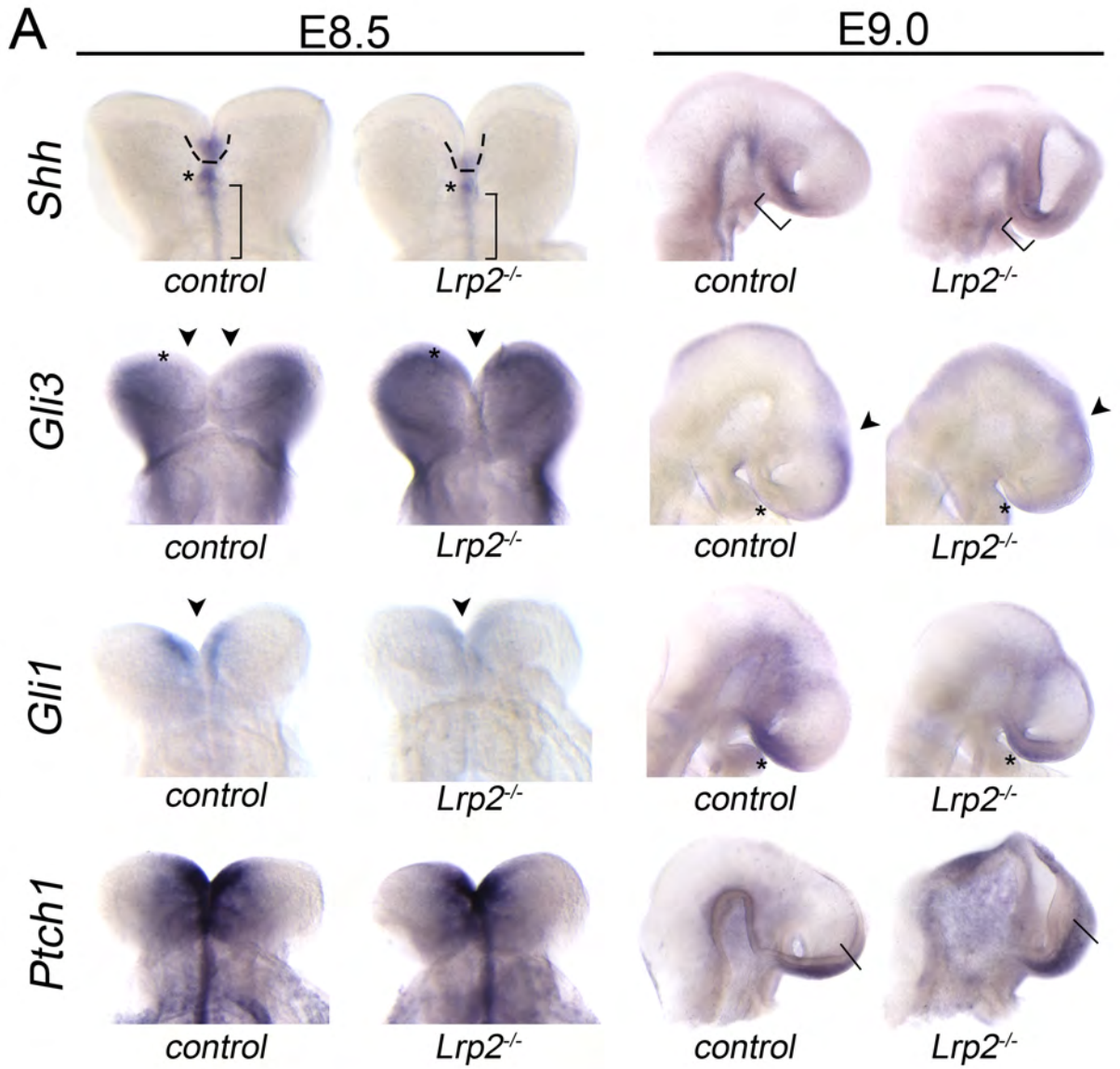

Figure 4.2.5 A: Expression analysis of *Shh* and its downstream targets during early forebrain development. Whole mount ISH for *Shh* indicating reduced expression in the RDVM (above dotted line) overlying the prechordal plate (asterisk) in *Lrp2*$^{-/-}$ embryos at E8.5 (ventral view) in comparison to strong expression in the control. At E9.0 reduced *Shh* expression in the preoptic area (bracket) is detected in *Lrp2* mutants (lateral view). The expression gradient of *Gli3* fails to be established in the *Lrp2*$^{-/-}$ embryos. In *Lrp2*$^{-/-}$ embryos at E8.5, *Gli3* expression reaches the neuroepithelium (asterisk) and spreads closer to the midline region (arrowhead) in comparison to the expression in control embryos. At E9.0 *Gli3* expression in the dorsal telencephalon of *Lrp2*$^{-/-}$ embryos is more diffuse and reaches the ventral telencephalon (asterisk) compared to control embryos. Starting from E8.5, *Gli1* expression in *Lrp2* mutants is significantly down-regulated in the neuroepithelium (arrowhead) compared to controls. This downregulation of *Gli1* expression persists at E9.0 when the expression in the ventral telencephalon is significantly reduced in *Lrp2*$^{-/-}$ embryos in comparison to the control embryos. There is no difference detectable in *Ptch*1 expression at E8.5 in *Lrp2*$^{-/-}$ embryos compared to control embryos. However at E9.0, the expression of *Ptch1* spreads into more dorsal regions of the developing telencephalon (above the line) in mutant embryos compared to control embryos.

To analyze if these changes in the SHH pathway are a direct consequence of LRP2 deficiency or rather caused by altered expression of other important genes that pattern the developing forebrain, I examined the BMP pathway next.

Noggin restricts *Bmp4* expression and inhibits binding of BMP4 to its receptor. At E8.5, *noggin* expression in the axial mesendoderm showed no differences between control and *Lrp2*$^{-/-}$ embryos. However, starting from E9.0 a clear difference in *noggin* expression was visible comparing the different genotypes. While *noggin* expression was spanning the rostral midline along the ventral to dorsal telencephalon in the controls (asterisk) expression of this BMP4 antagonist is reduced and disrupted in *Lrp2* mutant embryos (asterisk) (Figure 4.2.5 B).

Bmp4 is expressed in the developing foregut (fg, lateral view) and midline mesendoderm (mm, lateral view) in E8.5 old embryos (Figure 4.2.5 B). At this early stage, no *Bmp4* expression was detectable in the developing forebrain. The expression in the foregut as well as in the mesendoderm was comparable between control and *Lrp2*$^{-/-}$ embryos. In line with the decreased *noggin* expression in *Lrp2* mutants at E9.0, *Bmp4* showed an increased expression in the dorsal neuroepithelium (arrowheads) as well as a shifted expression in the ventral

telencephalon, sparing the optic stalk area (asterisk) at this embryonic stage (Figure 4.2.5 B).

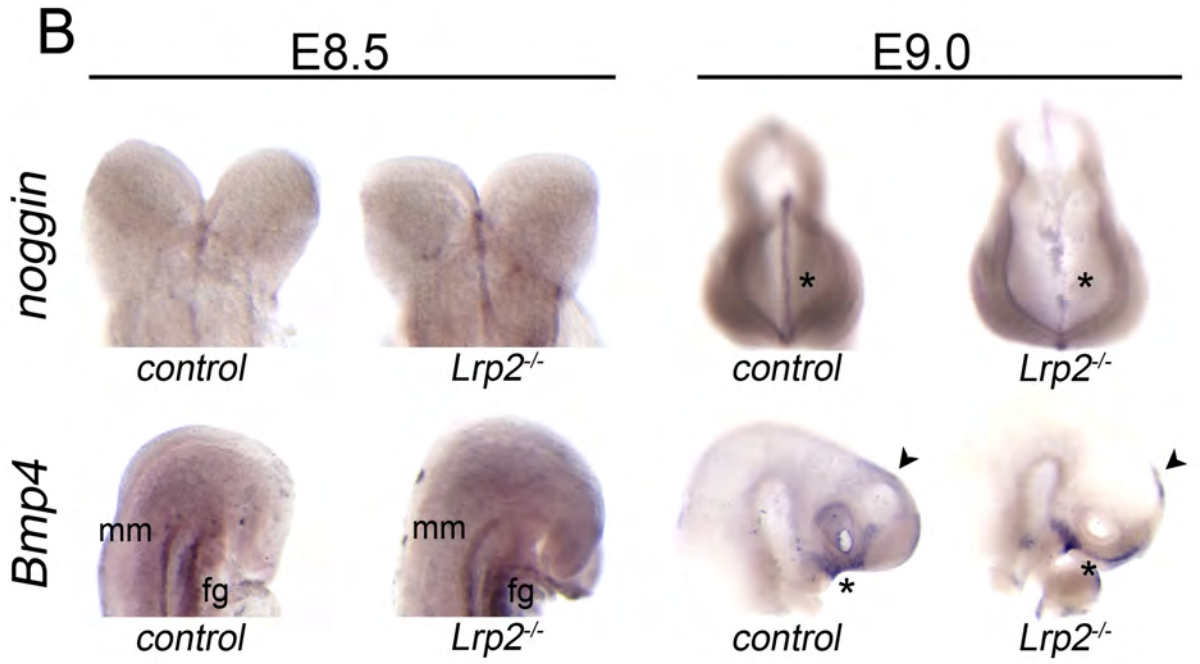

Figure 4.2.5 B: Expression analysis of the BMP pathway during early forebrain development. At E8.5, *Lrp2*$^{-/-}$ embryos display the same expression pattern for *noggin* in the axial mesendoderm as wild type controls (frontal view). At E9.0 however, the expression of *noggin* normally displaying a clear pattern in the ventral midline of the neuroepithelium is disrupted in the *Lrp2* mutant (asterisk), visible in frontal head aspects. At E8.5, *Bmp4* expression in the foregut (fg) and midline mesendoderm (mm, lateral view) is comparable between genotypes. In E9.0 old *Lrp2*$^{-/-}$ embryos, *Bmp4* expression was augmented in the dorsal telencephalon in *Lrp2*$^{-/-}$ embryos (arrowhead). In the ventral telencephalon, expression in the preoptic area is shifted to more rostral areas in *Lrp2*$^{-/-}$ embryos compared with control embryos.

Next, I analyzed the FGF pathway to investigate if the holoprosencephalic phenotype in LRP2-deficient embryos may be caused by changes in this pathway. To do so, I examined the expression pattern of *Fgf8*, a marker of the anterior neural ridge (ANR).

The initial expression of *Fgf8,* visible at E8.5, in the ANR is independent from SHH signaling and comparable between control and *Lrp2*$^{-/-}$ embryos (arrowheads) (Figure 4.2.5 C). At E9.0, the expression of *Fgf8* in the ventral and rostral neuroepithelium is decreased and shifted to more dorsal and caudal regions above the commissural plate (line) in the developing telencephalon of *Lrp2*$^{-/-}$ embryos in comparison to control embryos (Figure 4.2.5 C).

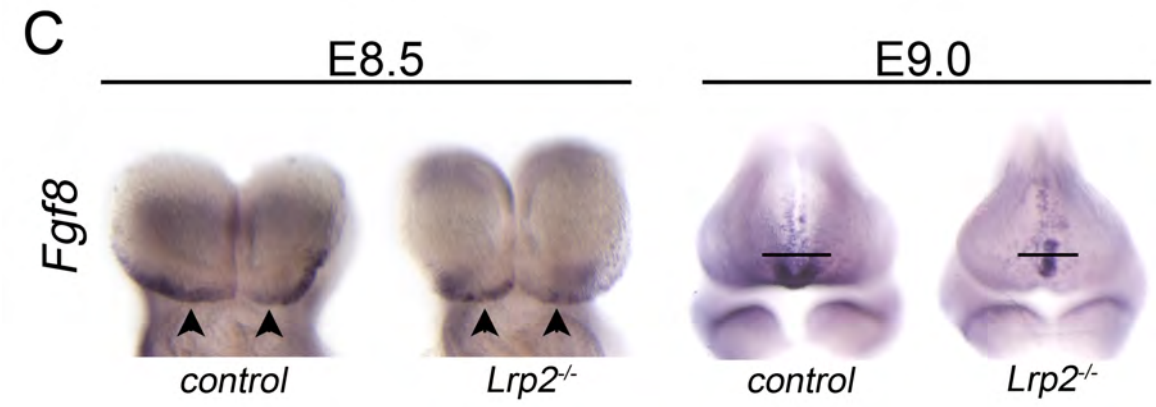

Figure 4.2.5 C: Analysis of the *Fgf8* expression during early forebrain development. Frontal head aspects show normal *Fgf8* expression in *Lrp2*$^{-/-}$ embryos at E8.5 (arrowheads) in comparison to the expression in control embryos. At E9.0, *Fgf8* expression is shifted and extended from the commissural plate along the midline into more dorsal and caudal regions of the forebrain (above the line). Additionally, the expression in the rostral ventral telencephalic area (below the line) is reduced in *Lrp2* mutants compared with control embryos (frontal view).

Based on the data described above, showing that the most pronounced and most earliest changes in *Lrp2*$^{-/-}$ embryos were alterations in SHH and its downstream targets (Figure 4.2.4 B), I concluded that the SHH pathway is the primary target of LRP2 activity in the developing forebrain.

4.2.6 Impaired development of the RDVM in *Lrp2* mutants caused by defects in SHH distribution

In the previous chapter, I demonstrated that *Shh* expression itself as well as the expression of its downstream targets is affected in the *Lrp2*$^{-/-}$ embryos. Changes in the expression pattern of *Shh* and its downstream targets might be caused by an altered SHH protein localization, as former studies demonstrated that correct distribution of SHH protein from the prechordal plate is an important step in establishing *Shh* expression in the overlying neuroepithelium, in particular in the RDVM (X. Huang *et al*., 2007b; X. Geng *et al*., 2008). This information, combined with data obtained in the lab of S. Argraves, that SHH can bind to LRP2 *in vitro* and *in vivo* (R. McCarthy *et al*., 2002; C. Morales *et al*., 2006), makes LRP2 a suitable candidate for controlling the proper SHH protein distribution in the RDVM. To investigate this hypothesis, I first examined SHH protein localization and a possible co-localization with LRP2 in early embryos (Figure 4.2.6 A). Thereafter, I analyzed SHH protein distribution in the prechordal plate and the overlying neuroepithelium in detail. In addition, I investigated the activation of SHH downstream targets in control embryos in comparison to *Lrp2*$^{-/-}$ embryos (Figure 4.2.6 B + C).

At E8.0, SHH was detected in the notochord as well as in the neuroepithelium overlying the notochord in control embryos using immunohistology (indicated by dotted line). In the apical neuroepithelium where LRP2 is also expressed, co-localization of LRP2 and SHH was obvious (Figure 4.2.6 A).

Similarly, in E8.5 old control embryos, SHH protein was visible in the prechordal plate and in the RDVM (above dotted line) showing partial co-localization with LRP2 on the apical side of the neuroepithelium (Figure 4.2.6. A). Co-localization of the two proteins on the apical side of the neuroepithelium (above dotted line) was also confirmed on sections of E8.75 old control embryos (figure 4.2.6. A).

To substantiate my data of a potential co-localization of SHH and LRP2, I also analyzed later embryonic stages. In the neuroepithelium of the ventral midline of E10.5 old control embryos SHH protein strongly co-localized with LRP2. Interestingly, the SHH protein was mainly seen on the apical neuroepithelial surface but nowhere else in the neural tube. On the apical side of the neuroepithelium, SHH strongly co-localized with LRP2 (Figure 4.2.6 A).

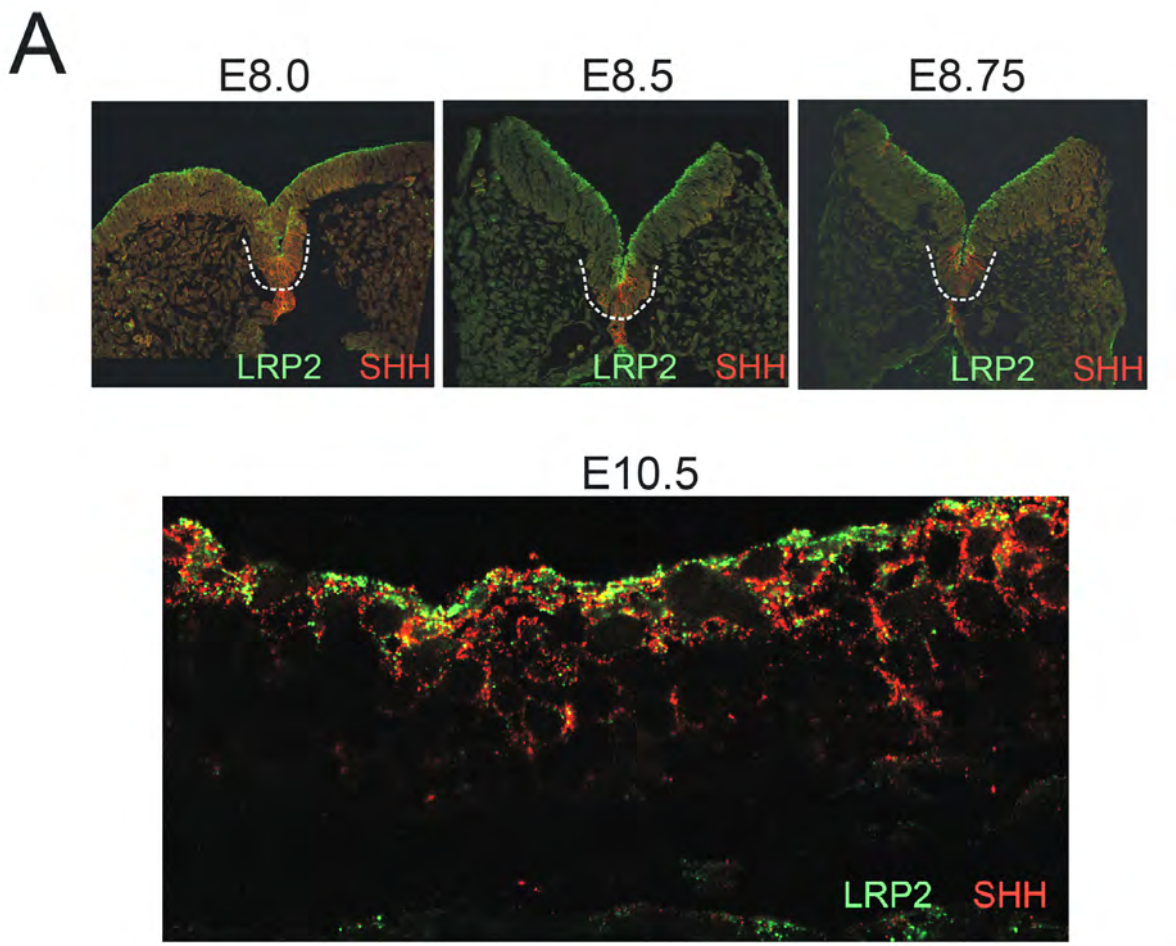

Figure 4.2.6 A: SHH protein co-localizes with LRP2. In coronal sections of E8.0 control embryos, SHH protein (red signal) localized to the prechordal plate (below the dotted line) and the overlying neuroepithelium (above dotted line). On the apical side of the neuroepithelium co-localization with LRP2 (green signal) is visible. At E8.5 the signal for SHH protein in the neuroepithelium is even more significant and co-localization of SHH with LRP2 is detected on the apical surface of the neuroepithelium in coronal forebrain sections. Co-localization of SHH with LRP2 on the apical surface of the neuroepithelium is confirmed in E8.75 control embryos. Finally, in a later embryonic stage at E10.5 a clear co-localization of SHH with LRP2 is demonstrated in the ventral neuroepithelium of the telencephalon in coronal sections.

Co-localization of SHH with LRP2 in control embryos (shown in Figure 4.2.6 A) supported my hypothesis that LRP2 plays a crucial role in proper SHH gradient formation. Therefore, I next investigated SHH protein distribution in *Lrp2*$^{-/-}$ embryos as well.

As shown in Figure 4.2.6 A, SHH protein from the prechordal plate already localized to the overlying neuroepithelium in control embryos at E8.0. At this stage SHH protein was also found in the prechordal plate of *Lrp2*$^{-/-}$ embryos with no apparent difference in signal intensities comparing both genotypes (control and *Lrp2*$^{-/-}$). However, no SHH protein was detected in the overlying neuroepithelium of *Lrp2*$^{-/-}$ embryos (Figure 4.2.6 B).

In the neuroepithelium of E8.5 control embryos a strong signal for SHH protein was discovered. In contrast, SHH protein was not detected in the neuroepithelium of *Lrp2*$^{-/-}$ embryos (Figure 4.2.6 B). Again, expression in the prechordal plate at this stage was comparable between the genotypes (Figure 4.2.6 B).

Starting from E8.75 old embryos, SHH protein was finally also visible in *Lrp2*$^{-/-}$ embryos in the RDVM like in the control embryos (Figure 4.2.6 B).

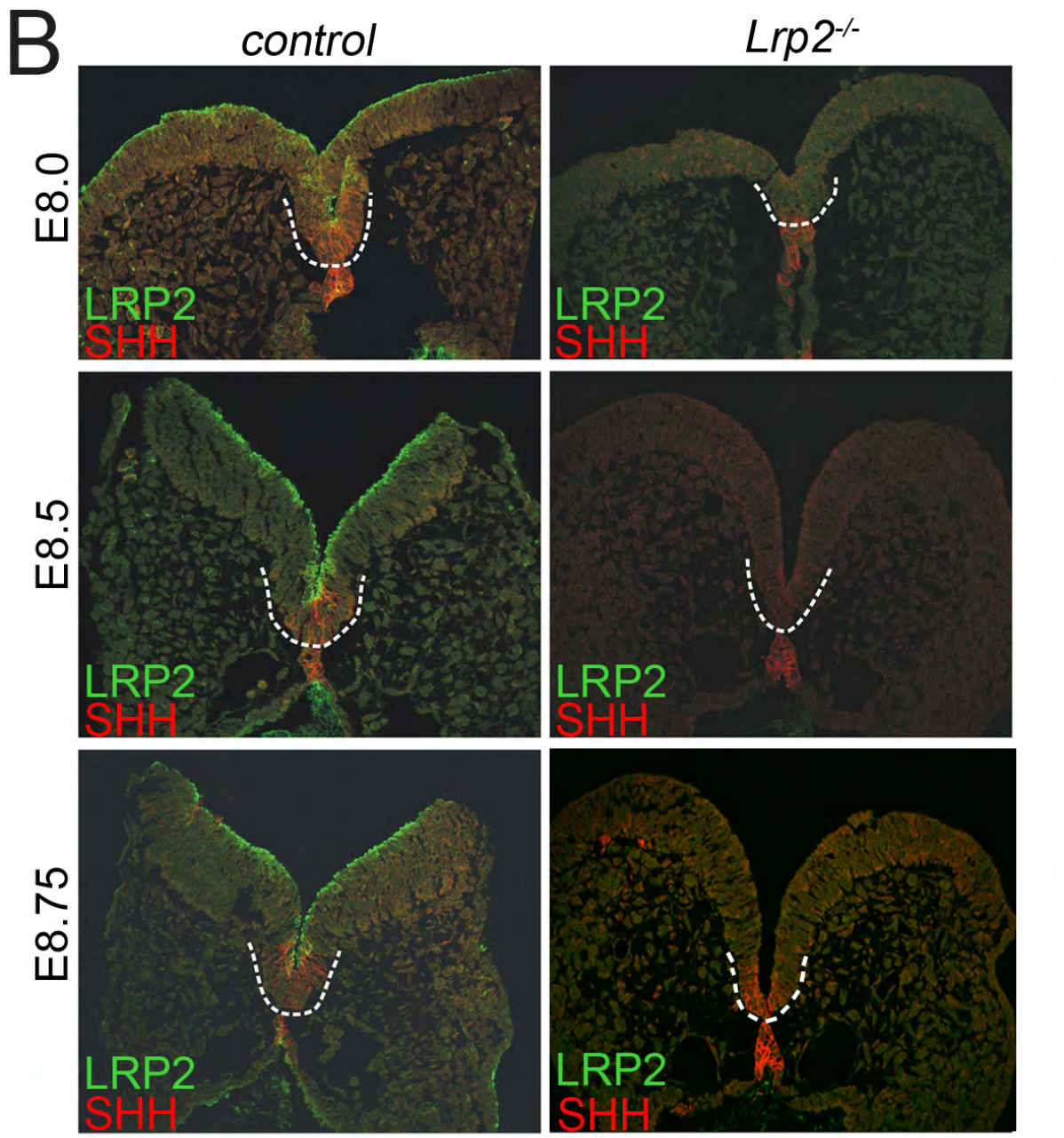

Figure 4.2.6 B: Altered SHH protein distribution in *Lrp2*$^{-/-}$ embryos. Coronal forebrain sections indicate that at E8.0, SHH protein from the prechordal plate localized to the overlying neuroepithelium, namely the RDVM, in control embryos. In contrast no SHH protein was detected in the RDVM of *Lrp2*$^{-/-}$ embryos. In E8.5 old control embryos, robust SHH protein levels are detected in the RDVM. Again, in *Lrp2*$^{-/-}$ embryos at E8.5, the RDVM showed no specific signal for SHH protein. First immuno-signals for SHH protein in the neuroepithelium of *Lrp2*$^{-/-}$ embryos were detected at E8.75.

The above set of experiments showed that there was a delay in SHH protein localization to the rostral neuroepithelium overlying the prechordal plate, a region referred to as RDVM, in *Lrp2*$^{-/-}$ embryos compared to somite-matched controls (Figure 4.2.6 B). It is well known that the RDVM acts as an important organizer for the developing forebrain (X. Geng *et al*., 2008; Y Jeong *et al*., 2008). Accordingly, I speculated that defects in establishing the RDVM might lead to the holoprosencephalic phenotype observed in *Lrp2*$^{-/-}$ embryos. To prove the delayed SHH protein localization and impaired development of the RDVM has an impact on downstream signalling pathways and is consequently causative for the occurance of the forebrain phenotype in LRP2 null embryos, I analyzed the expression of *Shh* and *Six3*, which are known downstream targets of SHH protein in this area (X. Huang *et al*., 2007b; X. Geng *et al*., 2008).

At E8.0 SHH protein from the notochord localized to the overlying neuroepithelium, the RDVM (also see Figure 4.2.6 A). At this early stage, I was unable to detect *Shh* expression itself in the RDVM. However, I detected a robust signal for *Six3* in the neuroepithelium of control embryos. In contrast, *Lrp2*$^{-/-}$ embryos at this stage showed neither SHH protein nor *Shh* mRNA expression, and for *Six3,* I detected a significantly down-regulated signal in the RDVM (Figure 4.2.6 C).

Obviously, in E8.5 control embryos, SHH protein in the RDVM, obviously, activates its own expression, as a robust signal for *Shh* mRNA was displayed and also *Six3* expression continued. In the *Lrp2* mutants, no SHH protein was detected in the RDVM and only low levels of *Shh* mRNA were seen. In addition, *Six3* expression still showed severe down-regulation at E8.5 in mutant mice (Figure 4.2.6 C).

At E8.75, I finally detected SHH protein in the RDVM of *Lrp2*$^{-/-}$ embryos. However, both downstream targets, *Shh* and *Six3,* displayed significantly reduced expression levels. In contrast, the control embryos showed not only robust SHH protein levels but also strong *Shh* and *Six3* expression (Figure 4.2.6 C).

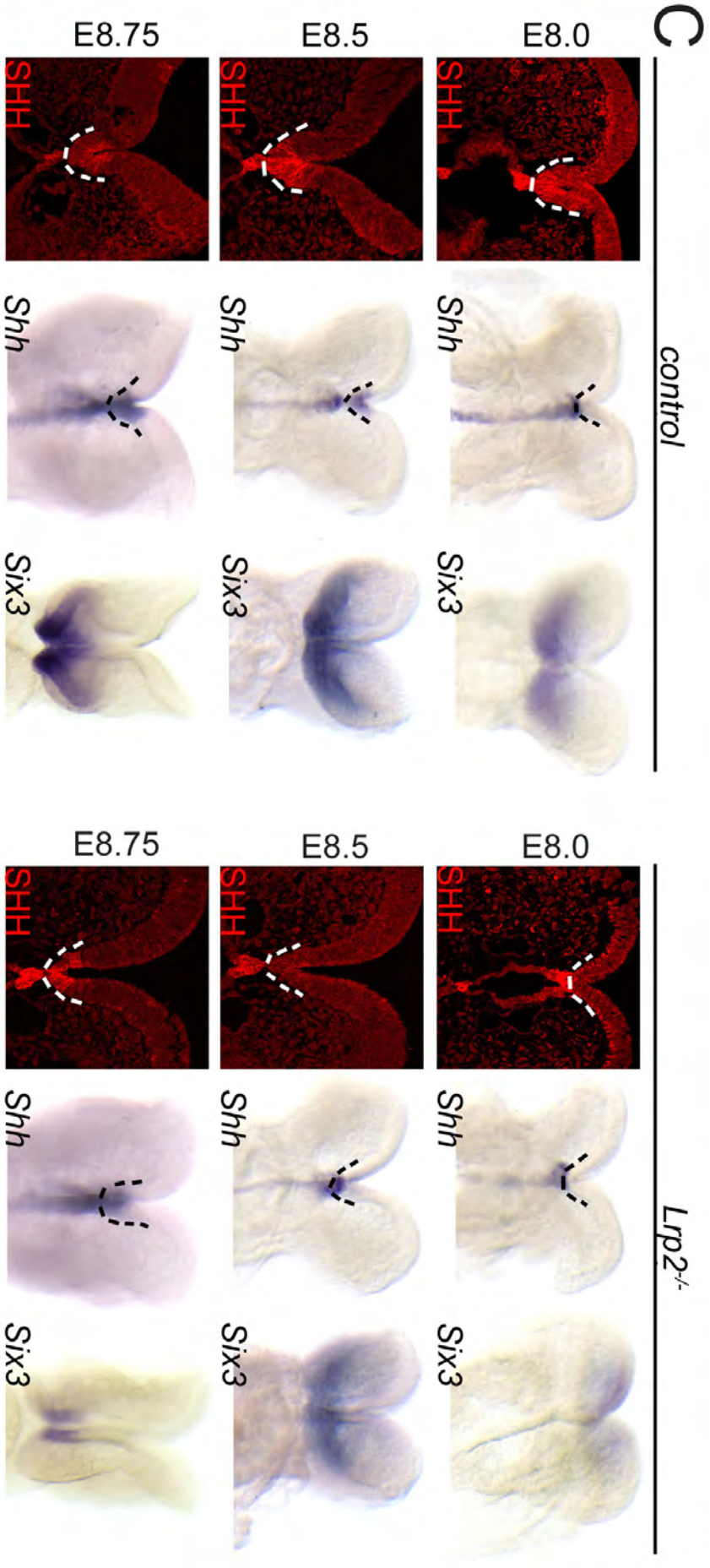
C
E8.75
E8.5
E8.0
SHH
Shh
Six3
control
Lrp2-/-

Figure 4.2.6 C: Impaired development of the RDVM in LRP2-deficient embryos. At E8.0, SHH protein localizes to the neuroepithelium in control embryos (coronal sections) but *Shh* mRNA expression itself cannot be detected yet (frontal view). *Six3* is robustly expressed in the RDVM in wild type embryos at E 8.0 (frontal view). In *Lrp2*$^{-/-}$ embryos, SHH protein fails to be established in the neuroepithelium. Similar to controls, *Shh* expression is not visible yet, but strongly reduced *Six3* expression levels are apparent in the mutant embryos at E 8.0. In E8.5 old control embryos, SHH protein and mRNA is found in the RDVM accompanied by a strong expression of *Six3*. In contrast to the control, in the *Lrp2*$^{-/-}$ E8.5 embryos SHH protein and its mRNA fail to be established in the RDVM. Consequently *Six3* expression is dramatically down-regulated. At E8.75, SHH protein is finally detected in the RDVM of *Lrp2*$^{-/-}$ embryos with an expression level comparable to control embryos, but the *Shh* mRNA signal is still reduced. Moreover, *Six3* expression levels are significantly lower in E8.75 *Lrp2*$^{-/-}$ embryos as compared with controls (magnification of sections: x40).

The results presented so far suggested a delay in the initial establishment of SHH protein in the RDVM and, subsequently, down-regulation of *Shh* and *Six3* expression in *Lrp2*$^{-/-}$ embryos. A delay in SHH protein localization from the prechordal plate to the overlying neuroepithelium would also explain the early changes in *Six3* expression detected already at E8.0 in receptor-deficient mice (Figure 4.2.4 B).

4.2.7 Defect in establishment of an early ventral midline in *Lrp2*$^{-/-}$ embryos

It has been reported that in HPE the cerebral hemispheres fail to separate along the midline due to a failure of midline induction (E. Monuki, 2007). Starting from E8.0, the RDVM in *Lrp2*$^{-/-}$ embryos fails to develop properly (Figure 4.2.6 B + C). Thus, my next aim was to investigate how this delay in SHH protein localization to the RDVM and subsequent loss of target gene expression may affect forebrain patterning after neural tube closure. Therefore, I analyzed control and *Lrp2*$^{-/-}$ embryos at E10.5 and compared localization of SHH protein and *Shh* transcript in the ventral midline of the neuroepithelium in more detail. I also tested expression of *Gli3*, a repressor of the SHH pathway (A. Ruiz i Altaba *et al*., 2003) and of *Bmp4*, both known to be inhibited by the SHH pathway (X. Huang *et al*., 2007a).

Strong signals for SHH protein (Figure 4.2.7 a + c) and *Shh* mRNA (Figure 4.2.7 e) were found in the ventral neuroepithelial midline in the anterior part of the diencephalon of control embryos at E10.5. In the overview, a strong signal for SHH protein was also detected in the *zona limitans intrathalamica* (ZLI) (Figure 4.2.7 a; asterisk) in these sections. In *Lrp2*$^{-/-}$ embryos, SHH protein level in the ZLI was comparable with signal intensity in somite-matched control embryos (Figure 4.2.7 b; asterisk) but the protein failed to establish in the ventral midline of the diencephalic neuroepithelium (Figure 4.2.7 d). This defect was also seen when looking at the corresponding *Shh* mRNA levels (Figure 4.2.7 f). Remarkably, SHH protein and *Shh* mRNA were seen in more lateral regions of the developing diencephalon in mutants. This region was analyzed in more detail by investigating the expression pattern of *Bmp4*, which is negatively regulated by SHH and of *Gli3*, a repressor of the SHH pathway. Interestingly, missing *Shh* expression in the ventral midline (Figure 4.2.7 f) in *Lrp2*$^{-/-}$ embryos led to the upregulation of *Bmp4* (Figure 4.2.7 h) and *Gli3* expression (Figure 4.2.7 j) (both provided by Oleg Lyubinskiy) in exactly this area, while there were no signals detectable in the control embryo.

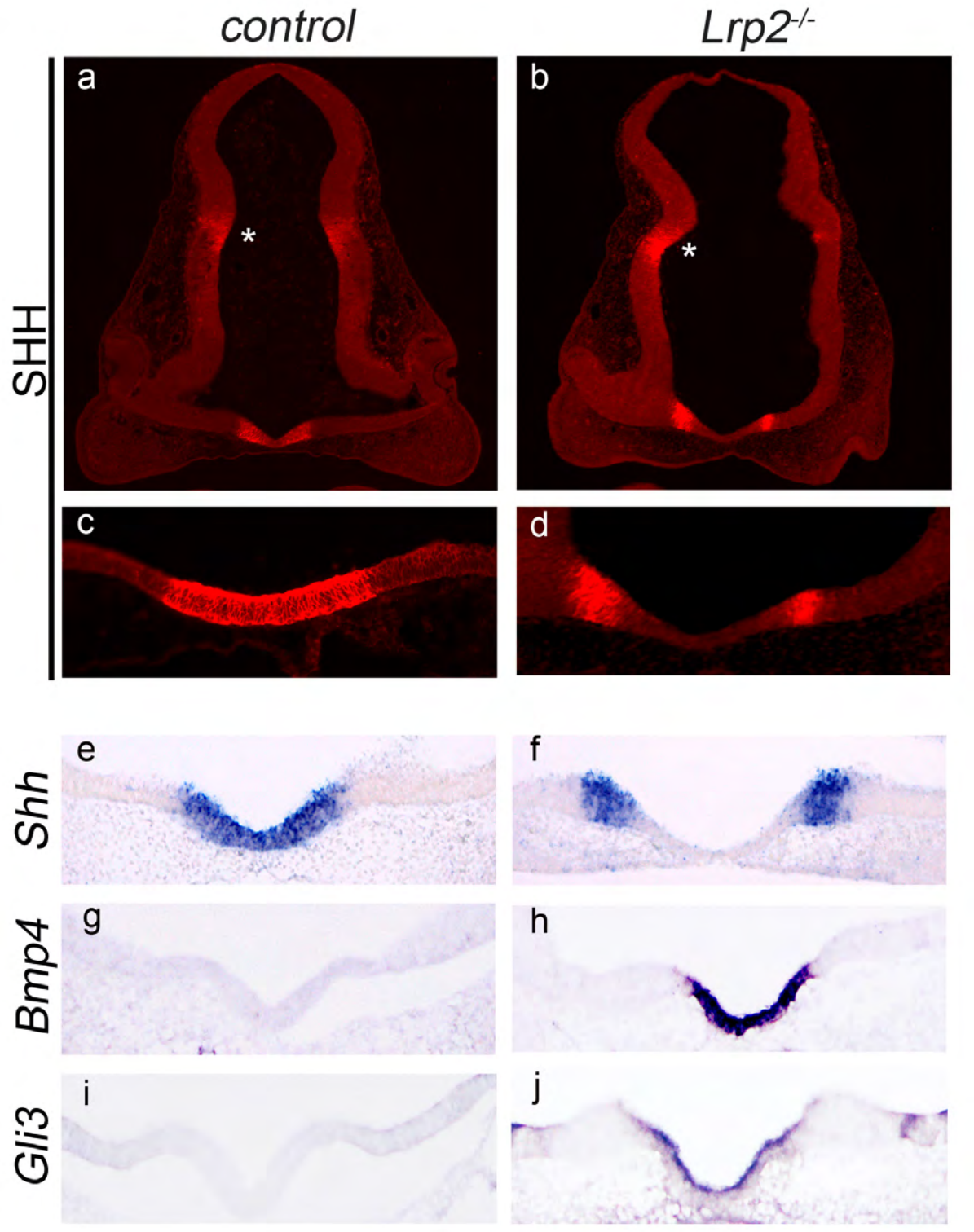
control
Lrp2-/-
SHH
a
b
c
d
Shh
e
f
Bmp4
g
h
Gli3
i
j

Figure 4.2.7: Malformation of the ventral neuroepithelial midline in E10.5 *Lrp2*$^{-/-}$ embryos. (a-f) Expression domains for SHH in control (a, c, e), and LRP2-deficient embryos (b, d, f). Distribution of SHH protein in the overview shows signals in the ventral neuroepithelial midline and in the ZLI (asterisk) of control embryos (a, magnification: x4). SHH protein (c) and *Shh* mRNA (e) signals overlap in the ventral midline at the level of the optic stalk in the control as shown in higher magnification micrographs (magnification: x20). Although there is a comparable signal for SHH in the ZLI in *Lrp2*$^{-/-}$ embryos (b; asterisk), in the immediate ventral midline of the diencephalon, SHH protein (d) and mRNA (f) are lost in the mutants. Rather, SHH protein localization as well as *Shh* expression shifts laterally. (g-j, provided by Oleg Lyubinskiy) *Bmp4* expression normally restricted to the dorsal midline is absent in the ventral midline of the rostral diencephalon in control embryos (g). In contrast, strong ectopic *Bmp4* expression in the ventral midline at the level of the optic stalk is now detected in *Lrp2*$^{-/-}$ embryos (h). *Gli3*, a repressor of the SHH pathway, is absent in areas where strong *Shh* expression occurs, such as in the ventral midline in control embryos (i). However, in *Lrp2*$^{-/-}$ embryos *Gli3* expression was detectable in this area (j).

The results described above suggested a midline defect in *Lrp2*$^{-/-}$ embryos, which is obvious already at E8.0 in the RDVM (Figure 4.2.6 A+B) and which manifests itself during subsequent developmental stages resulting in abnormal patterning of the ventral midline in affected embryos (Figure 4.2.7). Likely, the failure of establishment of RDVM is the reason for the holoprosencephalic phenotype in *Lrp2*$^{-/-}$ embryos. The loss of *Shh* expression in the ventral telencephalon at E10.5 (shown in Figure 4.2.2) might be a consequence of the lost *Shh* expression in the rostral ventral midline of the diencephalon, since it is known hat *Shh* expression in the ventral diencephalon acts in patterning of the telencephalon in concert with the downstream activator *Nkx2.1* (J. Ericson *et al*., 1995).

4.2.8 Analysis of the SHH signaling pathway in *ex vivo* model systems

So far my findings suggested a role for LRP2 in proper formation of the SHH signaling domain in the RDVM. However, the molecular and biochemical details of this defect were still unknown. In one scenario, LRP2 may be required for proper activity of the SHH signaling cascade downstream of Smoothened, the cognate SHH

receptor. To test this hypothesis and to study whether neuroepithelial cells lacking LRP2 are still responsive to the morphogen, I established two different *ex vivo* model systems.

Cephalic explants are an ideal model system to study the neuroepithelial SHH pathway in the context of organotypic structure and function.

I successfully established the preparation of these explants in the lab. To generate cephalic explants, heads from E9.5 mouse embryos are cut at the level of rhombomeres (r) r4/ r5. The otic vesicles are taken as a caudal reference. Following this step, the neural tube is opened along the dorsal midline (roof plate) by cutting from a caudal to rostral direction until the level of the *lamina terminalis* (Figure 4.2.8 A). To unfold the head, the floor plate is cut at the level of the cephalic flexure. The cephalic explants are transferred to sterile Petri dishes and placed on floating polycarbonate membrane filters in DMEM culture medium. They are cultured for 24 hours (hrs) before further analysis such as whole mount ISH. In my hands, cephalic explants displayed the proper expression pattern of *Shh* after 24 hrs in culture. Notably, they showed expression of *Shh* in the preoptic area (Figure 4.2.8 A; asterisk) indicating their suitability as experimental tool to investigate this expression domain in *Lrp2*$^{-/-}$ embryos.

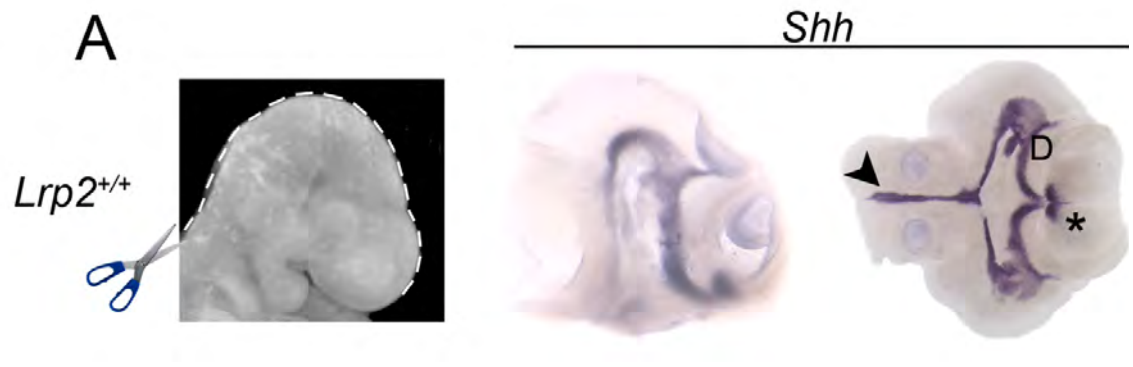

Figure 4.2.8 A: Cephalic explants as a tool for manipulating the SHH pathway in *Lrp2*$^{-/-}$ embryos. (A) Preparation of cephalic explants for whole mount ISH. The preparation of an E9.5 old cephalic explant is indicated. After opening the head along the dorsal midline the tissue is transferred on membrane filters and kept in culture for 24 hrs. *Shh* expression in the head of an embryo at E10.5 in comparison to the expression pattern of *Shh* visible in an E10.5 old cephalic explant. The cephalic explant is prepared from an E9.5 old embryo and kept in culture for 24 hrs. *Shh* expression is detected in the ventral neural tube (arrowhead) as well as in the ventral diencephalon (D) and the preoptic area (asterisk).

Analysis of control and *Lrp2*$^{-/-}$ cephalic explants recapitulated the specific loss of *Shh* expression in the ventral telencephalon in the preoptic area of *Lrp2*$^{-/-}$ embryos seen in utero before (Figure 4.2.8 B; -SAG; asterisk).

During 24 hrs of incubation, cephalic explants of control and *Lrp2*$^{-/-}$ embryos were treated with the Smoothened Agonist (SAG). SAG is a small molecule that activates the SHH receptor Smoothened and therefore activates the SHH intracellular signaling pathway and *Shh* expression itself (J. Chen *et al*., 2002). Because SHH can induce its own expression, SHH activity in the diencephalon not only precedes but is positively regulating *Shh* expression in the telencephalon at E 10.5 in control embryos (J. Ericson *et al*., 1995), a mechanism that does not occur in *Lrp2*$^{-/-}$ embryos. Addition of SAG might rescue the expression of *Shh* in the preoptic area, when the cells in this area are still able to respond to activation of the SHH pathway, because SAG directly activates Smoothened and thereby *Shh* expression.

Control cephalic explants treated with SAG for 24 hrs displayed normal *Shh* expression similar to control cephalic explants not treated with SAG (Figure 4.2.8 B). Cephalic explants prepared from *Lrp2*$^{-/-}$ embryos showed no expression of *Shh* in the telencephalon after one day in culture confirming the complete loss of telencephalic SHH signaling at E10.5 shown previously in whole mount ISH experiments. After SAG treatment however, I detected significant expression of *Shh* in the telencephalon of mutant explant cultures (Figure 4.2.8 B; asterisk). Out of a total of 15 mutant embryos treated, 28% of *Lrp2*$^{-/-}$ cephalic explants showed a rescue of *Shh* expression in the specific area of the telencephalon (Figure 4.2.8 B).

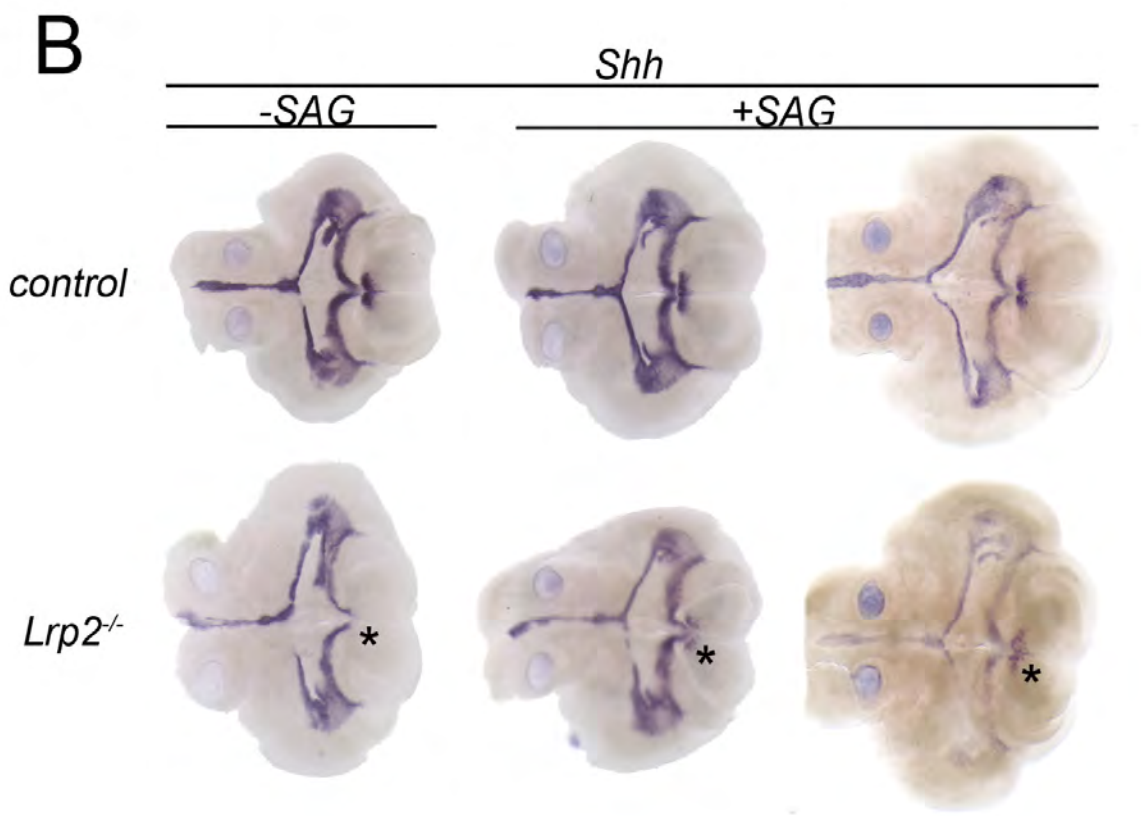

Figure 4.2.8 B: Cephalic explants as a tool for manipulating the SHH pathway in *Lrp2*$^{-/-}$ embryos. (B) Whole mount ISH of *Shh* in cephalic explants prepared from control and *Lrp2*$^{-/-}$ embryos and treated with or without SAG. *Lrp2*$^{-/-}$ cephalic explants show specific loss of *Shh* expression in the telencephalon (-SAG; asterisk), while more caudal parts of the neuroepithelium are unaffected. After 24 hrs in culture supplied with SAG, *Lrp2*$^{-/-}$ cephalic explants displayed a rescue of *Shh* expression in the preoptic area (asterisk) similar to the situation seen in control cephalic explants with or without SAG.

Cephalic explant cultures demonstrated that *Shh* expression in the preoptic area could be rescued by activating the intracellular signaling cascade of the SHH pathway. The fact that the ventral neuroepithelium of LRP2-deficient embryos can resume *Shh* transcription after SAG treatment shows that these cells are still responsive to Smoothened activation.

To confirm and substantiate this important finding, I established and tested a second *ex vivo* system of whole embryo cultures.

To prepare whole embryo cultures, E7.0 to E7.5 embryos were isolated and cultured for 24 hrs in whole embryo culture serum. During isolation of the embryos, it was important to fully remove tissue from the mother but not to destroy the yolk sac as damage to the yolk sac will result in malformed embryos. These isolated embryos were cultured for 24 hrs in whole embryo culture serum loaded with 200 nM SAG (Figure 4.2.9 A).

Effects of SAG application were analyzed in whole mount ISH for *Six3* expression. *Six3* is a known downstream target of SHH signaling, and *Six3* expression was significantly reduced throughout early embryonic development in *Lrp2*$^{-/-}$ embryos in the neuroepithelium compared with control embryos (Figure 4.2.9 B). Treatment with SAG was expected to rescue the reduced *Six3* expression in *Lrp2*$^{-/-}$ embryos.

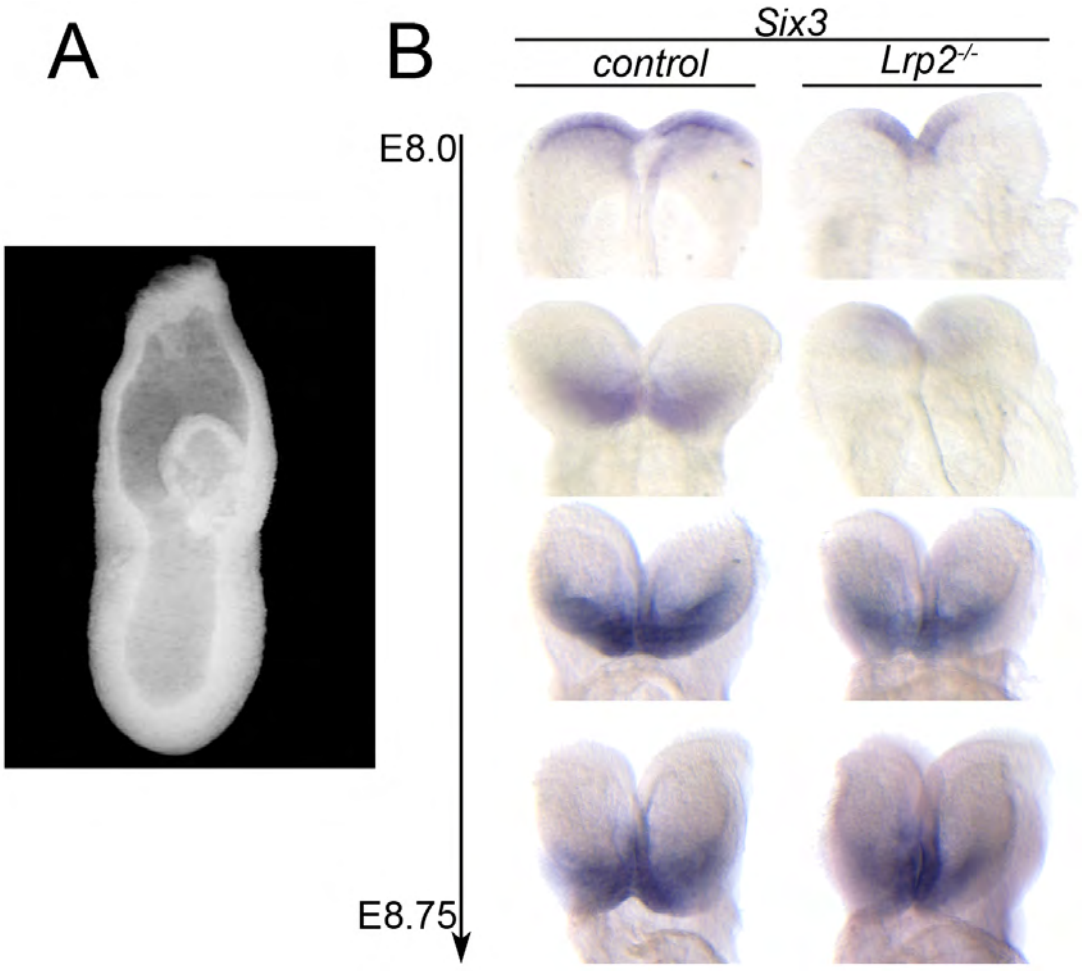

Figure 4.2.9 A + B: *Six3* expression as a readout for SHH pathway activation. (A) Picture of an isolated E7.5 old embryo for incubation in whole embryo culture experiments. During preparation it was important not to destroy the yolk sac, as damage to the yolk sac will result in malformed embryos. (B) Neuroepithelial *Six3* expression, specifically in the RDVM, is strongly reduced in *Lrp2*$^{-/-}$ embryos in comparison to control embryos throughout early embryonic forebrain development.

SAG can freely diffuse through the yolk sac and access the neuroepithelium to activate Smoothened. My aim was to investigate if the SAG treatment could activate the SHH pathway and consequently lead to higher *Six3* expression in the developing forebrain of *Lrp2*$^{-/-}$ embryos.

Control embryos, developed in a whole embryo culture, showed robust expression of *Six3* (Figure 4.2.10 A; -SAG; E8.5 and E8.75). Expression of *Six3* in *Lrp2*$^{-/-}$ embryos was significantly downregulated as shown for two different embryonic stages (E8.5 and E8.75), prepared for ISH after 24 hrs in culture without SAG (Figure 4.2.10 A; -SAG; E8.5 and E8.75).

After 24 hrs in culture supplied with SAG, control embryos demonstrated strong *Six3* expression (Figure 4.2.10 A; +SAG; E8.5 and E8.75). Also, *Lrp2*$^{-/-}$ embryos treated in culture with SAG displayed distinctly stronger *Six3* expression levels than *Lrp2*$^{-/-}$ embryos treated without SAG (Figure 4.2.10 A; +SAG; E8.5 and E8.75). In fact, *Six3* expression levels in the developing forebrain in *Lrp2*$^{-/-}$ embryos almost reached expression levels comparable to control embryos. Out of a total of 20 treated *Lrp2*$^{-/-}$ embryos, 55% showed a rescue in *Six3* expression.

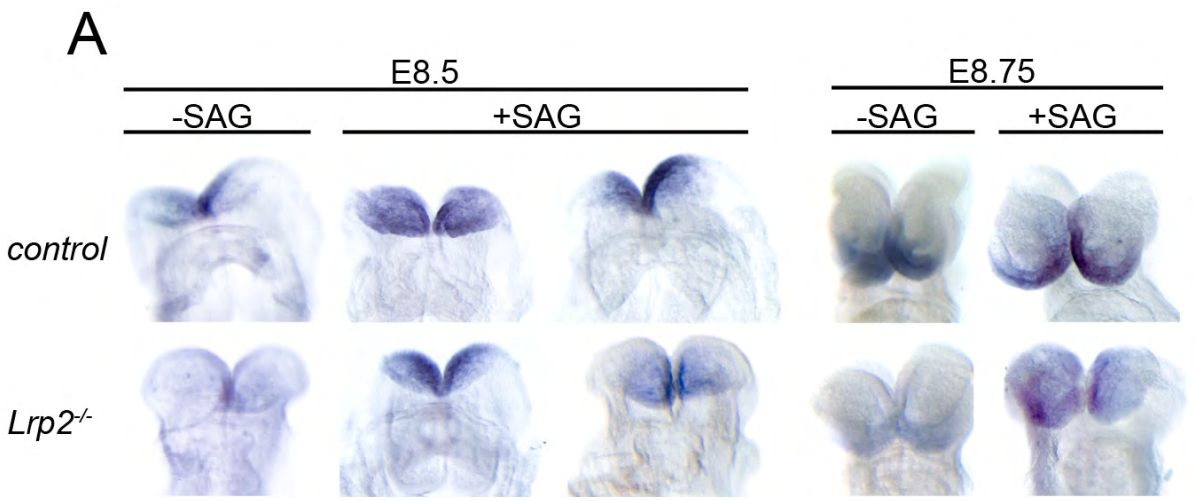

Figure 4.2.10 A: Whole embryo culture as a tool for manipulating the SHH pathway in *Lrp2*$^{-/-}$ embryos. (F) Whole mount ISH demonstrating *Six3* expression in control embryos as well as in *Lrp2*$^{-/-}$ embryos from whole embryo culture experiments with and without SAG. *Six3* expression is significantly decreased in *Lrp2*$^{-/-}$ embryos in comparison to control embryos developed in whole embryo cultures without SAG at E8.5 and E8.75. In contrast, *Lrp2*$^{-/-}$ whole embryo cultures supplied with SAG show increased *Six3* expression levels in the developing forebrain in comparison to LRP2-deficient embryos incubated without SAG.

In summary these data were in line with my results from cephalic explant cultures discussed above. In both models, the prospective forebrain region of *Lrp2*$^{-/-}$ embryos consisted of cells that were still responsive to signals activating the SHH pathway via Smoothened. Therefore, the defect in *Lrp2*$^{-/-}$ embryos that leads to impaired forebrain patterning had to be placed upstream of the intracellular signaling cascade, likely at the level of SHH binding to Patched1 to release its inhibitory effect on Smoothened.

4.2.9 Binding of SHH to LRP2

Based on the findings described above it is conceivable that LRP2 directly acts as a receptor for SHH in the developing forebrain. Since the intracellular signaling cascade of the SHH pathway was still responsive and functional upon activation it is plausible that loss of LRP2 rather affects the spatial and temporal gradient formation of SHH and consequently signaling through SHH. Previous studies using BIAcore assays and uptake studies in BN16 cells and in efferent duct epithelial cells already demonstrated that SHH binds to LRP2 (R. McCarthy *et al*., 2002; C. Morales *et al*., 2006).

To examine a direct interaction between LRP2 and SHH in more detail, I first performed cell culture experiments. My aim was to verify binding of SHH to LRP2 extending the findings described before and to establish binding conditions that could be transferred to experiments in whole embryo cultures subsequently. Ultimately, I wanted to demonstrate, that also in the neuroepithelium LRP2 is a functional receptor for SHH.

For assaying binding of SHH to LRP2, Brown Norway rat yolk sac carcinoma cells (BN16 cells) were used. These cells express LRP2 at high levels.

BN16 cells were incubated for 2 hrs with either GST-SHH-N fusion protein produced in bacteria (R. McCarthy *et al*., 2002) or recombinant amino-terminal SHH fragment (SHH-N) obtained commercially from R&D systems.

Before I used these proteins in binding assays, I tested their integrity and quality in Western blot analyses. By using an antibody directed against SHH, both GST-SHH-N and SHH-N protein were detected in the respective protein preparations (Figure 4.2.11). The recombinant SHH-N protein had a size of 19 kDa (asterisk) while the GST-SHH-N migrated around 50 kDa (arrowhead). An antibody against GST only detected the fusion protein GST-SHH-N (arrowhead) but not SHH-N.

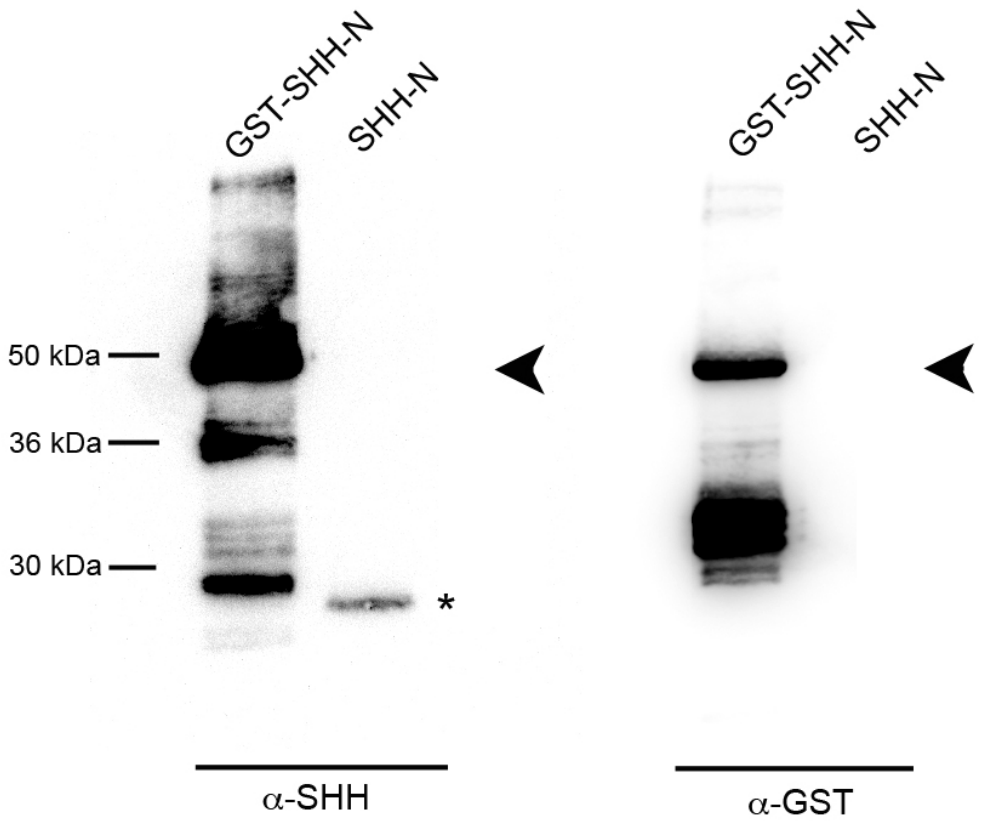

Figure 4.2.11: Western blot analysis of recombinant SHH proteins: 12,5 ng/μl of recombinant SHH-N protein were subjected to Western blot analysis. SHH-N protein was detected using an antibody directed against SHH and migrated at the expected size of 19 kDa (asterisk). To detect the GST-SHH-N fusion protein 3,1 μg/μl of the protein were subjected to Western blot analysis. The GST-SHH-N fusion protein was detected with both antibodies, against the SHH epitope and against the GST epitope, at an expected size of 50 kDa (arrowhead).

Using these two proteins in binding assays, I demonstrated binding of GST-SHH-N and SHH-N, respectively, to BN16 cells (Figure 4.2.12). I was able to detect binding of GST-SHH-N to BN16 cells using both antibodies against GST and SHH. Binding of recombinant SHH-N was demonstrated using an antibody against SHH.

Cellular binding and uptake of both SHH preparations could be blocked by co-incubation of the cells with receptor associated protein (RAP). RAP is an endogenous inhibitor of ligand binding to LRP2 and was shown previously also to block interaction of SHH with this receptor (S. Williams *et al*., 1992; C. Morales *et al*., 2006).

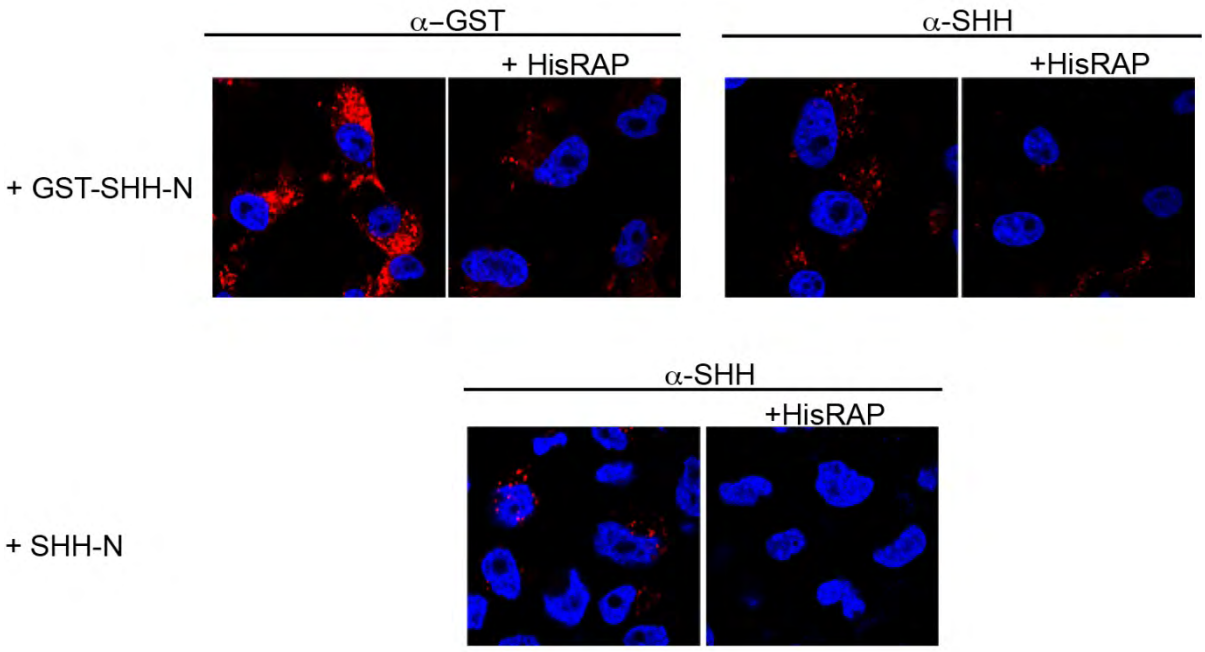

Figure 4.2.12: BN16 cells bind SHH. Cell culture experiments demonstrate binding of a GST-SHH-N fusion protein or recombinant SHH-N to BN16 cells expressing LRP2. Binding of GST-SHH-N to cells was detected by antibodies against the GST epitope or against the SHH epitope. Recombinant SHH-N protein binding was detected using the anti SHH antibody. Binding of GST-SHH-N and of SHH-N was inhibited by co-incubation with the LRP2 antagonist receptor-associated protein (RAP) indicating that SHH binding to BN16 cells is mediated via this receptor. (magnification: x63).

Having demonstrated the ability of LRP2 expressing BN16 cells to bind SHH, I also wanted to show binding of SHH to LRP2 in whole embryo culture experiments, here specific in the neuroepithelium.

I isolated E8.0 embryos and opened the yolk sac as well as the amnion. The embryos were incubated in DMEM with 1,5% BSA supplied with 5 μg/ml GST-SHH-N or 2,5 μg/ml recombinant SHH-N. After an incubation period of 2 hrs, I investigated binding of SHH to the neuroepithelium of the neural folds in control embryos and *Lrp2*$^{-/-}$ embryos (Figure 4.2.13) using immunohistology.

LRP2 is strongly expressed on the apical side of the neuroepithelium in control embryos, while the receptor was absent in the neuroepithelium in *Lrp2*$^{-/-}$ embryos. On the same coronal forebrain sections, where LRP2 localization was shown, binding of GST-SHH-N as well as recombinant SHH-N was demonstrated in the

neuroepithelium of control embryos. In contrast no binding of GST-SHH-N or SHH-N was detected in the neuroepithelium of *Lrp2*$^{-/-}$ embryos.

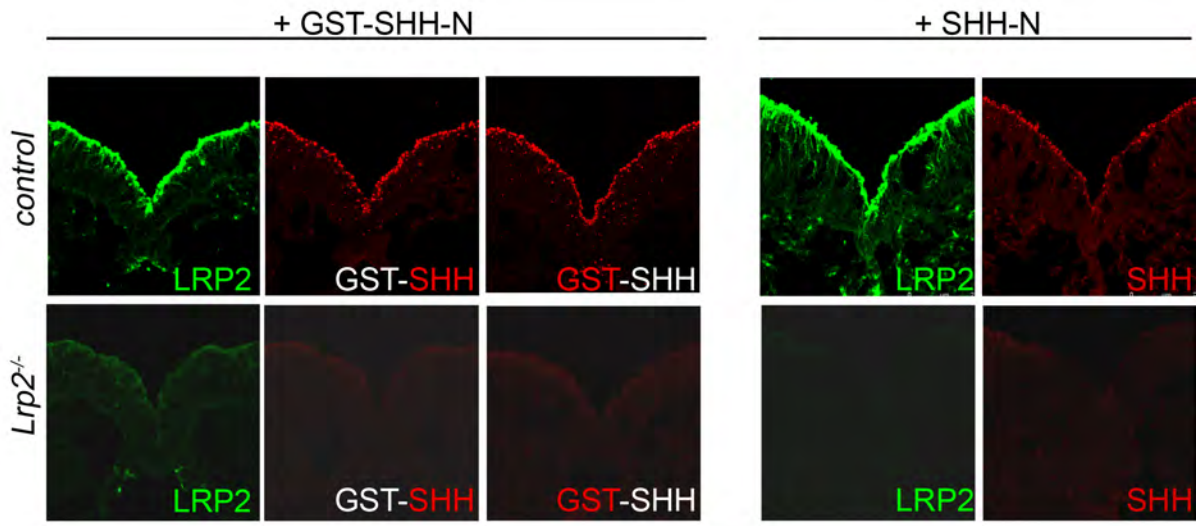

Figure 4.2.13: SHH binds to the neuroepithelium of control but not of *Lrp2*$^{-/-}$ embryos. Strong apical localization of LRP2 is demonstrated on coronal sections of the forebrain in control embryos whereas there is no signal detectable in sections of *Lrp2*$^{-/-}$ embryos. In the neuroepithelium of control embryos on the same section, strong binding of GST-SHH-N was detected using an antibody against SHH. On a different section of the same embryo binding of SHH to the neuroepithelium was confirmed by using an antibody against GST. In whole embryo cultures treated with recombinant SHH-N, LRP2 was detected on the apical side of the neuroepithelium. On the same section, binding of recombinant SHH-N to the neuroepithelium was demonstrated using an antibody against SHH.

My results uncovered a direct role for LRP2 in binding of SHH and subsequently forwarding the SHH signal to Patched to release its inhibitory effect on Smoothened and to activate the signal transduction pathway. Apparently, binding of SHH to LRP2 is an important step in establishing the proper gradient formation of SHH in the RDVM and thereby establishing the organizer function of this specific area during early forebrain development. Loss of LRP2 function causes a delayed establishment of SHH protein in the RDVM and results in ventral patterning defects in the neuroepithelium of the developing forebrain and consequently causes HPE.

5. Discussion

In my thesis, I have characterized the role for LRP2 in forebrain development using LRP2 receptor-deficient mouse embryos. The generation of LRP2-deficient mice has been described before (T. Willnow *et al*., 1996). These studies have uncovered the crucial contribution of this receptor to proper forebrain patterning and to HPE in the receptor-deficient mouse. However, the exact mechanism whereby LRP2 controls neural tube specification and forebrain formation remained enigmatic. Now, temporal and functional analyses performed in my thesis project demonstrate that the SHH pathway is the primary target of LRP2 activity. My data show that, LRP2 regulates the correct distribution of SHH in the early ventral prosencephalon, likely by acting as a cell surface receptor for this morphogen. LRP2-mediated sequestration of SHH on target cells may facilitate signaling via the Patched and Smoothened receptor pathway. Accordingly, loss of LRP2 leads to an abnormal SHH gradient formation in the developing brain. The delay and decrease in the activity of signaling pathways, which are crucial in initiating patterning of the ventral medial forebrain, cause a failure to establish normal forebrain patterning centers and consequently cause HPE.

5.1 LRP2 as a candidate gene for HPE

The phenotypes caused by loss of functional LRP2 in humans and in mice are similar. In humans, loss of LRP2 function leads to Donnai-Barrow syndrome (DBS) and/or facio-oculo-acoustico-renal syndrome (FOAR) (S. Kantarci *et al*., 2007). Additionally, deletions in the *LRP2* gene can also lead to microforms of HPE (J. Rosenfeld *et al*., 2010). In mice, most animals with a classical LRP2 null mutation die because of respiratory insufficiency (T. Willnow *et al*., 1996). Interestingly, patients with DBS syndrome show congenital diaphragmatic hernia (S. Kantarci *et al*., 2007). In diaphragmatic hernia an abnormal opening in the diaphragm, the muscle that is responsible for breathing, results in severe breathing difficulties due to ineffective

movement of the diaphragm. In addition, the small number of surviving LRP2-deficient mice suffer from proteinuria (J. Leheste *et al*., 1999) due to loss of LRP2 mediated retrieval pathway of filtered proteins. Likewise, patients with Donnai-Barrow/facio-oculo-acoustico-renal syndrome (DBS/FOAR syndrome) suffer from tubular resorption deficiency. In mice, loss of LRP2 leads to craniofacial anomalies and HPE. Similarly, patients with DBS show agenesis or hypoplasia of the corpus callosum, while patients with FOAR have macrocephaly (S. Kantarci *et al*., 2007). Additionally, some patients with deletions within the *LRP2* gene show microforms of HPE with milder craniofacial anomalies (J. Rosenfeld *et al*., 2010). The variability of brain phenotypes and craniofacial anomalies in humans has also been seen in LRP2-deficient mice with different genetic backgrounds (data shown). The most likely explanation is the presence of genetic modifiers, additional gene variants that affect the severity and penetrance of specific HPE-associated phenotypes. For example, mice on a mixed *129SvEmcTer* genetic background (*129SvEmcTer and C57BL/6N*) mostly die perinatally (T. Willnow *et al*., 1996) whereas mice on a mixed *FVB/NJ* genetic background (*FVB/NJ and C57BL/6J*) typically survive until adulthood (C. Gajera *et al*., 2010). Nevertheless, both mouse lines share all phenotypic characteristics associated with LRP2 null phenotypes like holoprosencephalic features and proteinuria (K. Zarbalis *et al*., 2004; R. Spoelgen *et al*., 2005).

5.2 LRP2 functions in proper SHH gradient formation and correct patterning of the ventral medial forebrain

5.2.1 LRP2 expression during early forebrain development in the mouse and consequences of loss of the receptor on morphogen pathways

Distinct and dynamic expression patterns of LRP2 during CNS development

Previous reports demonstrated LRP2 expression in neuroectodermal cells of E8.0 mouse embryos (D. Sahali *et al*., 1993) and in the neural tube at E9.5 (M. Kounnas *et al*., 1994). An important function of LRP2 in these tissues is strongly suggested by the neurodevelopmental abnormalities in LRP2-deficient mouse embryos including HPE (T. Willnow *et al*., 1996) as well as distinct changes in caudal spinal cord development (G. Wicher *et al*., 2008).

Here, I performed a detailed expression analysis of LRP2 during different stages of development to gain further insights into the exact developmental processes during early forebrain development that may require receptor activity.

As soon as the neuroectoderm forms, a robust LRP2 signal was observed in the neuroectoderm at E7.5 (Figure 4.2.1) using immunfluoresence. The receptor was uniformly distributed on the apical side of the neuroectoderm for as long as the neural tube was still open (Figure 4.2.1 B). No LRP2 protein was observed in the non-neural ectoderm tissue adjacent to the neural folds suggesting a specific role for this receptor in CNS development. After neural tube closure, the LRP2 expression was more dynamic with strong signals in the midline of the ventral and dorsal developing telencephalon but close to no detectable protein in the lateral neural tube (Figure 4.2.1 C). The early uniform expression pattern at the neural plate stage (E7.5) suggests a role for the receptor in establishing brain formation, which starts at E8.0. At this stage, local signaling centers in the neuroepithelium begin to refine the anterior-posterior specification of three main domains in the brain primordium, the prosencephalon, the mesencephalon and the rhombencephalon (J. Rubenstein *et al*., 1998). The later more restricted expression pattern in the ventral, dorsal and rostral midline of the developing telencephalon, and in the caudal ventral neural tube,

overlaps with important organizer regions: the ventral and dorsal midline and the anterior neural ridge (ANR) in the telencephalon as well as the floor plate cells in the more caudal regions of the ventral neural tube (R. Hoch *et al*., 2009; S. Gilbert, 2006). The presence of LRP2 in these regions suggested a role for the receptor in establishment of these patterning centers. Since LRP2 deficiency results only in minor changes in the development of the caudal neural tube (G. Wicher *et al*., 2008) my studies focused on the rostral development of the neural tube.

To further investigate the formation of the three patterning centers in the telencephalon and diencephalon (the ventral midline, the ANR, and the dorsal midline) I next analyzed the expression of key morphogens in these patterning centers, namely *Shh*, *Fgf8,* and *Bmp4* in control and LRP2-deficient embryos.

Impaired Shh expression in Lrp2$^{-/-}$ embryos

Shh expression is a key factor for anterior forebrain midline development (K. Shimamura *et al*., 1997) and previous studies already demonstrated that in *Shh*$^{-/-}$ mouse embryos, the telencephalon is reduced in size and ventral cell types are lost (J. Ericson *et al*., 1995).

LRP2-deficient embryos exhibit a severe reduction in *Shh* expression in the ventral midline at E8.5 (Figure 4.2.5 A). This reduction in *Shh* expression is followed by a specific loss of *Shh* expression in the ventral diencephalic midline (Figure 4.2.7) and at later embryonic stages in the ventral telencephalic midline (Figure 4.2.2). Normally, SHH signaling restricts the dorsalizing function of GLI3 and controls the positioning of the dorsoventral boundary (S. Kuschel *et al*., 2003). In *Lrp2*$^{-/-}$ embryos, the loss of *Shh* transcription in the neuroepithelium at E8.5 and E9.0 leads to an unrestricted expression of the SHH signaling repressor *Gli3* (Figure 4.2.5 A). Additionally, *Gli3* mRNA appears in ectopic regions, such as in the anterior diencephalic midline, where *Shh* expression would normally inhibit the expression of *Gli3* (Figure 4.2.7). Apparently, ectopic expression of *Gli3* in *Lrp2*$^{-/-}$ embryos and its dorsalizing effects may explain the abnormal expression of *Bmp4* specifically in the region of the anterior diencephalic midline (Figure 4.2.7). In contrast to *Gli3*, *Gli1* expression, which is tipically activated by SHH signaling, is down-regulated during embryonic development in *Lrp2*$^{-/-}$ embryos, reflecting the reduction of *Shh* expression in the anterior diencephalic midline (Figure 4.2.5 A).

Interestingly, *Ptch1* occupies an enlarged expression domain to more dorsal regions in the telencephalon of *Lrp2*$^{-/-}$ embryos (Figure 4.2.5 A). In the wild type situation, *Ptch1* expression is transcriptionally upregulated by SHH signaling and limits the extent of SHH signaling (V. Ribes *et al*., 2009). In *Drosophila* it was demonstrated that Patched, the *Drosophila* orthologue of Ptch1, limits the Hedgehog gradient. The upregulation of *Patched* in response to a HH signal results in sequestration of this ligand, limiting its spread in responding tissues and the internalization of Hedgehog in endosomes. Following endocytosis both Hedgehog and Patched are targeted to the lysosomal degradation pathway (C. Torroja *et al*., 2004). Therefore, activation of *Ptch1* expression in more dorsal regions suggests that the reduction in ventral midline activity is accompanied by an uncontrolled spread of the SHH protein into more dorsal regions where it aberrantly activates *Ptch1*. More evidence for uncontrolled spread of the SHH protein is the finding that *Fgf8* expression is shifted to more dorsal regions in the developing telencephalon in *Lrp2*$^{-/-}$ embryos (Figure 4.2.5 C). The fact that, unlike *Ptch1* and *Fgf8, Gli1* expression is downregulated and not shifted to more dorsal regions may be explained by the different threshold levels of the different downstream targets of the SHH pathway. For example in the neural tube, *Nkx2.2* expression requires higher SHH concentrations and longer SHH exposure than does *Olig2* (E. Dessaud *et al*., 2007).

At this point, my results confirmed an important role for LRP2 in the ventral forebrain, which was in line with the restricted expression pattern of LRP2 in the ventral midline in the developing forebrain. In subsequent experiments, I showed that the SHH pathway is the primary target of LRP2 activity in the ventral forebrain, data that is discussed in detail in section 5.2.3.

Aberrant Fgf8 expression in Lrp2$^{-/-}$ embryos caused by an imbalance of morphogen pathways in the forebrain patterning centers

Fgf8 is another key regulator in forebrain patterning and is typically expressed in a very specific expression pattern in the ANR. This gene showed a reduced expression in the ventral telencephalon, accompanied by a shift in expression from the commissural plate into more dorsal regions in the telencephalon of *Lrp2*$^{-/-}$ embryos (Figure 4.2.2).

The reduced ventral expression of *Fgf8* in LRP2-deficient embryos may be partially explained by the loss of ventral *Shh* expression. Previous studies demonstrated that SHH-mediated downregulation of GLI3 is necessary to sustain *Fgf8* expression (B. Rash *et al*., 2007). These data also support the hypothesis that the aberrant *Fgf8* expression in *Lrp2* mutants is secondary to the altered SHH signaling since I detected changes in *Fgf8* expression only after reduction of *Shh* expression (Figure 4.2.5 A+C). However, the shift in *Fgf8* expression to more dorsal regions of the neural tube is more difficult to reconcile with this hypothesis, as it seemingly contradicts the loss of *Shh* expression seen in mutant embryos. In the literature, a dorsally shifted expression pattern of *Fgf8* was reported in several mouse models. In *Gli3* mutants the loss of *Gli3* expression correlates with an impaired telencephalic roof plate. Usually, the roof plate expresses dorsal factors that restrict the expression of *Fgf8* and *Shh* to more rostral and ventral parts in the telencephalon. The impaired development of the roof plate as a consequence of loss of *Gli3* expression results in an expanded *Fgf8* expression to more dorsal regions in the telencephalon (T. Theil *et al*., 1999; S. Kuschel *et al*., 2003). Other important factors, which restrict *Fgf8* expression, are empty spiracles homolog 1 and 2 (EMX1 and EMX2). Lack of *Emx2* expression, which is also important for development of the dorsal telencephalon, leads to an expanded *Fgf8* expression (T. Fukuchi-Shimogori *et al*., 2003). In the two mouse models discussed above, the lack of factors important for the development of the dorsal telencephalon resulted in an expanded *Fgf8* expression to more dorsal regions of the telencephalon. In a more recent publication, Chiang and colleagues described a new mouse model with harbouring a mutated form of SHH lacking the cholesterol moiety. Mice heterozygous for this mutation (*ShhN/+*) show *Fgf8* expression ectopically extended to dorsal telencephalic regions (X. Huang *et al*., 2007a). Because the cholesterol moiety is believed to be important for membrane-tethering of SHH, mice that lack this moiety on the morphogen show a

more widespread signaling of SHH that also reaches more dorsal brain regions and ectopically activates *Fgf8*. In contrast in a mouse model that lacks the wild type allele (*ShhN/-*), ventral cell types in the telencephalon fail to be established, due to a failure of SHH gradient formation and rapid spread from its site of synthesis (X. Huang *et al*., 2007b).

The comparison of the LRP2-deficient phenotype with these above models suggests a function for the receptor in ventral sequestration of SHH. The loss of ventral *Fgf8* expression may be explained by reduced SHH signaling levels in the ventral telencephalon, while the expanded *Fgf8* expression fits with either a mis-specified telencephalic roof plate or with uncontrolled, overall widespread SHH signaling. Together with the data for SHH signaling in *Lrp2* mutants presented above, my data favor a model whereby LRP2 functions in the ventral sequestration of SHH whereby loss of LRP2 results in an uncontrolled signaling of SHH in more dorsal regions of the neural tube. This hypothesis is supported by the widespread *Ptch1* expression in *Lrp2* mutants, given the fact that *Ptch1* is a low threshold target gene responding to low concentrations of SHH.

Increased Bmp4 expression is a secondary consequence of the mispatterned telencephalon in Lrp2$^{-/-}$ embryos

Besides the altered morphogen expression in the ventral and rostral midline of the forebrain in LRP2-deficient mice, the dorsal midline patterning center is also affected. Thus, *Lrp2$^{-/-}$* mouse embryos displayed an increased and expanded *Bmp4* expression and enhanced pSMAD signals as shown previously (R. Spoelgen *et al*., 2005). The upregulated *Bmp4* expression in the dorsal telencephalon (Figure 4.2.2 and 4.2.5 B) may serve to protect dorsal midline formation from uncontrolled, and widespread SHH signaling. A consequence of the increased *Bmp4* expression might be the disrupted *noggin* expression visible at E9.0 in *Lrp2$^{-/-}$* embryos (Figure 4.2.5 B).

BMP4 is a dorso-medial marker, typically restricted to the immediate midline, important for proper dorso-ventral forebrain patterning. It was demonstrated that mutations in the BMP pathway lead to HPE. For example, deletion of the BMP receptor genes *Bmpr1b* and *Bmpr1a* in the mouse telencephalon results in holoprosencephalic syndrome, caused by a loss of dorsal midline cells (M. Fernandes *et al*., 2007). This observation indicates an important role for BMP signaling in establishing the dorsal organizer center. Not only loss of BMP signaling

but also increased BMP signaling leads to holoprosencephalic features as shown in *Chordin*$^{-/-}$*; Noggin*$^{+/-}$ mutants (R. Anderson *et al*., 2002). The loss of these BMP antagonists results in absence of ventral *Shh* expression and signaling in the prechordal plate, and in a decrease in *Fgf8* expression and signaling in the ANR. Both effects are caused by the increased BMP signal that inhibits the expression and activity of *Shh* and *Fgf8*.

In line with what has been shown for models with increased BMP4 activity, the enhanced BMP4 signaling in LRP2-deficient embryos could represent the primary cause of the holoprosencephalic phenotype seen in this model. Accordingly, loss of ventral *Shh* expression and reduced ventral *Fgf8* expression may be a secondary consequence of dorsalization of the neural tube. Previously published data from our lab support this hypothesis and demonstrated that LRP2 can bind specifically BMP4 (R. Spoelgen *et al*., 2005). Since BMP4 protein regulates its own expression in a positive feedback loop it was speculated that LRP2 may bind the morphogen to restrict its distribution and signaling in the dorsal medial midline. To address the question whether enhanced BMP4 signaling in the dorsal neural tube is the primary cause for the patterning defects in LRP2 deficient mice, I tried to rescue the mutant mice by partial ablation of BMP4 activity in the neural tube. To achieve *Bmp4* downregulation, I used the Bmp4^{tm1blh} mouse. According to published results (R. Stottmann *et al*., 2006), BMP4 levels are decreased in mice by crossing them onto the heterozygous haploinsufficient Bmp4^{tm1blh} background. Downregulation of BMP4 at the transcriptional level is now believed to play just as important a role in BMP regulation as Bmp4 antagonists like noggin, chordin, gremlin, or follistatin. Previous studies showed that decreasing the *Bmp4* levels partially rescued the phenotype, caused by mutations in noggin, which antagonizes BMP4 signaling (R. Stottmann *et al*., 2006).

RT-PCR analysis of embryos haploinsufficient for *Bmp4* confirmed a 50% downregulation of *Bmp4* RNA levels in our mice (Figure 4.2.3 A). Interestingly, no rescue of the phenotype of LRP2-deficient embryos was detected (Figure 4.2.3 B). *Shh* expression in the compound *Lrp2*$^{-/-}$*; Bmp4*$^{tm1blh/+}$ mutants was lost in the ventral telencephalic midline as in *Lrp2*$^{-/-}$ embryos (Figure 4.2.3 B). These results strongly suggest that the increased *Bmp4* expression is not the primary cause for the aberrant patterning of the telencephalon in *Lrp2*$^{-/-}$ mouse embryos, but is rather a secondary consequence of defects in the SHH pathway. This concept is also supported by my

finding that *Fgf8* as well as *Bmp4* expression was normal in E8.5 mutant mice compared to controls; a time point where I observed significant changes in the SHH pathway in *Lrp2*$^{-/-}$ embryos. These considerations will be discussed in detail in sections 5.2.2 and 5.2.3.

Nevertheless, considering the fact that LRP2 is a multi-ligand receptor with distinct roles in different tissues and during different developmental stages and in the adult it is still possible that LRP2-mediated uptake and degradation of BMP4 plays an important role at midgestation (E9 – E10). Recent data from our lab suggested that such a function of LRP2 as a negative regulator of BMP4 signaling might, at least exist in the adult mouse brain, where loss of the receptor causes aberrant induction of the BMP4 signaling pathway in the subventricular zone (SVZ) (C. Gajera *et al*., 2010). This enhanced BMP signaling as a consequence of LRP2 deficiency coincides with a significant decrease in proliferation of neural progenitors, substantiating the crucial role of LRP2 in reducing BMP signaling to promote SVZ neurogenesis.

5.2.2 The onset of the forebrain patterning phenotype in LRP2-deficient embryos starts with the initiation of neurulation and is caused by changes in the SHH pathway

Since all three forebrain patterning centers are affected in the LRP2-deficient embryos, and show complex interactions with each other, it is challenging to determine which patterning center disrubtion is central to causing the HPE phenotype. However a detailed expression analysis of early developmental stages may clarify the primary target of LRP2 activity.

The anterior visceral endoderm (AVE) in concert with the early gastrula organizer initiates the induction and patterning of the forebrain, while the axial mesendoderm (AME) emanating later from the node maintains and refines this initial pattern (S. Ang *et al*., 1994) (Figure 1.1). Alterations during these early patterning processes, disrupting anterior-posterior axis formation, result in HPE. Nodal signaling is important for the initial specification of the prechordal plate, developing from the AME (S. Wilson *et al*., 2004). Nodal null mutants fail to form the prechordal plate, resulting in lack of *Shh* expression and occurrence of HPE (K. Rohr *et al*., 2001).

I analyzed expression pattern of *Hesx1*, which marks the AVE, and *noggin*, which marks the node and the developing AME in wild types and *Lrp2*$^{-/-}$ mice. Both markers showed comparable expression patterns in *Lrp2*$^{-/-}$ mice and control embryos (Figure 4.2.4 A), suggesting that the forebrain is normally initiated in LRP2-deficient embryos. Also *Six3* and *Bmp4* showed an undisturbed expression pattern in *Lrp2*$^{-/-}$ mice (Figure 4.2.4 A). These results demonstrated that in LRP2-deficient embryos the AVE initiated normal forebrain gene expression in the anterior epiblast as indicated by proper *Six3* expression. The start of *Six3* expression also marks the onset of the forebrain specific gene expression program, which is properly initiated in *Lrp2*$^{-/-}$ embryos. Correct establishment of the AVE and subsequent activation of *Six3* expression is only possible with the BMP antagonizing activity from the early gastrula organizer, which forms the node and later the AME (Y. Yang *et al*., 2006). Proper function of the node and its derivatives together with the anterior epiblast is indicated by the restricted expression of *Bmp4*, which is also visible in the LRP2-deficient embryos. Thus gastrulation and initiation of forebrain development in LRP2-deficient embryos are normal.

Because gastrulation proceeded normally in *Lrp2*$^{-/-}$ embryos, I investigated the onset of neurulation at the transition from gastrulation to somitogenesis. At this stage, the AME is marked by *Shh* expression including the prechordal plate (PrCP) in the most rostral area as well as the notochord forming the rest of the AME. From the literature it is known that severe HPE is caused by removal of PrCP cells from amphibian and chick embryos (H. Li *et al*., 1997; E. Pera *et al*., 1997), or by lack of Nodal signaling resulting in the lack of prechordal plate cells in the mouse (K. Rohr *et al*., 2001).

In our mutant mouse model, *Shh* expression at this stage did not show any difference between *Lrp2*$^{-/-}$ embryos and control embryos (Figure 4.2.4 B). This observation suggests that the holoprosencephalic phenotype is not caused by aberrant development of PrCP cells, the essential organizing center for midline specification of brain and facial structures. The brain anlagen also developed properly as visualized with *Hesx1* expression in *Lrp2*$^{-/-}$ embryos at this developmental stage (Figure 4.2.4 B). But, as indicated by the severe reduction of *Six3* expression, later forebrain patterning is affected in mutants (Figure 4.2.4 B). In conclusion the expression analysis of gastrula stages and early neurulation stages demonstrated that the induction of brain specific genes is normal up to E7.75, and that the forebrain anlagen develop properly in LRP2-deficient embryos. However, the subsequent patterning and establishment of the forebrain anlagen from E8.0 onwards is affected in *Lrp2*$^{-/-}$ mutants.

SIX3 is a transcription factor that encodes an early regulator of different morphogens (F. Lacbawan *et al*., 2009). In zebrafish, SIX3 regulates nodal activity to establish early brain asymmetry (A. Inbal *et al*., 2007), while in *Xenopus* SIX3 inhibits *Bmp4* expression (G. Gestri *et al*., 2005). In the mouse it represses Wnt signaling (O. Lagutin *et al*., 2003) and acts as a direct regulator of *Shh* expression in the ventral forebrain (Y. Jeong *et al*., 2008). *Shh* expression itself regulates *Six3* expression in a positive feedback loop, resulting in a reciprocal positive interaction of the transcription factor SIX3 and the morphogen SHH in early midline formation in the developing forebrain (X. Geng *et al*., 2008).

In line with the reduction in the expression level of *Six3* in LRP2-deficient embryos I also detect significant changes in the *Shh* expression already at E8.5 (Figure 4.2.5 A), identifying the SHH pathway as a primary target of LRP2 activity in the developing forebrain. The defect in the SHH pathway at E8.5 suggests a failure

of ventral midline induction as *Shh* expression is significantly reduced in the ventral midline of *Lrp2*$^{-/-}$ embryos. Experimental evidence that other morphogen signaling pathways are not the primary target of LRP2 stems from the expression pattern of *Bmp4* and *noggin* within the BMP pathway and of *Fgf8* within the FGF pathway. No changes were detectable in the FGF and BMP (Figure 4.2.5 B-C) pathways at E8.5. That changes in the BMP pathway are secondary is underscored by the finding that *Bmp4* haploinsufficiency did not rescue the phenotype in *Lrp2*$^{-/-}$ embryos, The fact that alterations in *Fgf8* expression are seen later in development than changes in *Shh* expression supports the idea, that changes in the FGF pathway are secondary.

In summary, analysis of temporal aspects of LRP2 deficiency showed that the onset of the holoprosencephalic phenotype has to be placed at E8.0 and that the SHH pathway likely represents the primary affected pathway in LRP2-deficient embryos. Changes in the other pathways (e.g, BMP and FGF8) that are observed at later developmental stages are most likely secondary effects and a consequence of impaired SHH signaling.

5.2.3 Abnormal SHH signaling in early neurulation stages leads to defects in RDVM development and ultimately to an HPE phenotype in LRP2-deficient mice

The defects in midgestation in *Lrp2*$^{-/-}$ embryos are widespread affecting all patterning centers and several key morphogen pathways in the forebrain. However, I was able to narrow down the causative alterations to defects in the SHH pathway in a very specific time window during the developmental process of neurulation (starting with E8.0) and to a specific tissue organizer region, the rostral diencephalon ventral midline (RDVM).

SHH protein is first expressed in the prechordal plate. From there it is transferred to the apical side of the overlying neuroepithelium, the RDVM. In the RDVM, it forms a gradient and finally establishes it's own expression in neuroepithelial cells (X. Geng *et al*., 2008; J. Ericson *et al*., 1997). The very same process has also been described in detail for SHH in the notochord and the overlying neural tube (V. Ribes *et al*., 2010). Previous studies also showed that while located to the overlying neural tube SHH protein first accumulates at the apical region of ventral midline cells where patterning starts (C. Chamberlain *et al*., 2008). These results are in line with the observation that SHH protein co-localizes with LRP2 on the apical surface of the neuroepithelium. Lack of LRP2 leads to a delayed establishment of SHH in the RDVM (Figure 4.2.6 B). This observation suggests that initial low concentrations of SHH, which are already important for correct patterning in the caudal neural tube (V. Ribes *et al*., 2010), fail to be established in the rostral ventral midline of LRP2-deficient embryos. Only the higher concentrations that appear at later time points (E8.75) result in the appearance of SHH protein in the RDVM of LRP2-deficient embryos.

The delay of SHH protein localization to the RDVM in LRP2-deficient embryos results in severe patterning defects within this structure. The delayed establishment of SHH in the RDVM leads to a reduction of *Six3* expression in mutant mice, which subsequently fail to activate proper *Shh* expression in the midline (Figure 4.2.6 C). The expression of *Six3* together with *Shh* is important for the activation of a prosencephalon specific gene program. Loss of *Shh* expression in the RDVM as a consequence of reduced *Six3* expression and impaired SHH signaling from the prechordal plate causes the loss of *Shh* expression in later embryonic stages in the

ventral telencephalon (Figure 4.2.2) and leads to the holoprosencephalic phenotype observed in LRP2-deficient embryos. My hypothesis is supported by the phenotype observed in haploinsufficient *Six3* embryos (X. Geng *et al*., 2008). In this study, the authors showed that similar to the LRP2-deficient embryos, *Shh* expression in the prechordal plate in *Six3*$^{+/-}$ *was* unaffected, but its expression failed to extend anteriorly into the RDVM.

In conclusion, my studies demonstrated that proper development of the prosencephalon depends on the early establishment of SHH signaling in the RDVM. It seems that SHH from the prechordal plate needs to localize to the apical neuroepithelium as a prerequisite to activate SHH signaling within this tissue. Strong expression of LRP2 in this region (Figure 4.2.1) supports the idea that it is LRP2, that assists in proper localization and signaling of the SHH pathway in this special region of the ventral midline in the forebrain. Intriguingly, a proposed role for LRP2 in sequestration of SHH to the RDVM has already been documented for two other factors, Cdo and Gas1, in the neural tube. Cdo and Gas1 are cell surface proteins, which can bind to SHH and promote SHH signaling. How this occurs at the cellular level remains to be determined. As both factors bind SHH, one attractive hypothesis is that Gas1 and Cdo may form a physical complex through SHH binding, and that this complex promotes SHH signaling, possibly through ligand presentation to the SHH receptor Ptch1 (B. Allen *et al*., 2007). Cdo and Gas1 may contribute to the generation of an early burst of SHH signaling in the ventral neural tube, by sensitizing cells to low levels of SHH protein (V. Ribes *et al*., 2009). Removal of *Gas1* results in a *Shh* dose-dependent loss of cell identities in the ventral neural tube and in facial and skeletal defects, consistent with reduced SHH signaling. Whereas substantial experimental data describe the mechanisms responsible for establishment of the SHH activity domains in the caudal neural tube (E. Dessaud *et al*., 2008), surprisingly little is known for the much more complex processes of shaping the prosencephalon. Now my data shed some light on this unresolved issue. In LRP2-deficient embryos, loss of the receptor results in a failure of early SHH signaling in the RDVM. As a consequence of inappropriate concentrations of the morphogen in this region, proper specification and development of the RDVM is impaired. These data represent the first evidence for how establishment of SHH signaling in the ventral developing prosencephalon occurs and identifies LRP2 as a key component of this process.

5.2.4 LRP2 can bind SHH and functions in the establishment of SHH signaling in the RDVM

As described above LRP2 plays an important role in the establishment of SHH signaling in the RDVM at the onset of neurulation. In my thesis project, I was able to elucidate the likely underlying molecular mechanism of receptor function. These data are discussed below.

Previous studies demonstrated that LRP2 may act as a cell surface receptor for SHH, although the relevance of this interaction for embryonic development remained obscure. For example, McCarthy *et al* showed that LRP2 is able to bind SHH-N *in vitro* (surface plasmon resonance analysis) and to mediate endocytic uptake of the morphogen in BN16 cells. Since BN16 cells lack Ptch1, the known receptor for SHH, but express high levels of LRP2, it was highly suggestive that SHH-N uptake was mediated by LRP2 alone (R. McCarthy *et al*., 2002). This conclusion was supported by the fact that the uptake of SHH-N was inhibited by the LRP2 antagonist RAP. A few years later, the same group also showed that SHH-N was internalized *in vivo* via LRP2 in efferent duct epithelial cells when infused recombinantly into the rat epididymis (C. Morales *et al*., 2006).

In my studies, I have substantiated a possible role for LRP2 as a SHH-N receptor in the developing forebrain, which was supported by co-localization of the two proteins visible as early as E8.0 (Figure 4.2.6 A). To test the hypothesis that LRP2 is the physiological receptor for SHH-N in the neuroepithelium, I first established the binding conditions of SHH-N to LRP2 in cell culture. For this experiment, I also used BN16 cells. I was able to establish appropriate assay conditions where I detected strong binding of SHH-N to BN16 cells. Cell binding was largely abolished when I applied RAP (Figure 4.2.12). Next, I applied the very same binding conditions to test interaction of recombinant SHH-N with LRP2 in whole embryo cultures. Remarkably, in this *ex vivo* model I was able to demonstrate specific binding of SHH-N to the neuroectoderm of wild type but not LRP2-deficient embryos under physiological conditions (Figure 4.2.13). These data represent the first experimental proof that LRP2 acts as a SHH receptor in the neural tube, sequestering the morphogen in target tissues in the forebrain, similarly to the action of Cdo, Boc and Gas1 in the caudal neural tube.

To unambiguously demonstrate that impaired SHH signaling in the RDVM of LRP2-deficient embryos is caused by lack of morphogen sequestration rather than by impaired intracellular signal transduction, I tested the ability of LRP2-deficient neuroepithelial cells to respond to stimulation of Smo. To do so, I established whole embryo cultures and cephalic explants as two *ex vivo* model systems. In these models, the application of SAG (Smo agonist) in wild type and LRP2-deficient tissues was investigated. A previous study already showed that SAG activates the Hedgehog pathway by binding directly to Smo. Thus, SAG activity is independent of SHH binding to the receptor Ptch1 (J. Chen *et al*., 2002). At two different time points in embryonic development, in cephalic explants at E9.5 and whole embryo cultures at E7.0 to E7.5, application of SAG resulted in a comparable activation of the SHH pathway in control and in *Lrp2* mutant cultures (Figure 4.2.8 & 4.2.10). Thus, the rescue of *Shh* and *Six3* expression (as a readout of Smo activity) in LRP2-deficient explants or whole embryo cultures confirmed my hypothesis that LRP2 acts upstream of Smo (Figure 5.1).

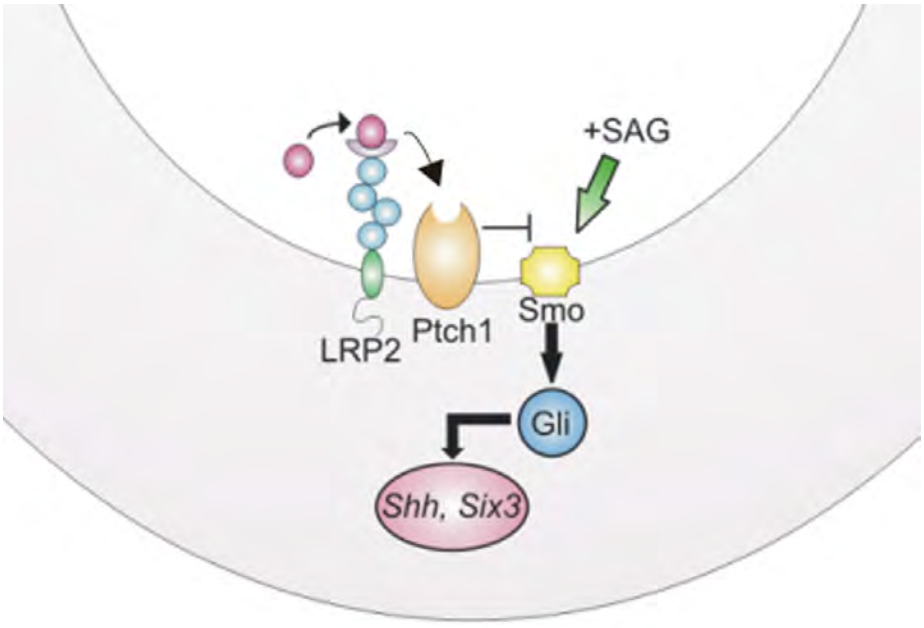

Figure 5.1: SAG dependent rescue of *Shh* and *Six3* expression in *ex vivo* model systems. SAG treatment acts at the level on Smo and activates the intracellular signaling cascade, resulting in the induction of *Shh* and *Six3* expression.

Intriguingly, rescue of the SHH signaling defect in LRP-deficient tissues was more efficient in whole embryo cultures (55%) compared with cephalic explants (28%). This observation is in line with data discussed in the literature that during telencephalic development changes in the competence of the telencephalic neuroepithelium to respond to SHH signaling occur with ongoing development (V. Sousa *et al*., 2010). It is possible that at E9.5 when patterning of the telencephalon is already initiated, the ventral midline loses its ability to respond to the activation of the SHH pathway and therefore is unable to acquire a midline identity in response to SHH, and like in the cephalic explants fails to efficiently induce *Shh* expression efficiently. Likely, the whole embryo culture, which is prepared from E7.5 old embryos is likely to be more suitable for rescuing midline cell identity, as it was demonstrated that floor plate cells in the ventral neural tube require high levels of SHH signaling in a specific time window between E8.0 and E8.5 to acquire their identity (V. Ribes *et al*., 2010). Similarly the *ex vivo* experiments in my study indicate that already with the transition from gastrula to neurula stages proper SHH signaling is required to induce correct midline induction and activation of the SHH pathway. In contrast to floor plate induction, which needs subsequent downregulation of SHH signaling (V. Ribes *et al*., 2010), midline cells of the developing prosencephalon seem to depend on sustained SHH signaling at least until the three organizer centers in the developing forebrain are established. The early disruption of SHH signaling in the RDVM manifests itself in defective midline development in the anteroventral diencephalon later on (Figure 4.2.7).

5.2.5 A model for LRP2 in establishment of SHH signaling in the RDVM

Proper sequestering of the SHH ligand is important within a specific time window as demonstrated for floor plate induction in the ventral neural tube. Inhibition of SHH signaling between 3-6 somites in the mouse embryo results in the absence of this most ventral cell type in the neural tube (V. Ribes *et al*., 2010).

Intriguingly, in LRP2-deficient embryos defective initial establishment of SHH signaling within the RDVM also results in mispatterning of the most ventral cell type, the midline cells. These findings suggest that like in the posterior neural tube, establishment of ventral midline cells in the rostral neural tube also depends on

proper SHH signaling, a pathway critically dependent on LRP2 activity. I propose a model whereby SHH protein produced in the prechordal plate (PrCP) shapes a ventral-to-dorsal gradient (Figure 5.2, T0). Initial low concentrations of SHH protein in the overlying rostral diencephalon ventral midline (RDVM) are sufficient to activate *Six3* expression (Figure 5.2, T1). SHH protein from the PrCP together with SIX3 now initiates strong *Shh* expression levels in the RDVM comparable to expression levels in the prechordal plate (Figure 5.2 T2).

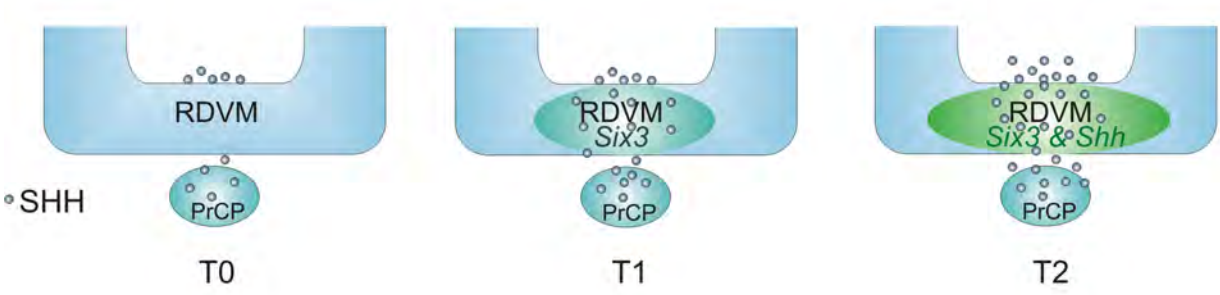

Figure 5.2: Model for SHH signaling during RDVM induction. At early time-points in development, initial low concentrations of SHH (T0) from the PrCP localize to the overlying neuroepithelium. With ongoing development (T1) SHH ligand concentrations are increasing in the RDVM and activate *Six3* expression. SHH protein from the PrCP together with SIX3 from the RDVM induces high *Shh* expression within the RDVM at a slightly later time-point (T2). Over time, SHH concentration in the RDVM increases with increasing number of cells producing SHH.

In LRP2-deficient embryos the initial activation of the SHH pathway in the RDVM is delayed (Figure 5.2, T0). All my data are consistent with a model in which LRP2 acts as a co-receptor for Ptch1 in the ventral neuroepithelium. In particular, it may facilitate binding of SHH to Ptch1, by increasing the local concentration of the morphogen on the apical surface of the neuroepithelium in the RDVM and acting as a reservoir to promote ligand binding to Ptch1. Alternatively, LRP2 may even directly associate with Ptch1 to form a high affinity receptor complex (Figure 5.3). Such a function was shown for LRP5/6 in the WNT pathway. LRP5 and LRP6 bind WNT proteins and act as co-receptors for Frizzled (Fz). The existence of multiple, independent Wnt binding sites on the LRP6 co-receptor suggests multiple possibilities for the architecture of Wnt signaling complexes (E. Bourhis *et al*., 2009).

In vitro, LRP2 has been shown to bind monomeric recombinant SHH-N produced in bacteria (McCarthy *et al*., 2002). Thus, binding epitopes recognized by the receptor must be localized in the polypetide chain of SHH-N. At present, I cannot exclude that distinct modification of SHH-N described in the literature may even further enhance (or decrease receptor binding). For example, SHH has been shown to exist in form of multimeric micelles. It was reported that the formation of micelles requires the presence of both N- and C-terminal lipid modification. Furthermore, it was demonstrated that the soluble SHH-Np, which is multimeric, is freely diffusible and biologically potent and therefore may act in gradient formation of the morphogen (X. Zeng *et al*., 2001). Also, association of SHH-Np with lipoprotein particles has been proposed to affect SHH activity. Thus, another possibility is that lipoprotein particles that bind to LRP2 act as a vehicle for the movement of lipid-linked morphogens like SHH, which was shown in *Drosophila* before (D. Panakova *et al*., 2005). In detail it was shown in this study that Hedgehog proteins in *Drosophila* travel on argosomes, lipoprotein-like particles. In larvae with reduced lipoprotein levels, Hedgehog accumulates near its site of production, and fails to signal over its normal range, identifying lipoprotein particles to be important for long-range signaling.

As well as simply sequestering SHH on the neuroepithelial cell surface, LRP2 may even participate in the process whereby SHH signals into cells. For the activation of the SHH pathway the morphogen needs to bind to Ptch1. Thereafter Ptch1 is endocytosed to release its inhibitory effect on Smo. Although quite speculative, LRP2 may directly take part in the SHH-dependend internalization of Ptch1. A similar function for LRP2 has already been documented for the co-receptor cubilin in the kidney (M. Kristiansen *et al*., 1999).

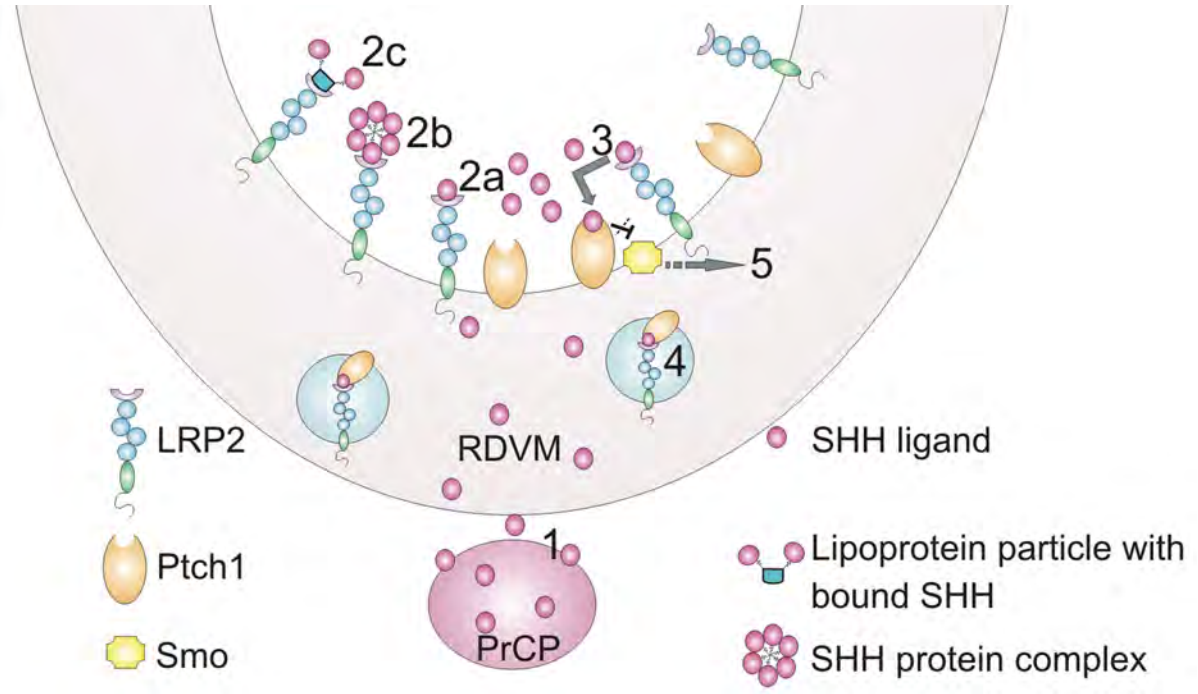

Figure 5.3: Model of LRP2 function during RDVM induction. (1) SHH protein from the prechordal plate (PrCP) localizes to the overlying RDVM. How the protein is transported to the apical site of the RDVM is still unknown. To establish SHH signaling within the RDVM, SHH protein needs to accumulate at the apical surface of the neuroepithelium, likely by binding to LRP2 (2a). As well as binding monomeric SHH-N, LRP2 may also sequester SHH ligand protein complexes (micelles) (2b) or bind to SHH ligand via lipoprotein particles that associate with multiple SHH ligands. In binding SHH at the apical cell surface, LRP2 may function as a reservoir for SHH ligand to be presented to Ptch1 (3) or it may promote endocytosis of the SHH-Ptch1 complex (4). Upon binding of SHH to Ptch1, the inhibitory effect on Smo is released and target gene transcription is activated (5).

5.3 The soluble LRP2 ICD appears not to play a major role in signal transduction pathways

Although members of the LDL receptor gene family were initially believed to function exclusively as clearance receptors, recent research has revealed that they also participate in signal transduction processes. The most prominent example is LRP6 and its function in the WNT pathway (X. Zeng *et al*., 2005). Upon Wnt stimulation, phosphorylation by GSK3 activates the intracellular domain of LRP6 (G. Davidson *et al*., 2005; X. Zeng *et al*., 2005), which consequently inhibits phosphorylation and degradation of β-catenin and results in the activation of β-catenin signaling (B. Mao *et al*., 2001).

How the different members of the LDL receptor gene family influence signal transduction pathways is still under investigation but one possible scenario is that the cell surface receptors undergo regulated intramembrane proteolysis (RIP). The role of RIP in nuclear signaling is most extensively described in the case of the Notch receptor. Ligand binding to Notch initiates ectodomain shedding and produces a membrane-associated C-terminal fragment (J. Mumm *et al*., 2000). The C-terminal fragment is cleaved by γ-secretase activity, which results in the release of the intracellular domain of Notch (NICD) (B. De Strooper *et al*., 1999). The NICD translocates to the nucleus where it interacts with transcription factors resulting in transcriptional regulation of target genes.

To test the hypothesis that LRP2 is subjected to this proteolytic cleavage event, I generated a new mouse model that expresses the soluble ICD endogenously. To ensure correct expression of the ICD in cells that also express the wild type receptor, the ICD was knocked in via homologous recombination, into the murine *Lrp2* gene locus, to get expression driven by the LRP2 promoter.

5.3.1 The soluble LRP2 ICD does not affect renal function of the wild type receptor

There have been hints from cell studies that LRP2 may be subjected to RIP in the kidney. At the brush border membrane of proximal tubular cells in the rat kidney high γ-secretase activity was demonstrated, suggesting that LRP2, may be cleaved by this protease. In addition, the soluble extracellular domain of LRP2 was identified on the microvillar surface, while the cytosolic domain was found in the dense apical tubules and coated pits in this cell type (Z. Zou *et al*., 2004). Further support for RIP of LRP2 in the kidney came from *in vitro* studies of the membrane-bound and soluble COOH-terminal fragment of LRP2, stably overexpressed in opossum kidney proximal tubule cells (OKP) (Y. Li *et al*., 2008). In these experiments, overexpression of the ICD resulted in a dramatic downregulation of *Lrp2* transcripts. Based on these data, the authors argued that RIP of LRP2 in the kidney may represent a pathway to downregulate receptor gene expression at the transcriptional level and to protect renal cells from the harmful effects of protein overload (A. Saito *et al*., 2010).

To substantiate a proposed role for the LRP2 ICD in renal gene expression and function, I initially focused my analysis on the consequences of ICD expression in this tissue from mice heterozygous for the wild type receptor and carrying one copy of the ICD transgene ($Lrp2^{+/TgICD}$).

In Western blot analysis and immunohistochemistry experiments I was able to detect a robust signal for the ICD in kidneys of mice heterozygous for the ICD transgene ($Lrp2^{+/TgICD}$) (Figure 4.1.2 B-D). Furthermore these data demonstrated that in contrast to the wild type receptor that localized to the apical surface of proximal tubular cells, the ICD showed a diffuse cytoplasmic pattern in the same cells. Co-immunoprecipitation of the ICD with Dab2 displayed the ability of the soluble ICD to bind to intracellular interaction partners (Figure 4.1.3). Although the ICD can bind to Dab2 it does not affect localization of the wild type LRP2 as supported by the immunohistochemistry results described above. Also cubilin, the co-receptor for LRP2 in the kidney, exhibited a normal localization pattern (Figure 4.1.4 A). Additionally, I demonstrated no effect of the ICD on endocytosis mediated by the wild type receptor LRP2 in PTCs and *in vivo.* In contrast to LRP2-deficient mice that suffer from proteinuria the ICD had no influence on the endocytosis of the wild type

receptor (Figure 4.1.4). These data demonstrate that the ICD has no function on the wild type receptor LRP2 in trafficking or sorting.

Also, lack of obvious nuclear localization of the ICD argued against a role for the soluble receptor intracellular domain in transcriptional regulation; still, a role in regulating gene transcription might be possible since even the Notch intracellular domain could not be detected *in vivo* after RIP, possibly due to a rapid turnover of the ICD in the nucleus. To test the hypothesis that LRP2 downregulates its own expression, I analyzed the protein and mRNA expression levels of LRP2 in the kidney of $Lrp2^{+/TgICD}$ mice. *In vivo*, the soluble ICD failed to mediate reduction of its own gene expression levels, which was also confirmed on the protein level by Western blot analysis (Figure 4.1.5). Furthermore the ICD had no effect on the gene expression profile in the kidney (Figure 4.1.5) as demonstrated by microarray experiments. The characterization of the ICD *in vivo* could not confirm the hypothesis that the soluble ICD itself has signaling function in the kidney.

5.3.2 The soluble LRP2 ICD cannot rescue the defects in forebrain development described in $Lrp2^{-/-}$ mice

A former study by A. Grigorenko *et al*. in 2004 suggested that the ICD of LRP2 may have signaling function during development. In this study, the authors showed that the intracellular soluble domain of *Ce*-LRP1 could rescue the molting defects caused by the RNAi mediated knockdown of *Ce-Imp-2. Ce*-IMP-2 is part of the γ-secretase complex, which mediates RIP of cell surface receptors, including LRP2. In conclusion of their data, Grigorenko argued that phenotypes in nematodes elicited by blockade of RIP of *Ce*-LRP1 can be overcome by expression of the ICD only.

To investigate if the soluble ICD may have a similar signaling function during mouse development and may even substitute for the activity of the full-length receptor, I generated embryos homozygous for the transgene but lacking the wild type receptor ($Lrp2^{TgICD/TgICD}$) by breeding of $Lrp2^{TgICD/+}$ animals. Remarkably, $Lrp2^{TgICD/TgICD}$ embryos showed similar forebrain malformations as LRP2-deficient embryos ($Lrp2^{-/-}$) (Figure 4.1.6), clearly demonstrating that the soluble ICD is unable to rescue the defects caused by the deficiency of the full-length receptor.

Obviously, my data are in contrast to the observations made in *C. elegans*. One obvious difference in the two experimental setups is that the nematodes tested by Grigorenko still expressed the full-length receptor together with the ICD. In contrast, in my mouse model the full-length receptor was replaced by the ICD transgene.

In conclusion, my results provide unequivocal proof that during forebrain development in mice it is the full-length receptor and not the isolated ICD that regulates embryonic patterning.

5.4 Perspectives

In this study a direct role for LRP2 in the SHH pathway has been investigated but still there are many open questions about this complex regulatory pathway that warrant further analysis.

For example, the mechanisms of SHH-N binding to the receptor needs to be studied in more detail. We need to find out whether it is mainly the monomeric form or the multimeric complex of the morphogen that binds and whether modifications shown to be biologically relevant (lipid modification, association with lipoproteins) regulate receptor and morphogen interaction. Studies in cultured cells expressing wild type or mutant forms of LRP2 may be helpful in this respect.

Also, we need to elucidate in detail how binding of SHH-N to LRP2 affects the SHH signaling pathways. Does LRP2 simply act as a scavenging receptor for SHH-N presenting this ligand to its receptor Ptch1 and this functions as a reservoir for SHH? Undoubtedly, such a function could be very important during early stages of forebrain pattering when limiting amounts of SHH-H diffuse from the PrCP into the overlying ventral telencephalic midline. Perhaps even more exciting may be the prospect that LRP2 could directly interact with Ptch1, affecting the affinity of the receptor for SHH-N or promoting internalization of receptor-ligand complexes, a prerequisite to Smoothened activation. The later hypothesis is particularly relevant given the fact that SHH signaling in the neuroepithelium is tightly controlled by the movement of Ptch1 and Smo along the cilium. Detailed immunohistoloical analysis of LRP2 localization in neuroepithelial cells or studies in *ex vivo* neuroepithelial cell cultures from wild type and LRP2 null embryos may clarify these issues.

Although the soluble ICD used in the present mouse model failed to substitute for complete loss of the LRP2 full-length receptor, these findings still do not completely rule out a role for RIP in LRP2 activity in forebrain development. In analogy to Notch and other proteins RIP is often induced by binding of ligands to the receptors. Thus, it is still conceivable that binding of SHH-N to LRP2 elicits ligand-dependent RIP, a concept that cannot be tested with the current Tg ICD mouse model. Generation of mouse models expressing a protease-resistant form of LRP2 or application of γ-secretase antagonists in *ex vivo* models of LRP2 activity in the neuroepithelium may aid in testing this hypothesis.

6. Bibliography

Allen, B. L., Tenzen, T., and McMahon, A. P. (2007). The Hedgehog-binding proteins Gas1 and Cdo cooperate to positively regulate Shh signaling during mouse development. Genes Dev *21*, 1244-1257.

Andersen, O. M., Reiche, J., Schmidt, V., Gotthardt, M., Spoelgen, R., Behlke, J., von Arnim, C. A. F., Breiderhoff, T., Jansen, P., Wu, X., et al. (2005). Neuronal sorting protein-related receptor sorLA/LR11 regulates processing of the amyloid precursor protein. Proc. Natl. Acad. Sci. U.S.A *102*, 13461-13466.

Anderson, R. M., Lawrence, A. R., Stottmann, R. W., Bachiller, D., and Klingensmith, J. (2002). Chordin and noggin promote organizing centers of forebrain development in the mouse. Development *129*, 4975-4987.

Ang, S. L., and Rossant, J. (1994). HNF-3 beta is essential for node and notochord formation in mouse development. Cell *78*, 561-574.

Aoto, K., Shikata, Y., Imai, H., Matsumaru, D., Tokunaga, T., Shioda, S., Yamada, G., and Motoyama, J. (2009). Mouse Shh is required for prechordal plate maintenance during brain and craniofacial morphogenesis. Dev. Biol *327*, 106-120.

Argraves, W. S., and Morales, C. R. (2004). Immunolocalization of cubilin, megalin, apolipoprotein J, and apolipoprotein A-I in the uterus and oviduct. Mol. Reprod. Dev *69*, 419-427.

Bachiller, D., Klingensmith, J., Kemp, C., Belo, J. A., Anderson, R. M., May, S. R., McMahon, J. A., McMahon, A. P., Harland, R. M., Rossant, J., *et al*. (2000). The organizer factors Chordin and Noggin are required for mouse forebrain development. Nature *403*, 658-661.

Bansal, A., and Gierasch, L. M. (1991). The NPXY internalization signal of the LDL receptor adopts a reverse-turn conformation. Cell *67*, 1195-1201.

Biemesderfer, D. (2006). Regulated intramembrane proteolysis of megalin: linking urinary protein and gene regulation in proximal tubule? Kidney Int *69*, 1717-1721.

Birn, H., Fyfe, J. C., Jacobsen, C., Mounier, F., Verroust, P. J., Orskov, H., Willnow, T. E., Moestrup, S. K., and Christensen, E. I. (2000). Cubilin is an albumin binding protein important for renal tubular albumin reabsorption. J. Clin. Invest *105*, 1353-1361.

Birn, H., Willnow, T. E., Nielsen, R., Norden, A. G. W., Bönsch, C., Moestrup, S. K., Nexø, E., and Christensen, E. I. (2002). Megalin is essential for renal proximal tubule reabsorption and accumulation of transcobalamin-B(12). Am. J. Physiol. Renal Physiol *282*, F408-416.

Blobel, C. P. (2000). Remarkable roles of proteolysis on and beyond the cell surface. Curr. Opin. Cell Biol *12*, 606-612.

Boycott, K. M., Flavelle, S., Bureau, A., Glass, H. C., Fujiwara, T. M., Wirrell, E., Davey, K., Chudley, A. E., Scott, J. N., McLeod, D. R., et al. (2005). Homozygous deletion of the very low density lipoprotein receptor gene causes autosomal recessive cerebellar hypoplasia with cerebral gyral simplification. Am. J. Hum. Genet *77*, 477-483.

Bourhis, E., Tam, C., Franke, Y., Bazan, F. J., Ernst, J., Hwang, J., Costa, M., Cochran, A. G., and Hannoush, R. N. (2010). Reconstitution of a Frizzled8 Wnt3a LRP6 Signaling complex reveals multiple Wnt and DKK1 binding sites on LRP6. JBC *285*, 9172-9179.

Brown, M. S., Ye, J., Rawson, R. B., and Goldstein, J. L. (2000). Regulated intramembrane proteolysis: a control mechanism conserved from bacteria to humans. Cell *100*, 391-398.

Brown, A. J., Dusso, A., Slatopolsky E. (1999). Vitamin D. J. Physiol *277*, 157-175.

Brown, S. D., Twells, R. C., Hey, P. J., Cox, R. D., Levy, E. R., Soderman, A. R., Metzker, M. L., Caskey, C. T., Todd, J. A., and Hess, J. F. (1998). Isolation and characterization of LRP6, a novel member of the low density lipoprotein receptor gene family. Biochem. Biophys. Res. Commun *248*, 879-888.

Bu, G. (1998). Receptor-associated protein: a specialized chaperone and antagonist for members of the LDL receptor gene family. Curr. Opin. Lipidol *9*, 149-155.

Bu, G., Sun, Y., Schwartz, A. L., and Holtzman, D. M. (1998). Nerve growth factor induces rapid increases in functional cell surface low density lipoprotein receptor-related protein. J. Biol. Chem *273*, 13359-13365.

Bujo, H., Yamamoto, T., Hayashi, K., Hermann, M., Nimpf, J., and Schneider, W. J. (1995). Mutant oocytic low density lipoprotein receptor gene family member causes atherosclerosis and female sterility. Proc. Natl. Acad. Sci. U.S.A *92*, 9905-9909.

Burmeister, R., Boe, I. M., Nykjaer, A., Jacobsen, C., Moestrup, S. K., Verroust, P., Christensen, E. I., Lund, J., and Willnow, T. E. (2001). A two-receptor pathway for catabolism of Clara cell secretory protein in the kidney. J. Biol. Chem *276*, 13295-13301.

Carey, R. M., Balcz, B. A., Lopez-Coviella, I., and Slack, B. E. (2005). Inhibition of dynamin-dependent endocytosis increases shedding of the amyloid precursor protein ectodomain and reduces generation of amyloid beta protein. BMC Cell Biol *6*, 30.

Caspary, T., García-García, M. J., Huangfu, D., Eggenschwiler, J. T., Wyler, M. R., Rakeman, A. S., Alcorn, H. L., and Anderson, K. V. (2002). Mouse Dispatched homolog1 is required for long-range, but not juxtacrine, Hh signaling. Curr. Biol *12*, 1628-1632.

Chamberlain, C. E., Jeong, J., Guo, C., Allen, B. L., and McMahon, A. P. (2008). Notochord-derived Shh concentrates in close association with the apically positioned basal body in neural target cells and forms a dynamic gradient during neural patterning. Development *135*, 1097-1106.

Chen, J. K., Taipale, J., Young, K. E., Maiti, T., and Beachy, P. A. (2002). Small molecule modulation of Smoothened activity. Proc. Natl. Acad. Sci. U.S.A *99*, 14071-14076.

Chen, W. J., Goldstein, J. L., and Brown, M. S. (1990). NPXY, a sequence often found in cytoplasmic tails, is required for coated pit-mediated internalization of the low density lipoprotein receptor. J. Biol. Chem *265*, 3116-3123.

Chiang, C., Litingtung, Y., Lee, E., Young, K. E., Corden, J. L., Westphal, H., and Beachy, P. A. (1996). Cyclopia and defective axial patterning in mice lacking Sonic hedgehog gene function. Nature *383*, 407-413.

Chow, R. L., and Lang, R. A. (2001). Early eye development in vertebrates. Annu. Rev. Cell Dev. Biol *17*, 255-296.

Christensen, E. I., Moskaug, J. O., Vorum, H., Jacobsen, C., Gundersen, T. E., Nykjaer, A., Blomhoff, R., Willnow, T. E., and Moestrup, S. K. (1999). Evidence for an essential role of megalin in transepithelial transport of retinol. J. Am. Soc. Nephrol *10*, 685-695.

Christensen, E. I., Nielsen, S., Moestrup, S. K., Borre, C., Maunsbach, A. B., de Heer, E., Ronco, P., Hammond, T. G., and Verroust, P. (1995). Segmental distribution of the endocytosis receptor gp330 in renal proximal tubules. Eur. J. Cell Biol *66*, 349-364.

Christensen, E. I., and Willnow, T. E. (1999). Essential role of megalin in renal proximal tubule for vitamin homeostasis. J. Am. Soc. Nephrol *10*, 2224-2236.

Chu, J., Ding, J., Jeays-Ward, K., Price, S. M., Placzek, M., and Shen, M. M. (2005). Non-cell-autonomous role for Cripto in axial midline formation during vertebrate embryogenesis. Development *132*, 5539-5551.

Chuang, P., Kawcak, T., and McMahon, A. P. (2003). Feedback control of mammalian Hedgehog signaling by the Hedgehog-binding protein, Hip1, modulates Fgf signaling during branching morphogenesis of the lung. Genes Dev *17*, 342-347.

Clevers, H. (2006). Wnt/beta-catenin signaling in development and disease. Cell *127*, 469-480.

Cohen, M. M. (2006). Holoprosencephaly: clinical, anatomic, and molecular dimensions. Birth Defects Res. Part A Clin. Mol. Teratol *76*, 658-673.

Cohen, M. M., and Shiota, K. (2002). Teratogenesis of holoprosencephaly. Am. J. Med. Genet *109*, 1-15.

Corbit, K. C., Aanstad, P., Singla, V., Norman, A. R., Stainier, D. Y. R., and Reiter, J. F. (2005). Vertebrate Smoothened functions at the primary cilium. Nature *437*, 1018-1021.

Couly, G., and Le Douarin, N. M. (1988). The fate map of the cephalic neural primordium at the presomitic to the 3-somite stage in the avian embryo. Development *103 Suppl*, 101-113.

Cowan, J. W., Wang, X., Guan, R., He, K., Jiang, J., Baumann, G., Black, R. A., Wolfe, M. S., and Frank, S. J. (2005). Growth hormone receptor is a target for presenilin-dependent gamma-secretase cleavage. J. Biol. Chem *280*, 19331-19342.

D'Arcangelo, G., Homayouni, R., Keshvara, L., Rice, D. S., Sheldon, M., and Curran, T. (1999). Reelin is a ligand for lipoprotein receptors. Neuron *24*, 471-479.

Davidson, G., Wu, W., Shen, J., Bilic, J., Fenger, U., Stannek, P., Glinka, A., and Niehrs, C. (2005). Casein kinase 1 gamma couples Wnt receptor activation to cytoplasmic signal transduction. Nature *438*, 867-872.

Dessaud, E., Yang, L. L., Hill, K., Cox, B., Ulloa, F., Ribeiro, A., Mynett, A., Novitch, B. G., and Briscoe, J. (2007). Interpretation of the sonic hedgehog morphogen gradient by a temporal adaption mechanism. Nature *450*: 717-20.

Dessaud, E., McMahon, A. P., and Briscoe, J. (2008). Pattern formation in the vertebrate neural tube: a sonic hedgehog morphogen-regulated transcriptional network. Development *135*, 2489-2503.

De Strooper, B., Annaert, W., Cupers, P., Saftig, P., Craessaerts, K., Mumm, J. S., Schroeter, E. H., Schrijvers, V., Wolfe, M. S., Ray, W. J., Goate, A., Kopan, R. (1999). A presenilin-1-dependent gamma-secretase-like protease mediates release of Notch intracellular domain. Nature *398*, 518-522.

Dethlefsen, S. M., Raab, G., Moses, M. A., Adam, R. M., Klagsbrun, M., and Freeman, M. R. (1998). Extracellular calcium influx stimulates metalloproteinase cleavage and secretion of heparin-binding EGF-like growth factor independently of protein kinase C. J. Cell. Biochem *69*, 143-153.

Drake, C. J., Fleming, P. A., Larue, A. C., Barth, J. L., Chintalapudi, M. R., and Argraves, W. S. (2004). Differential distribution of cubilin and megalin expression in the mouse embryo. Anat Rec A Discov Mol Cell Evol Biol *277*, 163-170.

Drögemüller, C., Leeb, T., Harlizius, B., Tammen, I., Distl, O., Höltershinken, M., Gentile, A., Duchesne, A., and Eggen, A. (2007). Congenital syndactyly in cattle: four novel mutations in the low density lipoprotein receptor-related protein 4 gene (LRP4). BMC Genet *8*, 5.

Dubourg, C., Bendavid, C., Pasquier, L., Henry, C., Odent, S., and David, V. (2007). Holoprosencephaly. Orphanet J Rare Dis *2*, 8.

Duchesne, A., Gautier, M., Chadi, S., Grohs, C., Floriot, S., Gallard, Y., Caste, G., Ducos, A., and Eggen, A. (2006). Identification of a doublet missense substitution in the bovine LRP4 gene as a candidate causal mutation for syndactyly in Holstein cattle. Genomics *88*, 610-621.

Dunn, N. R., Winnier, G. E., Hargett, L. K., Schrick, J. J., Fogo, A. B., and Hogan, B. L. (1997). Haploinsufficient phenotypes in Bmp4 heterozygous null mice and modification by mutations in Gli3 and Alx4. Dev. Biol *188*, 235-247.

Eagleson, G., Ferreiro, B., and Harris, W. A. (1995). Fate of the anterior neural ridge and the morphogenesis of the Xenopus forebrain. J. Neurobiol *28*, 146-158.

Ericson, J., Muhr, J., Placzek, M., Lints, T., Jessell, T. M., and Edlund, T. (1995). Sonic hedgehog induces the differentiation of ventral forebrain neurons: a common signal for ventral patterning within the neural tube. Cell *81*, 747-756.

Ericson, J., Briscoe, J., Rashbass, P., van Heyningen, V., Jessel, T. M. (1997). Graded sonic hedgehog signaling and the specification of cell fate in the ventral neural tube. Cold Spring Harb Symp Quant Biol *62*, 451-466.

Feng, J., White, B., Tyurina, O. V., Guner, B., Larson, T., Lee, H. Y., Karlstrom, R. O., and Kohtz, J. D. (2004). Synergistic and antagonistic roles of the Sonic hedgehog N- and C-terminal lipids. Development *131*, 4357-4370.

Fernandes, M., Gutin, G., Alcorn, H., McConnell, S. K., and Hébert, J. (2007). Mutations in the BMP pathway in mice support the existence of two molecular classes of holoprosencephaly. Development *134*, 3789-3794.

Fujino, T., Asaba, H., Kang, M., Ikeda, Y., Sone, H., Takada, S., Kim, D., Ioka, R. X., Ono, M., Tomoyori, H., et al. (2003). Low-density lipoprotein receptor-related protein 5 (LRP5) is essential for normal cholesterol metabolism and glucose-induced insulin secretion. Proc. Natl. Acad. Sci. U.S.A *100*, 229-234.

Fukuchi-Shimogori, T., and Grove E. A. (2003). Emx2 patterns the neocortex by regulating FGF positional signaling. Nat Neurosci. *6*, 825-31.

Gåfvels, M. E., Paavola, L. G., Boyd, C. O., Nolan, P. M., Wittmaack, F., Chawla, A., Lazar, M. A., Bucan, M., Angelin, B. O., and Strauss, J. F. (1994). Cloning of a complementary deoxyribonucleic acid encoding the murine homolog of the very low density lipoprotein/apolipoprotein-E receptor: expression pattern and assignment of the gene to mouse chromosome 19. Endocrinology *135*, 387-394.

Gajera, C. R., Emich, H., Lioubinski, O., Christ, A., Beckervordersandforth-Bonk, R., Yoshikawa, K., Bachmann, S., Christensen, E. I., Götz, M., Kempermann, G., et al. (2010). LRP2 in ependymal cells regulates BMP signaling in the adult neurogenic niche. J. Cell. Sci *123*, 1922-1930.

Geng, X., and Oliver, G. (2009). Pathogenesis of holoprosencephaly. J. Clin. Invest *119*, 1403-1413.

Geng, X., Speirs, C., Lagutin, O., Inbal, A., Liu, W., Solnica-Krezel, L., Jeong, Y., Epstein, D. J., and Oliver, G. (2008). Haploinsufficiency of Six3 fails to activate Sonic hedgehog expression in the ventral forebrain and causes holoprosencephaly. Dev. Cell *15*, 236-247.

Gerbe, F., Cox, B., Rossant, J., and Chazaud, C. (2008). Dynamic expression of Lrp2 pathway members reveals progressive epithelial differentiation of primitive endoderm in mouse blastocyst. Dev. Biol *313*, 594-602.

Gestri, G., Carl, M., Appolloni, I., Wilson, S. W., Barsacchi, G., and Andreazzoli, M. (2005). Six3 functions in anterior neural plate specification by promoting cell proliferation and inhibiting Bmp4 expression. Development *132*, 2401-2413.

Gilbert, S. F. (2006). Principles of Development: 8th Edition. Sinauer Associates 402.

Goldstein, J. L., Hobbs, H. H. and Brown, M. S. (2001). Familial hypercholesterolemia. In *The Metabolic and Molecular Basis of Inherited Disease* (ed. C. R. Scriver, A. L. Beaudet, W. S. Sly, D. Valle, B. Childs, K. W. Kinzler and B. Vogelstein), pp. 2863-2913. New York: McGraw-Hill.

Gong, Y., Slee, R. B., Fukai, N., Rawadi, G., Roman-Roman, S., Reginato, A. M., Wang, H., Cundy, T., Glorieux, F. H., Lev, D., et al. (2001). LDL receptor-related protein 5 (LRP5) affects bone accrual and eye development. Cell *107*, 513-523.

Gotthardt, M., Trommsdorff, M., Nevitt, M. F., Shelton, J., Richardson, J. A., Stockinger, W., Nimpf, J., and Herz, J. (2000). Interactions of the low density lipoprotein receptor gene family with cytosolic adaptor and scaffold proteins suggest diverse biological functions in cellular communication and signal transduction. J. Biol. Chem *275*, 25616-25624.

Grant, B., and Hirsh, D. (1999). Receptor-mediated endocytosis in the Caenorhabditis elegans oocyte. Mol. Biol. Cell *10*, 4311-4326.

Grigorenko, A. P., Moliaka, Y. K., Soto, M. C., Mello, C. C., and Rogaev, E. I. (2004). The Caenorhabditis elegans IMPAS gene, imp-2, is essential for development and is functionally distinct from related presenilins. Proc. Natl. Acad. Sci. U.S.A *101*, 14955-14960.

Grove, E. A., Tole, S., Limon, J., Yip, L., and Ragsdale, C. W. (1998). The hem of the embryonic cerebral cortex is defined by the expression of multiple Wnt genes and is compromised in Gli3-deficient mice. Development *125*, 2315-2325.

Gutin, G., Fernandes, M., Palazzolo, L., Paek, H., Yu, K., Ornitz, D. M., McConnell, S. K., and Hébert, J. M. (2006). FGF signalling generates ventral telencephalic cells independently of SHH. Development *133*, 2937-2946.

Hammad, S. M., Stefansson, S., Twal, W. O., Drake, C. J., Fleming, P., Remaley, A., Brewer, H. B., and Argraves, W. S. (1999). Cubilin, the endocytic receptor for intrinsic factor-vitamin B(12) complex, mediates high-density lipoprotein holoparticle endocytosis. Proc. Natl. Acad. Sci. U.S.A *96*, 10158-10163.

Hammes, A., Andreassen, T. K., Spoelgen, R., Raila, J., Hubner, N., Schulz, H., Metzger, J., Schweigert, F. J., Luppa, P. B., Nykjaer, A., et al. (2005). Role of endocytosis in cellular uptake of sex steroids. Cell *122*, 751-762.

Haycraft, C. J., Banizs, B., Aydin-Son, Y., Zhang, Q., Michaud, E. J., and Yoder, B. K. (2005). Gli2 and Gli3 localize to cilia and require the intraflagellar transport protein polaris for processing and function. PLoS Genet *1*, e53.

Hayhurst, M., and McConnell, S. K. (2003). Mouse models of holoprosencephaly. Curr. Opin. Neurol *16*, 135-141.

Herz, J., Clouthier, D. E., and Hammer, R. E. (1992). LDL receptor-related protein internalizes and degrades uPA-PAI-1 complexes and is essential for embryo implantation. Cell *71*, 411-421.

Herz, J., Couthier, D. E., and Hammer, R. E. (1993). Correction: LDL receptor-related protein internalizes and degrades uPA-PAI-1 complexes and is essential for embryo implantation. Cell *73*, 428.

Herz, J., and Strickland, D. K. (2001). LRP: a multifunctional scavenger and signaling receptor. J. Clin. Invest *108*, 779-784.

Herz, J., and Bock, H. H. (2002). Lipoprotein receptors in the nervous system. Annu. Rev. Biochem *71*, 405-434.

Hiesberger, T., Trommsdorff, M., Howell, B. W., Goffinet, A., Mumby, M. C., Cooper, J. A., and Herz, J. (1999). Direct binding of Reelin to VLDL receptor and ApoE receptor 2 induces tyrosine phosphorylation of disabled-1 and modulates tau phosphorylation. Neuron *24*, 481-489.

Hilpert, J., Nykjaer, A., Jacobsen, C., Wallukat, G., Nielsen, R., Moestrup, S. K., Haller, H., Luft, F. C., Christensen, E. I., and Willnow, T. E. (1999). Megalin antagonizes activation of the parathyroid hormone receptor. J. Biol. Chem *274*, 5620-5625.

Hilpert, J., Wogensen, L., Thykjaer, T., Wellner, M., Schlichting, U., Orntoft, T. F., Bachmann, S., Nykjaer, A., and Willnow, T. E. (2002). Expression profiling confirms the role of endocytic receptor megalin in renal vitamin D3 metabolism. Kidney Int *62*, 1672-1681.

Hoch, R. V., Rubenstein, J. L. R., and Pleasure, S. (2009). Genes and signaling events that establish regional patterning of the mammalian forebrain. Semin. Cell Dev. Biol *20*, 378-386.

Hooper, J. E., and Scott, M. P. (2005). Communicating with Hedgehogs. Nat. Rev. Mol. Cell Biol *6*, 306-317.

Huang, X., Litingtung, Y., and Chiang, C. (2007a). Ectopic sonic hedgehog signaling impairs telencephalic dorsal midline development: implication for human holoprosencephaly. Hum. Mol. Genet *16*, 1454-1468.

Huang, X., Litingtung, Y., and Chiang, C. (2007b). Region-specific requirement for cholesterol modification of sonic hedgehog in patterning the telencephalon and spinal cord. Development *134*, 2095-2105.

Inbal, A., Kim, S., Shin, J., and Solnica-Krezel, L. (2007). Six3 represses nodal activity to establish early brain asymmetry in zebrafish. Neuron *55*, 407-415.

Ingham, P. W., and McMahon, A. P. (2001). Hedgehog signaling in animal development: paradigms and principles. Genes Dev *15*, 3059-3087.

Ishibashi, S., Brown, M. S., Goldstein, J. L., Gerard, R. D., Hammer, R. E., and Herz, J. (1993). Hypercholesterolemia in low density lipoprotein receptor knockout mice and its reversal by adenovirus-mediated gene delivery. J. Clin. Invest *92*, 883-893.

Jeong, J., and McMahon, A. P. (2005). Growth and pattern of the mammalian neural tube are governed by partially overlapping feedback activities of the hedgehog antagonists patched 1 and Hhip1. Development *132*, 143-154.

Jeong, Y., Leskow, F. C., El-Jaick, K., Roessler, E., Muenke, M., Yocum, A., Dubourg, C., Li, X., Geng, X., Oliver, G., et al. (2008). Regulation of a remote Shh forebrain enhancer by the Six3 homeoprotein. Nat. Genet *40*, 1348-1353.

Johnson, E. B., Hammer, R. E., and Herz, J. (2005). Abnormal development of the apical ectodermal ridge and polysyndactyly in Megf7-deficient mice. Hum. Mol. Genet *14*, 3523-3538.

Kantarci, S., Al-Gazali, L., Hill, R. S., Donnai, D., Black, G. C. M., Bieth, E., Chassaing, N., Lacombe, D., Devriendt, K., Teebi, A., et al. (2007). Mutations in LRP2, which encodes the multiligand receptor megalin, cause Donnai-Barrow and facio-oculo-acoustico-renal syndromes. Nat. Genet *39*, 957-959.

Kato, M., Patel, M. S., Levasseur, R., Lobov, I., Chang, B. H., Glass, D. A. 2nd., Hartmann, C., Li, L., Hwang, T. H., Brayton, C. F., Lang, R. A., Karsenty, G., Chan, L. (2002). Cbfa1-independent decrease in osteoblast proliferation, osteopeniy, and persistent embryonic eye vascularization in mice deficient in Lrp5, a Wnt coreceptor. J Cell Biol. *157*, 303-314.

Kawano, Y., Okamoto, I., Murakami, D., Itoh, H., Yoshida, M., Ueda, S., and Saya, H. (2000). Ras oncoprotein induces CD44 cleavage through phosphoinositide 3-OH kinase and the rho family of small G proteins. J. Biol. Chem *275*, 29628-29635.

Kim, N., Stiegler, A. L., Cameron, T. O., Hallock, P. T., Gomez, A. M., Huang, J. H., Hubbard, S. R., Dustin, M. L., and Burden, S. J. (2008). Lrp4 is a receptor for Agrin and forms a complex with MuSK. Cell *135*, 334-342.

Klingensmith, J., Ang, S. L., Bachiller, D., and Rossant, J. (1999). Neural induction and patterning in the mouse in the absence of the node and its derivatives. Dev. Biol *216*, 535-549.

Kohtz, J. D., Baker, D. P., Corte, G., and Fishell, G. (1998). Regionalization within the mammalian telencephalon is mediated by changes in responsiveness to Sonic Hedgehog. Development *125*, 5079-5089.

Kounnas, M. Z., Haudenschild, C. C., Strickland, D. K., and Argraves, W. S. (1994). Immunological localization of glycoprotein 330, low density lipoprotein receptor related protein and 39 kDa receptor associated protein in embryonic mouse tissues. In Vivo *8*, 343-351.

Kozyraki, R., Fyfe, J., Verroust, P. J., Jacobsen, C., Dautry-Varsat, A., Gburek, J., Willnow, T. E., Christensen, E. I., and Moestrup, S. K. (2001). Megalin-dependent cubilin-mediated endocytosis is a major pathway for the apical uptake of transferrin in polarized epithelia. Proc. Natl. Acad. Sci. U.S.A *98*, 12491-12496.

Kozyraki, R., Kristiansen, M., Gerdes, C., Jacobsen, C., Cui, S., Christensen, E. I., Aminoff, M., de la Chapelle, A., Krahe, R., Verroust, P. J., Moestrup, S. K. (1999). The intrinsic factor-vitamin B12 receptor, cubilin, is a high-affinity apolipoprotein A-I receptor facilitating endocytosis of high-density lipoprotein. Nat Med. *5*, 656-661.

Krauss, R. S. (2007). Holoprosencephaly: new models, new insights. Expert Rev Mol Med *9*, 1-17.

Kristiansen, M., Kozyraki, R., Jacobsen, C., Nexø, E., Verroust, P. J., and Moestrup, S. K. (1999). Molecular dissection of the intrinsic factor-vitamin B12 receptor, cubilin, discloses regions important for membrane association and ligand binding. J. Biol. Chem *274*, 20540-20544.

Kuschel, S., Rüther, U., and Theil, T. (2003). A disrupted balance between Bmp/Wnt and Fgf signaling underlies the ventralization of the Gli3 mutant telencephalon. Dev. Biol *260*, 484-495.

Kutejova, E., Briscoe, J., and Kicheva, A. (2009). Temporal dynamics of patterning by morphogen gradients. Curr. Opin. Genet. Dev *19*, 315-322.

Lacbawan, F., Solomon, B. D., Roessler, E., El-Jaick, K., Domené, S., Vélez, J. I., Zhou, N., Hadley, D., Balog, J. Z., Long, R., et al. (2009). Clinical spectrum of SIX3-associated mutations in holoprosencephaly: correlation between genotype, phenotype and function. J. Med. Genet *46*, 389-398.

Lagutin, O. V., Zhu, C. C., Kobayashi, D., Topczewski, J., Shimamura, K., Puelles, L., Russell, H. R. C., McKinnon, P. J., Solnica-Krezel, L., and Oliver, G. (2003). Six3 repression of Wnt signaling in the anterior neuroectoderm is essential for vertebrate forebrain development. Genes Dev *17*, 368-379.

Lee, J. H., Cheng, R., Schupf, N., Manly, J., Lantigua, R., Stern, Y., Rogaeva, E., Wakutani, Y., Farrer, L., St George-Hyslop, P., et al. (2007). The association between genetic variants in SORL1 and Alzheimer disease in an urban, multiethnic, community-based cohort. Arch. Neurol *64*, 501-506.

Leheste, J. R., Rolinski, B., Vorum, H., Hilpert, J., Nykjaer, A., Jacobsen, C., Aucouturier, P., Moskaug, J. O., Otto, A., Christensen, E. I., et al. (1999). Megalin knockout mice as an animal model of low molecular weight proteinuria. Am. J. Pathol *155*, 1361-1370.

Leheste, J. R., Melsen, F., Wellner, M., Jansen, P., Schlichting, U., Renner-Müller, I., Andreassen, T. T., Wolf, E., Bachmann, S., Nykjaer, A., et al. (2003). Hypocalcemia and osteopathy in mice with kidney-specific megalin gene defect. FASEB J *17*, 247-249.

Lewis, A. J., Simon, E. M., Barkovich, A. J., Clegg, N. J., Delgado, M. R., Levey, E., and Hahn, J. S. (2002). Middle interhemispheric variant of holoprosencephaly: a distinct cliniconeuroradiologic subtype. Neurology *59*, 1860-1865.

Li, H., Tierney, C., Wen, L., Wu, J. Y., and Rao, Y. (1997). A single morphogenetic field gives rise to two retina primordia under the influence of the prechordal plate. Development *124*, 603-615.

Li, Y., Cam, J., and Bu, G. (2001a). Low-density lipoprotein receptor family: endocytosis and signal transduction. Mol. Neurobiol *23*, 53-67.

Li, Y., van Kerkhof, P., Marzolo, M. P., Strous, G. J., and Bu, G. (2001b). Identification of a major cyclic AMP-dependent protein kinase A phosphorylation site within the cytoplasmic tail of the low-density lipoprotein receptor-related protein: implication for receptor-mediated endocytosis. Mol. Cell. Biol *21*, 1185-1195.

Li, Y., Marzolo, M. P., van Kerkhof, P., Strous, G. J., and Bu, G. (2000). The YXXL motif, but not the two NPXY motifs, serves as the dominant endocytosis signal for low density lipoprotein receptor-related protein. J. Biol. Chem *275*, 17187-17194.

Li, Y., Cong, R., and Biemesderfer, D. (2008). The COOH terminus of megalin regulates gene expression in opossum kidney proximal tubule cells. Am. J. Physiol., Cell Physiol *295*, C529-537.

Little, R. D., Carulli, J. P., Del Mastro, R. G., Dupuis, J., Osborne, M., Folz, C., Manning, S. P., Swain, P. M., Zhao, S., Eustace, B., et al. (2002). A mutation in the LDL receptor-related protein 5 gene results in the autosomal dominant high-bone-mass trait. Am. J. Hum. Genet *70*, 11-19.

Liu, C. X., Musco, S., Lisitsina, N. M., Forgacs, E., Minna, J. D., and Lisitsyn, N. A. (2000). LRP-DIT, a putative endocytic receptor gene, is frequently inactivated in non-small cell lung cancer cell lines. Cancer Res *60*, 1961-1967.

Logan, C. Y., and Nusse, R. (2004). The Wnt signaling pathway in development and disease. Annu. Rev. Cell Dev. Biol *20*, 781-810.

Lowe, L. A., Yamada, S., and Kuehn, M. R. (2001). Genetic dissection of nodal function in patterning the mouse embryo. Development *128*, 1831-1843.

Lu, C. C., Brennan, J., and Robertson, E. J. (2001). From fertilization to gastrulation: axis formation in the mouse embryo. Curr. Opin. Genet. Dev *11*, 384-392.

Lundgren, S., Carling, T., Hjälm, G., Juhlin, C., Rastad, J., Pihlgren, U., Rask, L., Akerström, G., and Hellman, P. (1997). Tissue distribution of human gp330/megalin, a putative Ca(2+)-sensing protein. J. Histochem. Cytochem *45*, 383-392.

Ma, Y., Erkner, A., Gong, R., Yao, S., Taipale, J., Basler, K., and Beachy, P. A. (2002). Hedgehog-mediated patterning of the mammalian embryo requires transporter-like function of dispatched. Cell *111*, 63-75.

Mahley, R. W. (1988). Apolipoprotein E: cholesterol transport protein with expanding role in cell biology. Science *240*, 622-630.

Mani, A., Radhakrishnan, J., Wang, H., Mani, A., Mani, M., Nelson-Williams, C., Carew, K. S., Mane, S., Najmabadi, H., Wu, D., et al. (2007). LRP6 mutation in a family with early coronary disease and metabolic risk factors. Science *315*, 1278-1282.

Mao, B., Wu, W., Li, Y., Hoppe, D., Stannek, P., Glinka, A., and Niehrs, C. (2001). LDL-receptor-related protein 6 is a receptor for Dickkopf proteins. Nature *411*, 321-325.

Marschang, P., Brich, J., Weeber, E. J., Sweatt, J. D., Shelton, J. M., Richardson, J. A., Herz, J. (2004). Normal development and fertility of knockout mice lacking the tumor suppressor gene LRP1b suggest functional compensation by LRP1. Mol Cell Biol. *24*, 3782-3793.

Martinelli, D. C., and Fan, C. (2007a). Gas1 extends the range of Hedgehog action by facilitating its signaling. Genes Dev *21*, 1231-1243.

Martinelli, D. C., and Fan, C. (2007b). The role of Gas1 in embryonic development and its implications for human disease. Cell Cycle *6*, 2650-2655.

Matsunaga, E., and Shiota, K. (1977). Holoprosencephaly in human embryos: epidemiologic studies of 150 cases. Teratology *16*, 261-272.

May, P., Bock, H. H., and Herz, J. (2003). Integration of endocytosis and signal transduction by lipoprotein receptors. Sci. STKE *2003*, PE12.

May, P., Reddy, Y. K., and Herz, J. (2002). Proteolytic processing of low density lipoprotein receptor-related protein mediates regulated release of its intracellular domain. J. Biol. Chem *277*, 18736-18743.

McCarthy, R. A., and Argraves, W. S. (2003). Megalin and the neurodevelopmental biology of sonic hedgehog and retinol. J. Cell. Sci *116*, 955-960.

McCarthy, R. A., Barth, J. L., Chintalapudi, M. R., Knaak, C., and Argraves, W. S. (2002). Megalin functions as an endocytic sonic hedgehog receptor. J. Biol. Chem *277*, 25660-25667.

Medina, M., and Dotti, C. G. (2003). RIPped out by presenilin-dependent gamma-secretase. Cell. Signal *15*, 829-841.

Meyers, E. N., Lewandoski, M., and Martin, G. R. (1998). An Fgf8 mutant allelic series generated by Cre- and Flp-mediated recombination. Nat. Genet *18*, 136-141.

Milenkovic, L., Scott, M. P., and Rohatgi, R. (2009). Lateral transport of Smoothened from the plasma membrane to the membrane of the cilium. J. Cell Biol *187*, 365-374.

Moestrup, S. K., Birn, H., Fischer, P. B., Petersen, C. M., Verroust, P. J., Sim, R. B., Christensen, E. I., and Nexø, E. (1996). Megalin-mediated endocytosis of transcobalamin-vitamin-B12 complexes suggests a role of the receptor in vitamin-B12 homeostasis. Proc. Natl. Acad. Sci. U.S.A *93*, 8612-8617.

Monuki, E. S. (2007). The morphogen signaling network in forebrain development and holoprosencephaly. J. Neuropathol. Exp. Neurol *66*, 566-575.

Morales, C. R., Zeng, J., El Alfy, M., Barth, J. L., Chintalapudi, M. R., McCarthy, R. A., Incardona, J. P., and Argraves, W. S. (2006). Epithelial trafficking of Sonic hedgehog by megalin. J. Histochem. Cytochem *54*, 1115-1127.

Morris, S. M., Tallquist, M. D., Rock, C. O., and Cooper, J. A. (2002). Dual roles for the Dab2 adaptor protein in embryonic development and kidney transport. EMBO J *21*, 1555-1564.

Muenke, M., and Beachy, P. A. (2000). Genetics of ventral forebrain development and holoprosencephaly. Curr. Opin. Genet. Dev *10*, 262-269.

Muenke, M., and Cohen, M. M. (2000). Genetic approaches to understanding brain development: holoprosencephaly as a model. Ment Retard Dev Disabil Res Rev *6*, 15-21.

Mumm, J. S., Schroeter, E. H., Saxena, M. T., Griesemer, A., Tian, X., Pan, D. J., Ray, W. J., and Kopan, R. (2000). A ligand-induced extracellular cleavage regulates gamma-secretase-like proteolytic activation of Notch1. Mol. Cell *5*, 197-206.

Nagai, J., Christensen, E. I., Morris, S. M., Willnow, T. E., Cooper, J. A., and Nielsen, R. (2005). Mutually dependent localization of megalin and Dab2 in the renal proximal tubule. Am. J. Physiol. Renal Physiol *289*, F569-576.

Nagai, T., Aruga, J., Minowa, O., Sugimoto, T., Ohno, Y., Noda, T., and Mikoshiba, K. (2000). Zic2 regulates the kinetics of neurulation. Proc. Natl. Acad. Sci. U.S.A *97*, 1618-1623.

Nykjaer, A., Dragun, D., Walther, D., Vorum, H., Jacobsen, C., Herz, J., Melsen, F., Christensen, E. I., and Willnow, T. E. (1999). An endocytic pathway essential for renal uptake and activation of the steroid 25-(OH) vitamin D3. Cell *96*, 507-515.

Nykjaer, A., Fyfe, J. C., Kozyraki, R., Leheste, J. R., Jacobsen, C., Nielsen, M. S., Verroust, P. J., Aminoff, M., de la Chapelle, A., Moestrup, S. K., et al. (2001). Cubilin dysfunction causes abnormal metabolism of the steroid hormone 25(OH) vitamin D(3). Proc. Natl. Acad. Sci. U.S.A *98*, 13895-13900.

Nykjaer, A., and Willnow, T. E. (2002). The low-density lipoprotein receptor gene family: a cellular Swiss army knife? Trends Cell Biol *12*, 273-280.

Ohkubo, Y., Chiang, C., and Rubenstein, J. L. R. (2002). Coordinate regulation and synergistic actions of BMP4, SHH and FGF8 in the rostral prosencephalon regulate morphogenesis of the telencephalic and optic vesicles. Neuroscience *111*, 1-17.

Oleinikov, A. V., Zhao, J., and Makker, S. P. (2000). Cytosolic adaptor protein Dab2 is an intracellular ligand of endocytic receptor gp600/megalin. Biochem. J *347 Pt 3*, 613-621.

Orlando, R. A., and Farquhar, M. G. (1993). Identification of a cell line that expresses a cell surface and a soluble form of the gp330/receptor-associated protein (RAP) Heymann nephritis antigenic complex. Proc. Natl. Acad. Sci. U.S.A *90*, 4082-4086.

Panáková, D., Sprong, H., Marois, E., Thiele, C., and Eaton, S. (2005). Lipoprotein particles are required for Hedgehog and Wingless signalling. Nature *435*, 58-65.

Pepinsky, R. B., Zeng, C., Wen, D., Rayhorn, P., Baker, D. P., Williams, K. P., Bixler, S. A., Ambrose, C. M., Garber, E. A., Miatkowski, K., et al. (1998). Identification of a palmitic acid-modified form of human Sonic hedgehog. J. Biol. Chem *273*, 14037-14045.

Pera, E. M., and Kessel, M. (1997). Patterning of the chick forebrain anlage by the prechordal plate. Development *124*, 4153-4162.

Petryk, A., Anderson, R. M., Jarcho, M. P., Leaf, I., Carlson, C. S., Klingensmith, J., Shawlot, W., and O'Connor, M. B. (2004). The mammalian twisted gastrulation gene functions in foregut and craniofacial development. Dev. Biol *267*, 374-386.

Pinson, K. I., Brennan, J., Monkley, S., Avery, B. J., and Skarnes, W. C. (2000). An LDL-receptor-related protein mediates Wnt signalling in mice. Nature *407*, 535-538.

Porter, J. A., von Kessler, D. P., Ekker, S. C., Young, K. E., Lee, J. J., Moses, K., and Beachy, P. A. (1995). The product of hedgehog autoproteolytic cleavage active in local and long-range signalling. Nature *374*, 363-366.

Rash, B. G., and Grove, E. A. (2007). Patterning the dorsal telencephalon: a role for sonic hedgehog? J. Neurosci *27*, 11595-11603.

Rawson, R. B. (2002). Regulated intramembrane proteolysis: from the endoplasmic reticulum to the nucleus. Essays Biochem *38*, 155-168.

Raychowdhury, R., Niles, J. L., McCluskey, R. T., and Smith, J. A. (1989). Autoimmune target in Heymann nephritis is a glycoprotein with homology to the LDL receptor. Science *244*, 1163-1165.

Ribes, V., Balaskas, N., Sasai, N., Cruz, C., Dessaud, E., Cayuso, J., Tozer, S., Yang, L. L., Novitch, B., Marti, E., et al. (2010). Distinct Sonic Hedgehog signaling dynamics specify floor plate and ventral neuronal progenitors in the vertebrate neural tube. Genes Dev *24*, 1186-1200.

Ribes, V., and Briscoe, J. (2009). Establishing and interpreting graded Sonic Hedgehog signaling during vertebrate neural tube patterning: the role of negative feedback. Cold Spring Harb Perspect Biol *1*, a002014.

Roach, E., Demyer, W., Conneally, P. M., Palmer, C., and Merritt, A. D. (1975). Holoprosencephaly: birth data, benetic and demographic analyses of 30 families. Birth Defects Orig. Artic. Ser *11*, 294-313.

Roebroek, A. J. M., Reekmans, S., Lauwers, A., Feyaerts, N., Smeijers, L., and Hartmann, D. (2006). Mutant Lrp1 knock-in mice generated by recombinase-mediated cassette exchange reveal differential importance of the NPXY motifs in the intracellular domain of LRP1 for normal fetal development. Mol. Cell. Biol *26*, 605-616.

Roessler, E., Lacbawan, F., Dubourg, C., Paulussen, A., Herbergs, J., Hehr, U., Bendavid, C., Zhou, N., Ouspenskaia, M., Bale, S., et al. (2009). The full spectrum of holoprosencephaly-associated mutations within the ZIC2 gene in humans predicts loss-of-function as the predominant disease mechanism. Hum. Mutat *30*, E541-554.

Rogaeva, E., Meng, Y., Lee, J. H., Gu, Y., Kawarai, T., Zou, F., Katayama, T., Baldwin, C. T., Cheng, R., Hasegawa, H., et al. (2007). The neuronal sortilin-related receptor SORL1 is genetically associated with Alzheimer disease. Nat. Genet *39*, 168-177.

Rohr, K. B., Barth, K. A., Varga, Z. M., Wilson, S. W. (2001). The nodal pathway acts upstream of hedgehog signaling to specify ventral telencephalic identity. Neuron *29*,341-351.

Rosenfeld, J. A., Ballif, B. C., Martin, D. M., Aylsworth, A. S., Bejjani, B. A., Torchia, B. S., and Shaffer, L. G. (2010). Clinical characterization of individuals with deletions of genes in holoprosencephaly pathways by aCGH refines the phenotypic spectrum of HPE. Hum Genet. Available at: http://www.ncbi.nlm.nih.gov/pubmed/20066439 [Accessed July 5, 2010].

Rubenstein, J. L., Shimamura, K., Martinez, S., and Puelles, L. (1998). Regionalization of the prosencephalic neural plate. Annu. Rev. Neurosci *21*, 445-477.

Ruiz i Altaba, A., Nguyên, V., and Palma, V. (2003). The emergent design of the neural tube: prepattern, SHH morphogen and GLI code. Curr. Opin. Genet. Dev *13*, 513-521.

Ruiz i Altaba, A. (1999). Gli proteins encode context-dependent positive and negative functions: implications for development and disease. Development *126*, 3205-3216.

Sahali, D., Mulliez, N., Chatelet, F., Laurent-Winter, C., Citadelle, D., Sabourin, J. C., Roux, C., Ronco, P., and Verroust, P. (1993). Comparative immunochemistry and ontogeny of two closely related coated pit proteins. The 280-kd target of teratogenic antibodies and the 330-kd target of nephritogenic antibodies. Am. J. Pathol *142*, 1654-1667.

Saito, A., Pietromonaco, S., Loo, A. K., and Farquhar, M. G. (1994). Complete cloning and sequencing of rat gp330/"megalin," a distinctive member of the low density lipoprotein receptor gene family. Proc. Natl. Acad. Sci. U.S.A *91*, 9725-9729.

Saito, A., Sato, H., Lino, N., Takeda, T. (2010). Molecular mechanismus of receptor-mediated endocytosis in the renal proximal tubular epithelium. J Biomed Biotechnol. *2010*, 403272.

Sakthivel, R., Zhang, J. C., Strickland, D. K., Gåfvels, M., and McCrae, K. R. (2001). Regulation of the ligand binding activity of the human very low density lipoprotein receptor by protein kinase C-dependent phosphorylation. J. Biol. Chem *276*, 555-562.

Schonbaum, C. P., Lee, S., and Mahowald, A. P. (1995). The Drosophila yolkless gene encodes a vitellogenin receptor belonging to the low density lipoprotein receptor superfamily. Proc. Natl. Acad. Sci. U.S.A *92*, 1485-1489.

Shimamura, K., and Rubenstein, J. L. (1997). Inductive interactions direct early regionalization of the mouse forebrain. Development *124*, 2709-2718.

Simon-Chazottes, D., Tutois, S., Kuehn, M., Evans, M., Bourgade, F., Cook, S., Davisson, M. T., and Guénet, J. (2006). Mutations in the gene encoding the low-density lipoprotein receptor LRP4 cause abnormal limb development in the mouse. Genomics *87*, 673-677.

Sisodia, S. S., and St George-Hyslop, P. H. (2002). gamma-Secretase, Notch, Abeta and Alzheimer's disease: where do the presenilins fit in? Nat. Rev. Neurosci *3*, 281-290.

Sonoda, I., Imoto, I., Inoue, J., Shibata, T., Shimada, Y., Chin, K., Imamura, M., Amagasa, T., Gray, J. W., Hirohashi, S., et al. (2004). Frequent silencing of low density lipoprotein receptor-related protein 1B (LRP1B) expression by genetic and epigenetic mechanisms in esophageal squamous cell carcinoma. Cancer Res *64*, 3741-3747.

Sousa, V. H., and Fishell, G. (2010). Sonic hedgehog functions through dynamic changes in temporal competence in the developing forebrain. Curr Opin Genet Dev. Available at: http://www.ncbi.nlm.nih.gov/pubmed/20466536 [Accessed July 5, 2010].

Spoelgen, R., Hammes, A., Anzenberger, U., Zechner, D., Andersen, O. M., Jerchow, B., and Willnow, T. E. (2005). LRP2/megalin is required for patterning of the ventral telencephalon. Development *132*, 405-414.

Steinhusen, U., Weiske, J., Badock, V., Tauber, R., Bommert, K., and Huber, O. (2001). Cleavage and shedding of E-cadherin after induction of apoptosis. J. Biol. Chem *276*, 4972-4980.

Storm, E. E., Garel, S., Borello, U., Hebert, J. M., Martinez, S., McConnell, S. K., Martin, G. R., and Rubenstein, J. L. R. (2006). Dose-dependent functions of Fgf8 in regulating telencephalic patterning centers. Development *133*, 1831-1844.

Storm, E. E., Rubenstein, J. L. R., and Martin, G. R. (2003). Dosage of Fgf8 determines whether cell survival is positively or negatively regulated in the developing forebrain. Proc. Natl. Acad. Sci. U.S.A *100*, 1757-1762.

Stottmann, R. W., Berrong, M., Matta, K., Choi, M., and Klingensmith, J. (2006). The BMP antagonist Noggin promotes cranial and spinal neurulation by distinct mechanisms. Dev. Biol *295*, 647-663.

Südhof, T. C., Goldstein, J. L., Brown, M. S., and Russell, D. W. (1985). The LDL receptor gene: a mosaic of exons shared with different proteins. Science *228*, 815-822.

Sussel, L., Marin, O., Kimura, S., and Rubenstein, J. L. (1999). Loss of Nkx2.1 homeobox gene function results in a ventral to dorsal molecular respecification within the basal telencephalon: evidence for a transformation of the pallidum into the striatum. Development *126*, 3359-3370.

Tam, P. P., and Steiner, K. A. (1999). Anterior patterning by synergistic activity of the early gastrula organizer and the anterior germ layer tissues of the mouse embryo. Development *126*, 5171-5179.

Tamai, K., Semenov, M., Kato, Y., Spokony, R., Liu, C., Katsuyama, Y., Hess, F., Saint-Jeannet, J. P., and He, X. (2000). LDL-receptor-related proteins in Wnt signal transduction. Nature *407*, 530-535.

Tamai, K., Zeng, X., Liu, C., Zhang, X., Harada, Y., Chang, Z., and He, X. (2004). A mechanism for Wnt coreceptor activation. Mol. Cell *13*, 149-156.

Tanzawa, K., Shimada, Y., Kuroda, M., Tsujita, Y., Arai, M., and Watanabe, H. (1980). WHHL-rabbit: a low density lipoprotein receptor-deficient animal model for familial hypercholesterolemia. FEBS Lett *118*, 81-84.

Tenzen, T., Allen, B. L., Cole, F., Kang, J., Krauss, R. S., and McMahon, A. P. (2006). The cell surface membrane proteins Cdo and Boc are components and targets of the Hedgehog signaling pathway and feedback network in mice. Dev. Cell *10*, 647-656.

Terryn, S., Jouret, F., Vandenabeele, F., Smolders, I., Moreels, M., Devuyst, O., Steels, P., Van Kerkhove, E. (2007). A primary culture of mouse proximal tubular cells, established on collagen-coated membranes. Am J Physiol Renal Physiol. *293*, 476-485.

Theil, T., Alvarez-Bolado, G., Walter, A., and Rüther, U. (1999). Gli3 is required for Emx gene expression during dorsal telencephalon development. Development *126*, 3561-3571.

Torroja, C., Gorfinkiel, N., Guerrero, I. (2004). Patched controls the Hedgehog gradient by endocytosis in a dynamin-dependent manner, but this internalization does not play a major role in signal transduction. Development *131*, 2395-2408.

Tousseyn, T., Jorissen, E., Reiss, K., and Hartmann, D. (2006). (Make) stick and cut loose--disintegrin metalloproteases in development and disease. Birth Defects Res. C Embryo Today *78*, 24-46.

Trommsdorff, M., Gotthardt, M., Hiesberger, T., Shelton, J., Stockinger, W., Nimpf, J., Hammer, R. E., Richardson, J. A., and Herz, J. (1999). Reeler/Disabled-like disruption of neuronal migration in knockout mice lacking the VLDL receptor and ApoE receptor 2. Cell *97*, 689-701.

Urban, S., and Freeman, M. (2002). Intramembrane proteolysis controls diverse signalling pathways throughout evolution. Curr. Opin. Genet. Dev *12*, 512-518.

Van Praet, O., Argraves, W. S., and Morales, C. R. (2003). Co-expression and interaction of cubilin and megalin in the adult male rat reproductive system. Mol. Reprod. Dev *64*, 129-135.

Wallis, D. E., and Muenke, M. (1999). Molecular mechanisms of holoprosencephaly. Mol. Genet. Metab *68*, 126-138.

Weatherbee, S. D., Anderson, K. V., and Niswander, L. A. (2006). LDL-receptor-related protein 4 is crucial for formation of the neuromuscular junction. Development *133*, 4993-5000.

Wehrli, M., Dougan, S. T., Caldwell, K., O'Keefe, L., Schwartz, S., Vaizel-Ohayon, D., Schejter, E., Tomlinson, A., and DiNardo, S. (2000). arrow encodes an LDL-receptor-related protein essential for Wingless signalling. Nature *407*, 527-530.

Wicher, G., and Aldskogius, H. (2008). Megalin deficiency induces critical changes in mouse spinal cord development. Neuroreport *19*, 559-563.

Williams, S. E., Ashcom, J. D., Argraves, W. S., and Strickland, D. K. (1992). A novel mechanism for controlling the activity of alpha 2-macroglobulin receptor/low density lipoprotein receptor-related protein. Multiple regulatory sites for 39-kDa receptor-associated protein. J. Biol. Chem *267*, 9035-9040.

Willnow, T. E., Hilpert, J., Armstrong, S. A., Rohlmann, A., Hammer, R. E., Burns, D. K., and Herz, J. (1996). Defective forebrain development in mice lacking gp330/megalin. Proc. Natl. Acad. Sci. U.S.A *93*, 8460-8464.

Willnow, T. E., Hammes, A., and Eaton, S. (2007). Lipoproteins and their receptors in embryonic development: more than cholesterol clearance. Development *134*, 3239-3249.

Willnow, T. E., and Nykjaer, A. (2010). Cellular uptake of steroid carrier proteins--mechanisms and implications. Mol. Cell. Endocrinol *316*, 93-102.

Wilson, S. W., Houart, C. (2004). Early steps in the development of the forebrain. Dev Cell *6*,167-181.

Winnier, G., Blessing, M., Labosky, P. A., and Hogan, B. L. (1995). Bone morphogenetic protein-4 is required for mesoderm formation and patterning in the mouse. Genes Dev *9*, 2105-2116.

Yang, Y., and Klingensmith, J. (2006). Roles of organizer factors and BMP antagonism in mammalian forebrain establishment. Dev. Biol *296*, 458-475.

Yochem, J., Tuck, S., Greenwald, I., and Han, M. (1999). A gp330/megalin-related protein is required in the major epidermis of Caenorhabditis elegans for completion of molting. Development *126*, 597-606.

Zaki, P. A., Quinn, J. C., Price, D. J. (2003). Mouse models of telencephalic development. Curr Opin Genet Dev. *13*, 423-437.

Zarbalis, K., May, S. R., Shen, Y., Ekker, M., Rubenstein, J. L., Peterson, A. S. (2004). A focused and efficient genetic screening strategy in the mouse: identification of mutations that disrupt cortical development. PLoS Biol. *2*, E219.

Zeng, X., Goetz, J. A., Suber, L. M., Scott, J. W. Jr., Schreiner, C. M., and Robbins, D J. (2001). A freely diffusible form of Sonic hedgehog mediates long-range signalling. Nature *411*, 716-720.

Zeng, X., Tamai, K., Doble, B., Li, S., Huang, H., Habas, R., Okamura, H., Woodgett, J., and He, X. (2005). A dual-kinase mechanism for Wnt co-receptor phosphorylation and activation. Nature *438*, 873-877.

Zhang, W., Kang, J., Cole, F., Yi, M., and Krauss, R. S. (2006). Cdo functions at multiple points in the Sonic Hedgehog pathway, and Cdo-deficient mice accurately model human holoprosencephaly. Dev. Cell *10*, 657-665.

Zheng, G., Bachinsky, D. R., Abbate, M., Andres, G., Brown, D., Stamenkovic, I., Niles, J. L., and McCluskey, R. T. (1994). gp330: receptor and autoantigen. Ann. N. Y. Acad. Sci *737*, 154-162.

Zhou, W., and Carpenter, G. (2000). Heregulin-dependent trafficking and cleavage of ErbB-4. J. Biol. Chem *275*, 34737-34743.

Zou, Z., Chung, B., Nguyen, T., Mentone, S., Thomson, B., and Biemesderfer, D. (2004). Linking receptor-mediated endocytosis and cell signaling: evidence for regulated intramembrane proteolysis of megalin in proximal tubule. J. Biol. Chem *279*, 34302-34310.

7. Appendix

7.1. Curriculum Vitae

The curriculum vitae is not inclosed in the online version for data privacy protection reasons

Der Lebenslauf ist in der Online-Version aus Gründen des Datenschutzes nicht enthalten

The curriculum vitae is not inclosed in the online version for data privacy protection reasons

Der Lebenslauf ist in der Online-Version aus Gründen des Datenschutzes nicht enthalten

Publications:

Zhang, J, Piontek, J, Wolburg, H, Piehl, C, Liss, M, Otten, C, **Christ, A**, Willnow, TE, Blasig, IE and Abdelilah-Seyfried, S.
Estabilshment of a neuroepithelial barrier by Claudin5a is essential for zebrafish brain ventricular lumen expansion.
Proc. Natl. Acad. Sci USA (1/2010), Vol. 107, 1425-1430.

Gajera C, Emich H, Lioubinski, **Christ A**, Beckervordersandforth-Bonk R, Yoshikawa K, Bachmann S, Christensen EI, Götz M, Kempermann G, Peterson AS, Willnow TE, Hammes A.
LRP2 in ependymal cells regulate BMP signaling in the adult neurogenic niche
Journal of Cell Science (6/2010). Vol. 123, 1922-1930.

Christ A, Terryn S, Schmidt V, Christiansen EI, Huska MR, .Andrade-Navarro MA, Hübner N, Devuyst O, Hammes A, Willnow TE
The soluble intracellular domain of megalin does not affect renal proximal tubular function in vivo
Kidney International (9/2010). Vol. 78, 473-477

7.2 Selbstständigkeitserklärung

Hiermit erkläre ich, dass ich die vorliegende Arbeit mit dem Titel ”The role of LRP2 in forebrain development of the mouse” selbstständig und ohne Hilfe Dritter angefertigt habe. Sämtliche Hilfsmittel, Hilfen sowie Literaturquellen sind als solche kenntlich gemacht. Ausserdem erkläre ich hiermit, dass ich mich nicht anderweitig um einen entsprechenden Doktorgrad beworben habe. Die Promotionsordnung des Fachbereichs Biologie, Chemie, Pharmazie der Freien Universität Berlin habe ich gelesen und akzeptiert.

Annabel Christ

Berlin, September 2010

7.3 Danksagung

Ich bedanke mich herzlichst bei Prof. Dr. Thomas E. Willnow und Dr. Annette Hammes-Lewin für die Überlassung dieses Projekts, die ausgezeichnete und enthusiastische Betreuung meiner Arbeit und die erstklassigen Arbeitsbedingungen im Labor.

Mein besonderer Dank gilt Prof. Dr. Volker Haucke von der Freien Universität Berlin für die Betreuung und Begutachtung meiner Arbeit.

Ich bedanke mich bei Erik I. Christensen, Sarah Terrin, Vanessa Schmidt, Tilman Breiderhoff und Oleg Liubinsky für die Hilfe in der ICD Studie und BMP4 Haploinsuffizienz Studie, die in dieser Arbeit präsentiert wurden.

Ein großes Dankeschön gilt meinen Arbeitskollegen der AG Willnow. Die Hilfsbereitschaft jedes Einzelnen hat zum Gelingen dieser Doktorarbeit beigetragen.
Mein besonderer Dank gilt Dr. Oleg Lyubinskiy der, nicht nur, in unzähligen und umfangreichen Diskussion immer wieder neue Denkanstöße und Mut lieferte, sondern auch dafür sorgte, dass ich in New York nicht verloren ging. Im Besonderen danke ich der gesamten Megalin-Gruppe für hilfreiche Diskussionen rund ums Projekt. Ebenso möchte ich Dr. Tilman Breiderhoff danken. Ohne ihn würde ich immer noch mit Lasergene kämpfen. Dr. Anne-Sophie Carlo möchte ich für die wunderbare, abwechslungsreiche Zeit an der „Bench“ danken! Bei Tatjana Pantzlaff und Juliane Reiche möchte ich mich für den regen Informationsaustausch bedanken. Ebenso möchte ich mich bei Verona Kuhle für Ihre Unterstützung bedanken.
Bei den technischen Assistentinnen, Maria Schmeisser, Christine Kruse, Kristin Kampf und Donathe Vetter möchte ich mich für Ihre Unterstützung bedanken.

Meiner Familie und meinem Freund möchte ich ganz besonders für die aufmunternde Unterstützung während meines Studiums und meiner Doktoranden-Zeit danken!